

Frej Wasastjerna

Using MCNP for fusion neutronics

VTT PUBLICATIONS 699

Using MCNP for fusion neutronics

Frej Wasastjerna

Dissertation for the degree of Doctor of Science in Technology to be presented with due permission of the Department of Engineering Physics, Faculty of Information and Natural Sciences, for public examination and debate in Room 326 of the Department of Engineering Design and Production of the Helsinki University of Technology, Otakaari 4, on the 19th of December, 2008, at 12 o'clock noon.



ISBN 978-951-38-7129-1 (soft back ed.)

ISSN 1235-0621 (soft back ed.)

ISBN 978-951-38-7130-7 (URL: <http://www.vtt.fi/publications/index.jsp>)

ISSN 1455-0849 (URL: <http://www.vtt.fi/publications/index.jsp>)

Copyright © VTT 2008

JULKAISIJA – UTGIVARE – PUBLISHER

VTT, Vuorimiehentie 5, PL 1000, 02044 VTT

puh. vaihde 020 722 111, faksi 020 722 7001

VTT, Bergsmansvägen 5, PB 1000, 02044 VTT

tel. växel 020 722 111, fax 020 722 7001

VTT Technical Research Centre of Finland, Vuorimiehentie 5, P.O. Box 1000, FI-02044 VTT, Finland
phone internat. +358 20 722 111, fax + 358 20 722 7001

VTT, Otakaari 3 A, PL 1000, 02044 VTT

puh. vaihde 020 722 111, faksi 020 722 5000

VTT, Otsvängen 3 A, PB 1000, 02044 VTT

tel. växel 020 722 111, fax 020 722 5000

VTT Technical Research Centre of Finland, Otakaari 3 A, P.O. Box 1000, FI-02044 VTT, Finland
phone internat. +358 20 722 111, fax +358 20 722 5000

Text preparing Tarja Haapalainen

Edita Prima Oy, Helsinki 2008

Wasastjerna, Frej. Using MCNP for fusion neutronics [Fusionsneutronik med MCNP]. Espoo 2008. VTT Publications 699. 68 p. + app. 136 p.

Keywords fusion neutronics, MCNP, variance reduction, importances, weight windows, tally source method

Abstract

Any fusion reactor using tritium-deuterium fusion will be a prolific source of 14 MeV neutrons. In fact, 80% of the fusion energy will be carried away by these neutrons. Thus it is essential to calculate what will happen to them, so that such quantities as the tritium breeding ratio, the neutron wall loading, heat deposition, various kinds of material damage and biological dose rates can be determined. Monte Carlo programs, in particular the widely-used MCNP, are the preferred tools for this. The International Fusion Materials Irradiation Facility (IFMIF), intended to test materials in intense neutron fields with a spectrum similar to that prevailing in fusion reactors, also requires neutronics calculations, with similar methods.

In some cases these calculations can be very difficult. In particular shielding calculations – such as those needed to determine the heating of the superconducting field coils of ITER or the dose rate, during operation or after shutdown, outside ITER or in the space above the test cell of IFMIF – are very challenging. The thick shielding reduces the neutron flux by many orders of magnitude, so that analog calculations are impracticable and heavy variance reduction is needed, mainly importances or weight windows. On the other hand, the shields contain penetrations through which neutrons may stream. If the importances are much higher or the weight windows much lower at the outer end of such a penetration than at the inner end, this may lead to an excessive proliferation of tracks, which may even make the calculation break down.

This dissertation describes the author's work in fusion neutronics, with the main emphasis on attempts to develop improved methods of performing such calculations. Two main approaches are described: trying to determine near-optimal importances or weight windows, and testing the “tally source” method suggested by John Hendricks as a way of biasing the neutron flux in angle.

Wasastjerna, Frej. Using MCNP for fusion neutronics [Fusionsneutronik med MCNP]. Espoo 2008. VTT Publications 699. 68 s. + bil. 136 s.

Nyckelord fusion neutronics, MCNP, variance reduction, importances, weight windows, tally source method

Sammanfattning

En fusionsreaktor som använder sig av tritium-deuteriumfusion kommer att vara en mycket stark källa till neutroner med en energi av 14 MeV. Dessa kommer i själva verket att bära med sig 80 % av fusionsenergin. Det är alltså väsentligt att beräkna vad som kommer att hända med dem, så att man kan bestämma sådana storheter som tritiumbräckvidden, den av neutronerna förorsakade väggbelastningen, värmedepositionen, olika slags materialskador och biologiska dosrater. Monte Carlo-program, speciellt MCNP, är det mest allmänt använda redskapet för sådana beräkningar. IFMIF (International Fusion Materials Irradiation Facility), avsedd att testa material i ett intensivt neutronflöde med ett spektrum som liknar det i fusionsreaktorer, kräver också neutronberäkningar, med liknande metoder.

I vissa fall kan dessa beräkningar vara mycket svåra. I synnerhet strålskyddsberäkningar, sådana som behövs för att bestämma värmeutvecklingen i ITERs supraledande fältspolar eller dosraten, i verksamhet eller efter avstängning, utanför ITER eller i utrymmet ovanför IFMIFs testcell, är särdeles krävande. Det tjocka strålskyddet minskar neutronflödet med många storleksordningar, så att analoga beräkningar är ogenomförbara och stark variansreduktion är nödvändig, främst med viktighet eller viktfönster. Å andra sidan innehåller skyddet genomföringar längs vilka neutroner kan strömma. Om viktigheterna är mycket högre eller viktfönstren mycket lägre i yttre ändan av en sådan genomföring än i den inre ändan, kan en partikelhistoria yngla av sig i ett orimligt antal spår, vilket kan få beräkningen att bryta samman.

Denna avhandling beskriver disputandens arbete i fusionsneutronikbranschen med huvudvikten lagd vid hans försök att utveckla förbättrade beräkningsmetoder. Två huvudsakliga sätt att göra detta beskrivs: försök att bestämma närapå optimala viktigheter eller viktfönster, och testning av "tally source"-metoden, föreslagen av John Hendricks som ett sätt att biasera neutronflödet med avseende på vinkel.

Preface

The work described here was carried out during the period 1996–2007 under the auspices of Association Euratom-Tekes, as part of the EU work on the development of fusion power.

It is not feasible to thank everybody who has helped me in the course of this work; the list would be too long. However, special thanks are due to Drs Seppo Karttunen and Petri Kotiluoto for handling the associated administrative tasks and to Drs Robert Santoro, Hiromasa Iida and Ulrich Fischer for supervising the work. Drs Stanislav Simakov and John Hendricks were also particularly helpful, as noted in the main text. Dr Petri Kotiluoto, Professor Rainer Salomaa, Professor Emeritus Heikki Kalli and Assistant Professor Robert Jeraj also deserve thanks for providing useful comments on this dissertation.

The funding for the work was provided by Tekes, VTT and Euratom, and is hereby gratefully acknowledged.

List of publications

This dissertation is based on the following publications:

- I Heikinheimo, L., Heikkinen, J., Linden, J., Kaye, A., Orivuori, S., Saarelma, S., Tähtinen, S., Walton, R. and Wasastjerna, F. Dielectric window for reactor like ICRF vacuum transmission line. *Fusion Engineering and Design* **55**(2001), pp. 419–436.
- II Bibet, Ph., Mirizzi, F., Bosia, P., Doceul, L., Kuzikov, S., Rantamäki, K., Tuccillo, A.A. and Wasastjerna, F. Overview of the ITER-FEAT LH system. *Fusion Engineering and Design* **66–68**(2003), pp. 525–529.
- III Fischer, U., Pereslavitsev, P., Kotiluoto, P. and Wasastjerna, F. Nuclear performance analyses for HCPB test blanket modules in ITER. *Fusion Engineering and Design* **82**(2007), pp. 2140–2146.
- IV Norajitra, P., Bühler, L., Buenaventura, A., Diegele, E., Fischer, U. Gordeev, S., Hutter, E., Kruessmann, R., Malang, S., Maisonnier, D., Orden, A., Reimann, G., Reimann, J., Vieider, G., Ward, D. and Wasastjerna, F. Conceptual design of the EU dual-coolant blanket (model C). 20th IEEE/NPSS Symposium on Fusion Engineering (SOFE). San Diego, CA, USA 2003.
- V Simakov, S.P, Fischer, U., Möslang, A., Vladimirov, P., Wasastjerna, F. and Wilson, P.P.H. Neutronics and activation characteristics of the international fusion material irradiation facility. *Fusion Engineering and Design* **75–79**(2005), pp. 813–817.
- VI Fischer, U., Chen, Y., Simakov, S.P., Wilson, P.P.H., Vladimirov, P. and Wasastjerna, F. Overview of recent progress in IFMIF neutronics. *Fusion Engineering and Design* **81**(2006), pp. 1195–1202.

- VII Simakov, S.P., Vladimirov, P., Fischer, U., Heinzl, V., Möslang, A. and Wasastjerna, F. Tungsten spectral shifter: neutronics analysis (dpa evaluation, H, He and other impurities generation, recoil spectrum, etc) of different positions and geometries. Final report on the EFDA task TW5-TTMI-003, Deliverable 8. FZK (Forschungszentrum Karlsruhe) report (2006). 11 p.
- VIII Kotiluoto, P. and Wasastjerna, F. Calculating the neutron current emerging through the beam tubes in IFMIF (EFDA Task TW6-TTMI-001-D3a). VTT Research Report (2006). 9 p.
- IX Wasastjerna, F. A study of variance reduction methods in MCNP4C in a slot with a dogleg. 12th Biennial Topical Meeting of the Radiation Protection and Shielding Division of the American Nuclear Society. Paper 14, Santa Fe, NM, USA 2002. 11 p.
- X Wasastjerna, F. Importances for MCNP Calculations on a Shield with a Penetration. 14th Biennial Topical Meeting of the Radiation Protection and Shielding Division of the American Nuclear Society, Carlsbad, NM, USA 2006. Pp. 478–488.
- XI Wasastjerna, F. Application of importances or weight windows in MCNP4C to a geometry similar to an ITER equatorial port. *Annals of Nuclear Energy* **35/3** (2008), pp. 425–431.
- XII Wasastjerna, F. Calculating streaming with the “tally source” method, as applied to IFMIF. *Annals of Nuclear Energy* **35/3** (2008), pp. 438–445.

In Publications I through III the contribution of the disputant was to model one or more port plugs for an equatorial and/or upper port in ITER, fit this into the general ITER model prepared by a team of other people, and perform the required neutron shielding calculations. In Publication III the modeling was limited to the rear (shield) part of the plug, and even this modeling was shared with one co-author. In Publication IV the disputant modeled the whole reactor, at a more modest level of detail than for ITER or IFMIF, and performed the neutronics calculations. In Publications V through VIII the IFMIF test cell and

its contents were modeled in considerable detail. The author also performed some of the calculations described in Publication VIII.

In more detail, the disputant was responsible for the following:

- Publication I: Section 2
- Publication II: Subsection 3.5
- Publication III: most of Section 5, with a contribution from P. Kotiluoto.

Note that the disputant's share of the modeling in these three publications was mostly limited to the port plug being investigated, and in Publication III only to part of that. For the rest of the reactor, existing standard models were used, though they often had to be modified slightly, e.g. by subdividing the port walls into smaller cells to permit sufficient resolution for importances or weight windows.

- Publication IV: Subsection IIC
- Publication V: The model described in the second paragraph of Section 2 and used in the calculations
- Publication VI: Again, the model used in the Monte Carlo calculations
- Publication VII: All of the several geometry model variants used in the calculations
- Publication VIII: The model and the initial calculations
- All of Publications IX through XII.

Contents

Abstract.....	3
Sammanfattning.....	4
Preface.....	5
List of publications.....	6
1. Introduction.....	11
1.1 The need for fusion neutronics.....	11
1.2 The international magnetic confinement fusion program.....	12
1.3 Typical features of fusion reactors and related facilities.....	14
1.4 What method to use?.....	15
1.5 Shutdown dose rate calculations.....	17
1.6 Variance reduction.....	18
2. Applications.....	25
2.1 ITER (Publications I, II and III).....	25
2.2 PPCS, model C (Publication IV).....	27
2.2.1 Geometry modeling.....	28
2.2.2 Neutron wall loading.....	29
2.2.3 Tritium breeding ratio.....	31
2.2.4 Shielding calculations.....	32
2.3 IFMIF (Publications V–VIII).....	33
2.3.1 Background and geometry.....	33
2.3.2 Calculating neutron transport through the beam tubes.....	38
2.3.3 Cover shielding calculations.....	41
3. Method development.....	44
3.1 Background.....	44
3.2 Choosing importances (Publications IX, X and XI).....	48
3.2.1 The longitudinal importance distribution: the Handy Method.....	49
3.2.2 Transverse importance distribution.....	51
3.2.3 Testing the methods.....	56
3.3 The “tally source” method (Publication XII).....	58

4. Summary and conclusions	62
----------------------------------	----

References.....	65
-----------------	----

Appendices

Appendix A: An Analytic Estimate of the Spatial Discretization Error in the Rigorous Two-Step Method for Calculating Shutdown Dose Rates

Appendix B: Publications I–XII

Appendix B: Publications I, II, III, V, VI, XI, XII are not included in the PDF version. Please order the printed version to get the complete publication (<http://www.vtt.fi/publications/index.jsp>)

1. Introduction

1.1 The need for fusion neutronics

In a fission reactor, approximately one neutron gets released for each 80 MeV of fission energy, and the average energy of fission neutrons is about 2 MeV. In deuterium-tritium fusion, one neutron is released per 17.6 MeV of fusion energy, and the neutrons initially have a kinetic energy of about 14.1 MeV. In other words, a fusion reactor relying on the D-T reaction is a much more prolific source of neutrons than a fission reactor, and in addition the neutrons are much more energetic.

While fusion reactors do not depend on neutrons to maintain a chain reaction the way fission reactors do, neutrons are needed to generate the fuel they burn. Tritium does not exist in significant quantities in nature, so it must be produced by neutrons reacting with lithium (e.g., ${}^6\text{Li}(n,t){}^4\text{He}$). Since every fusion reaction consumes one tritium atom (ignoring such side reactions as D-D fusion) and provides only one neutron, and since losses of both neutrons and tritium are unavoidable, a certain amount of neutron multiplication in materials such as beryllium or lead is required. The lithium also needs to be enriched in ${}^6\text{Li}$. Checking that the tritium breeding ratio (TBR) is adequate is one of the problems in fusion neutronics.

The neutrons carry away 80% of the fusion energy, depositing it mostly in the blanket. Calculating the energy deposition rate as a function of position is essential, so that the designers know how much heat the coolant must be able to remove in each location.

The neutrons also have harmful effects. They induce radioactivity in the materials of which a fusion reactor is constructed and in the coolant flowing through it, e.g., through the ${}^{16}\text{O}(n,p){}^{16}\text{N}$ reaction. They may damage materials through displacement of atoms, affecting mechanical and electric properties. They produce hydrogen and helium, which make welding difficult in concentrations above about 1 atomic ppm, and they heat superconducting coils in devices using magnetic confinement. These effects also need to be calculated.

1.2 The international magnetic confinement fusion program

The current centerpiece of the international magnetic confinement fusion program is ITER [1, 2], which will be built at Cadarache in France. It is a tokamak with a fusion power of 500 MW, with superconducting coils and a water-cooled blanket, with the coolant temperature limited to 150°C. It will lack equipment to convert the produced power into electricity, since the low temperature and low duty cycle would make such conversion uneconomic. The goal of ITER is to achieve a substantial energy gain¹ and long pulses (at least 400 s), thus demonstrating the practicality of fusion as an energy source. It will provide experience of operating an industrial-scale fusion reactor, enabling scientists and engineers to design reactors suitable for actual power production.

In order to be economic, future fusion reactors will probably need to be more compact than ITER, with a higher wall loading (the power carried as kinetic energy by neutrons per square meter of wall surface) and will also need a high capacity factor. This will mean that, at least near the plasma, the materials will be exposed to high fluences of high-energy neutrons. Developing materials capable of standing such fluences is a major challenge and will require lots of testing. With its modest wall loading and low duty cycle, ITER will be unable to provide the required fluence. Therefore, a dedicated facility for material testing will be needed. This is the reasoning behind IFMIF, the International Fusion Materials Irradiation Facility [3]. IFMIF will use two beams of 40 MeV deuterons, each with an intensity of 125 mA, impinging on a jet of liquid lithium to produce an intense flux of neutrons with energies up to 55 MeV over a volume of several liters and a lower flux over a larger volume. Although the maximum neutron energy of 55 MeV will be substantially higher than the 14.1 MeV maximum in a fusion reactor, most of the neutrons will actually be born at much lower energies. In any case, it has been estimated that the ratios of different types of material damage, such as displacements and hydrogen and helium production, will be similar to what can be expected in a fusion reactor. Thus IFMIF can, in a few years, provide data about the behavior of materials at fluences corresponding to decades of exposure in a fusion reactor. It can also test

¹ The ratio Q of the fusion power to the power fed in to heat the plasma and drive the current is intended to be at least 10.

the behavior of materials under simultaneous stress and irradiation or test tritium retention and release under irradiation, all at different temperatures.

In addition to facilities intended to actually be built, such as ITER and IFMIF, the fusion community has also prepared a number of preliminary designs for future reactors. These are not supposed to be built as such; their purpose is to get some idea of what future fusion reactors might be like and thus to clarify what research is needed. One such study is the European Power Plant Conceptual Study (PPCS). In the words of Andreani et al. [4],

“Within the European Power Plant Conceptual Study (PPCS) four fusion power plant “models”, delivering 1500 MW of electric power to the network, have been developed, named PPCS-A to PPCS-D, which are illustrative of a wider spectrum of possibilities. For the two “near-term” models, PPCS-A and PPCS-B, the plasma physics scenarios are based on parameters slightly better than the design basis of ITER. The high plasma currents, the high current-drive power and the divertor heat load constraints drive these devices to larger size. The technology employed stems from the use of near-term solutions for the blanket, respectively the “water-cooled lithium-lead” concept for model A and the “helium-cooled pebble bed” concept for model B, on which large amount of work has already been performed in Europe. Associated with these are water-cooled and helium-cooled divertors. The water-cooled divertor is an extrapolation of the ITER design and can resist peak heat loads of 15 MW/m². A helium-cooled divertor has been chosen for model B to prevent the risk of hydrogen formation resulting from the water-beryllium reaction in case of accident and to simplify the balance of plant by using the same coolant for all internal components. This divertor must resist a peak heat load of at least 10 MW/m² and, to achieve a reasonable system efficiency, the high pressure helium pumping power should be limited to no more than 10% of the thermal power. Operating temperature however is limited below 550 °C by the use of EUROFER as structural material so that the benefit of the use of helium on thermodynamic efficiency is limited by the high pumping power.

“PPCS-C and PPCS-D are based on progressive improvements in plasma physics, especially in relation to plasma shaping, stability and density

limit, and on minimisation of divertor loads without penalisation of the core plasma conditions. In both cases higher fusion power densities and higher operating temperatures of the coolant and, consequently, higher efficiencies in energy conversion are foreseen. The blanket technology stems from a “dual-coolant” blanket concept for model C (helium for the first wall and high temperature self cooled lithium-lead breeder with steel structures protected by silicon carbide inserts acting as thermal insulators) and from a “self-cooled” blanket concept (even higher temperature lithium-lead coolant with a silicon carbide structure) for model D.”

The present author performed some neutronics calculations for PPCS-C (Publication IV).

1.3 Typical features of fusion reactors and related facilities

Fusion reactors and related facilities have some characteristic differences from fission reactors, which influence the neutronics calculations. One obvious difference is that (assuming deuterium-tritium fusion and ignoring side reactions) all source neutrons will be born at an energy in the neighborhood of 14.1 MeV, though an exact representation of the source spectrum will require accounting for the thermal motion of the fusing nuclei. This is not a problem, since cross section libraries for neutronics calculations usually extend to energies above 14.1 MeV, typically 17.33 or 20 MeV.

Another, more problematic aspect is that fusion reactors contain lots of voids. To begin with, the plasma where the neutrons are born is essentially a void, as far as the neutrons are concerned. More difficult for the neutronics specialist is the fact that the structures surrounding the plasma contain voids that provide streaming paths for neutrons, with deleterious effects on the shielding capability of these components. For instance, in ITER the innermost structure, the blanket, consists of modules separated by gaps of about 2 cm thickness. Similar gaps separate the plugs to be inserted into the ports from the port walls, and these gaps perforate run right through both the blanket and the vacuum vessel, to locations where humans may have to work during shutdowns. The plugs themselves may contain

waveguides or other ducts. The designers try to insert bends or doglegs into these penetrations, but even so they represent weak spots in the shielding.

The situation is even worse in such locations as the neutral beam injection (NBI) ports, where large, straight void channels are unavoidable. Such cases will, however, not be considered in this thesis, being outside the scope of the author's work.

1.4 What method to use?

In principle, shielding calculations, like other neutronics calculations, can be performed using either deterministic or Monte Carlo methods. However, deterministic methods have difficulties in coping with the geometrically-complex mixture of shielding materials and voids typical of ITER and presumably other fusion reactors. Typically they use one or the other of two opposite methods of representing the angular dependence of the flux. The S_N method and the method of characteristics use a limited number of discrete flight directions. The P_L method expands the flux in terms of Legendre polynomials of the angular variables. The former method is plagued by ray effects when applied in voids, and the latter introduces a spurious angular spreading. On the other hand, it would presumably be possible to develop methods of calculating neutron fluxes in a geometry consisting mainly of voids, but such methods would be confounded by the fact that there are large amounts of shielding materials present in fusion reactors and by the geometric complexity.

Thus we have to resort to Monte Carlo². Jaakko Leppänen's doctoral thesis [35] contains a very good introduction to this method, so it would be superfluous to provide one here.

Monte Carlo programs are capable of handling both material-filled cells and voids in a correct fashion, subject only to the need to accumulate enough histories to give adequate statistics. The method is also straightforward and intuitive, at least in particle transport problems. That does not necessarily mean

² Calculation of fluxes and related quantities through the simulation of individual particle histories, using pseudo-random numbers.

that it is easy to use, however. Getting good statistics can sometimes be a very challenging task, as will become apparent below.

In the ITER project, the MCNP program [5–9] has been chosen as a standard. This is a versatile, accurate, well-tested and widely used program. The calculations reported below were performed using MCNP4B, MCNP4C and MCNP5.1.40. In some cases modifications were made (not by the author personally). Specifically, three different modifications were used.

One was intended to model the source in a tokamak more accurately than the standard MCNP source description allows. In a tokamak geometry, this would require modeling the plasma as a number of discrete cells, each with a constant source density. This step-like representation was considered somewhat unsatisfactory and an alternative method was developed at the UKAEA to represent the source in r - θ - z geometry. A mesh of (r,z) points is used, in practice typically some 40×40 points, and each point is assigned an appropriate source intensity, calculated by an auxiliary program on the basis of the plasma density and temperature. The source is considered constant in the θ direction. This method is well adapted to a tokamak geometry.

Another source modification was needed for calculations on IFMIF. Stanislav Simakov at Forschungszentrum Karlsruhe wrote a modified version of MCNP called McDeLicious [10, 11], which calculates the neutron source produced by deuteron beams impinging on lithium. In principle this could presumably also have been calculated using MCNPX [12], but at the time McDeLicious was written, MCNPX did not give satisfactory accuracy. Note that in McDeLicious, the source normalization factor should be the number of deuterons hitting the target per second, not the number of neutrons emitted by the source.

The third modification is required for the Direct 1-Step (D1S) method of activation calculations, described in the next section. In addition to a program, one also needs to decide on a nuclear data library to be used with it. In the ITER project, FENDL, the Fusion Evaluated Nuclear Data Library, was chosen as a standard. The latest version is FENDL-2.1 (Dec. 2004) [13].

1.5 Shutdown dose rate calculations

A prominent issue in neutronics calculations for ITER is the calculation of dose rates with the reactor shut down. The specifications say that it must be possible to carry out hands-on maintenance at the ends of the ports 10^6 seconds (about 11.5 days) after shutdown. Assuming a maximum annual dose of 20 mSv and 200 hours of work per year, this means that the dose rate must be less than 100 μ Sv/h [14]. This has turned out to be the most difficult requirement to fulfill for the port shielding, much more difficult than limiting the heating in the superconducting coils to an acceptable level.

Calculating shutdown dose rates requires three things. First, one must calculate the neutron flux. Secondly, a calculation of the resulting activation is required. Note that this may be quite sensitive to certain trace materials, such as europium in concrete. Finally, one must then calculate the transport of the delayed gammas and tally the dose rates in the relevant locations.

There are two ways of going about this. One possibility is to do all these calculations separately. This requires two separate MCNP calculations and is accordingly called the Rigorous Two-Step (R2S) method [15]. Between the neutron and gamma calculations, an activation calculation is performed. FISPACT [16] is the preferred program for this purpose. In addition, certain auxiliary programs have been written to facilitate the use of FISPACT on a mass production basis for a large number of geometry cells.

A disadvantage of the R2S method is that the averaging of the flux over each tally cell results in a distortion of the spatial distribution of the activation reaction. The true distribution is approximated by a stepwise distribution. Appendix A provides a rough estimate of this discretization error.

On the other hand, the R2S method permits a full activation calculation, including multi-step reactions. It also allows one to use different geometries in the neutron and gamma calculations.

The other possibility is to handle the neutron and gamma calculations as a single MODE N P (combined neutron-photon) calculation. Then the photons will be born exactly where the neutrons collide, and the spatial discretization error is

eliminated. This method is called the Direct One-Step (D1S) method [17–19]. It requires some changes in MCNP and the data libraries, since the program is intended to handle only prompt gammas. It uses a kind of pseudo-time bins to separate the contributions from different radioactive nuclides. Each such contribution is multiplied by a factor taking into account the irradiation history and subsequent decay.

The D1S method obviously has an advantage in that it avoids the discretization error. It is also simpler to use, at least once the above-mentioned factors have been calculated – and provided one can get the modified program and data libraries to work, which may sometimes be problematic. It requires the activation to be directly proportional to the neutron flux, so multi-step reactions or depletion effects cannot be taken into account. However, one would not expect these to be important at the relatively modest fluences prevailing at the ends of ITER ports.

In principle, combining the neutron and gamma calculations requires the geometry to be the same in both steps. However, the modified version of MCNP currently allows some cells to be void in one step but not the other.

Activity levels after irradiation may be strongly affected by low levels of certain impurities such as europium. This is typically not taken into account in ITER dose rate calculations, which simply use some given composition, not including trace materials, for both transport and activation calculations. However, this is reasonable, since the materials to be used in those parts of ITER subject to significant neutron flux are designed for minimum activation, so the levels of problematic trace materials will presumably be kept low.

1.6 Variance reduction

A few of the calculations described in this work did not require variance reduction. For instance, the wall loading calculation for PPCS-C was easy. However, most of the cases were shielding calculations, and shielding calculations with the Monte Carlo method generally require a lot of variance

reduction³. After all, the purpose of shielding is to stop particles from getting where they are not wanted, and, as a result, an analog calculation will have very poor statistics.

The variance reduction techniques most used in the work reported here are implicit capture and splitting / Russian roulette. A few other techniques were occasionally used and will be mentioned in those contexts.

Implicit capture is used by default for neutrons in MCNP. In analog capture, when a particle collides, the track⁴ is terminated with a probability equal to the probability of the particle being captured. In implicit capture, the track is not terminated, but its weight⁵ is reduced through multiplication by the probability of not being captured. The track will thus continue until it leaks out of the system, by entering a cell with importance zero or a negative sill (weight window lower boundary),⁶ or until it is terminated by some other means, typically weight cutoff.

The advantage of implicit capture is that it decreases the risk that a track will be terminated just as it is about to reach a region where it will be tallied. However, there must be some means of terminating a track. For some small systems, it may be feasible to rely on leakage to accomplish this. If an energy or time cutoff is used, they can also terminate tracks effectively. However, in large systems without an energy or time cutoff it is necessary to use some kind of weight cutoff. In this case, the track will be rouletted when the weight drops below a certain limit, so that it will either terminate or continue with an increased weight.

³ Due to its dependence on random sampling, the Monte Carlo method suffers from stochastic uncertainty. This is usually expressed in terms of the **variance** or the **fractional standard deviation** (also called estimated relative error).

⁴ In MCNP, a **history** begins when a particle is emitted from the source. It may split into several **tracks**, for instance due to splitting or (n,2n) reactions. Each track is terminated individually. A history ends when all its tracks have been terminated.

⁵ In **analog** Monte Carlo, a particle is tracked until it is absorbed or leaves the relevant space, energy or time domain. In non-analog techniques, the number of particles tracked may differ from the physical number, and to compensate for this each track, is assigned a statistical **weight**. The calculation tries to determine the correct total weight in each element of phase space rather than the actual number of particles.

⁶ The word “sill” for “weight window lower boundary” was introduced by Hodgdon [25]. Since it is a handy and vivid substitute for a frequently occurring, long and awkward term, it is used in this thesis.

If weight windows are used, the lower boundary of the weight window automatically provides such a cutoff. However, in many of the calculations described here, importances were used instead. Then the weight cutoff defined by the CUT:N card is needed. This card contains the parameters $WC1$ and $WC2$. As the MCNP manual [8] (p. 3–135) says,

“If a neutron’s weight WGT falls below $WC2$ times the ratio R of the source cell importance to the current cell importance, then with probability $WGT/(WC1*R)$, the neutron survives and is assigned $WGT = WC1*R$. If negative values are entered for the weight cutoffs, the values

$$|WC1|*W_s \text{ and } |WC2|*W_s$$

will be used for $WC1$ and $WC2$, respectively, where W_s is the minimum weight assigned to a source neutron from an MCNP general source. These negative entries are recommended for most problems.”

The default values are $WC1 = -0.50$ and $WC2 = -0.25$. However, anybody who wishes to use MCNP with a modified source subroutine should bear in mind that the combination of negative $WC1$ and $WC2$ values with a non-standard source may not work. It has been observed to produce zero or negative weights. Therefore, it is the opinion of the author that when a non-standard source is used, $WC1$ and $WC2$ should be set to positive values. If the source produces particles with a weight of 1, $WC1 = 0.50$ and $WC2 = 0.25$ may be appropriate. In McDeLicious, on the other hand, the source particle weight varies but is typically about 0.08 (related to the probability that a deuteron produces a neutron). Then $WC1 = 0.04$ and $WC2 = 0.02$ may be appropriate.

Probably the most important variance reduction method is geometry splitting; that is, splitting when a particle moves into more important parts of the geometry (closer to a tally cell) and Russian roulette when it moves away. In MCNP this can be implemented using either importances or weight windows.

When importances are used, each cell is assigned an importance. If a particle moves into a cell with a higher importance than the cell it just left, it splits into the number of tracks given by the ratio of the importance in the cell entered to that in the cell it left, while the weight is divided by that same ratio. If the

importance ratio is not an integer, the splitting is done probabilistically so that the average number of tracks will be correct. The weight is still adjusted by the importance ratio, so in individual cases a non-integer ratio of importances will lead to a gain or loss of weight, but on average the figures come out right.

When a particle moves from a more important cell into a less important one, it undergoes Russian roulette. It survives with a probability equal to the ratio of the importance in the cell entered to that in the cell it left, and the weight is adjusted accordingly.

When weight windows are used, the lower boundary of the weight window is specified for each particle type and each cell (or mesh interval, when mesh-based weight windows are used). In addition, weight windows may also be energy or time dependent (not both in MCNP). Angle dependence is not allowed, which is unfortunate in shielding problems such as those considered here, but angle-dependent weight windows would presumably introduce too much additional complexity in the code and input to be practical.

If the weight of a particle drops below the lower boundary, the particle is rouletted. If the weight exceeds the upper bound, the particle is split. The details of the roulette or splitting are determined by parameters on the WWP card, which give the upper bound and the weight after surviving roulette as multiples of the lower bound.

MCNP contains an automatic weight window generator, which calculates weight windows on the basis of the total score from particles in each cell and energy or time bin. However, before the weight window generator can be used, the problem must be run with manually-supplied importances or weight windows. Moreover, the stochastic nature of the weight window generator means that it gives good results only when the variance reduction is already fairly effective. Iterative use of the generator will then produce successively improved results. The manual points out that the generated weight windows should be scrutinized by the user and unreasonable ones adjusted. This is good advice, but unfortunately such scrutiny and adjustment is very time-consuming and laborious when the model consists of thousands of cells, especially if it must be done repeatedly.

A much more extensive description of variance reduction techniques is given in the MCNP manual. In the MCNP5 manual, this description occupies pages 2–134 to 2–163 of Volume I [7].

There is, however, one important point where earlier editions of the MCNP manual are wrong and the MCNP5 manual dated 10/3/05 is somewhat unclear. This concerns the use of weight windows in universes.⁷ For importances, the manual says correctly that “an importance in a cell that is in a universe is interpreted as a multiplier of the importance of the filled cell”. The MCNP4C manual states that sills are treated similarly, but this is false. Test calculations show that only the weight window of the lowest-level cell is taken into account, any weight windows in filled cells are ignored. (In fact, the manual recommends that mesh-based weight windows be used when the geometry model uses repeated structures, i.e., universes or lattices. This way the issue is avoided. However, mesh-based weight windows may be unable to fit the geometry with sufficient precision.)

So, should one use importances or weight windows?

Weight windows have a number of advantages [7] (p. 2–145). However, entering them manually is even more laborious than doing this for importances, so usually it’s best to do the first calculation with importances. Then one can use the weight window generator and recalculate with the resulting weight windows.

Moreover, it’s often hard or impossible to avoid the use of universes in modeling complicated geometries. But the fact that only the weight windows for the lowest-level cells are taken into account often means that weight windows will not work as required with universes. Therefore, in such cases one has to use importances.

Fortunately importances and weight windows can be fairly easily converted into each other. There is an inverse relationship between them, so that a high importance means that the weights in that cell will be low, and consequently the sill should also be low. In fact, the WWP card in MCNP provides an option to

⁷ In MCNP, a cell or a collection of cells can constitute a **universe**, which **fills** another cell.

calculate sills through dividing a constant by the importance for each cell. Similarly, importances can be obtained through dividing a constant by the sills. This is not available as an option in MCNP, but it can be done separately, using a spreadsheet program, so, if necessary, generated weight windows can be translated into importances.

There is also the issue of how large a part of the problem to solve at once. For instance, in shutdown dose rate calculations with the DIS method and in many other applications, combined neutron-photon calculations are necessary. However, it is more practical to start with a calculation covering only fast neutrons (using a CUT:N card to impose an energy cutoff). This can be performed relatively quickly, and the generated weight windows can then be extended to slower neutrons and to photons (suggestions on how to do this are given below). Then one can run a MODE N P calculation and generate improved weight windows, iterating as long as necessary. (If weight windows cannot be used, the generated weight windows must be converted to importances, which must apply to all energies, but one can still have different importances for different particle types.)

One can go further in subdividing the problem. Some analysts prefer to generate a first set of weight windows only for the part of the geometry nearest the source, by using a tally located only a short way into the shielding. It is then possible to get adequate statistics even with very crude starting importances, for instance setting all importances to 1. The generated weight windows can then be used to extend the calculation somewhat farther into the shielding, and so on until good weight windows have been generated for all cells. This stepwise approach is perfectly reasonable, but it involves a large number of calculations. Whether it is preferable to a more direct approach, tackling the whole geometry at once, comes down to a question of how much confidence one has in one's own ability to choose good starting importances. Advice is offered below on how to choose the starting importances, oriented toward the direct approach.

A common problem in shielding calculations with MCNP is that the program "freezes", "locks up" or "hangs", i.e., it keeps running indefinitely without producing any output or dumps. Ctrl-c has no effect, except that if it is repeated a sufficient number of times the run is killed.

It is not known for certain what causes this behavior. However, there are grounds for suspecting that it may be due to excessive splitting. Consider a shielding problem with a long and narrow duct, modeled as a void, running through the shield. The optimum importance will be much higher at the end of the duct furthest from the source than at the near end (or the weight window will be lower). Once in a long while a high-weight particle from the near end will fly straight along the duct, reaching the far end without any collisions on the way. It will then split into a very large number of tracks, so that this history will take a very long time (hours, days or more). Thus we call this the long history problem.

This diagnosis is supported by the fact that such behavior is usually observed in cases where there are voids connecting regions with very different importances. It also appears to be more common in calculations covering the whole energy range for neutrons, and especially in MODE N P calculations, than in calculations considering only fast neutrons, and likewise appears to be more common when absorption in the shielding material is weak. This is consistent with the above diagnosis, since an energy cutoff and high absorption both make for shorter histories.

Possible remedies for the long history problem include minimizing the importance ratio between cells at opposite ends of ducts or other penetrations, but this makes for less effective variance reduction. If only a single duct, of more or less circular cross section, is present, the use of DXTRAN is worth considering, but the geometries encountered in fusion neutronics typically involve numerous or awkwardly-shaped penetrations. John Hendricks has proposed using analog capture, which may help somewhat by terminating tracks sooner.

This dissertation essentially consists of two parts. In the first, the application of MCNP to practical problems in fusion neutronics is described. These calculations often proved to be very difficult, providing an impetus for investigations of how to use variance reduction methods (in particular, importances) as effectively as possible. These studies are described in the second part.

2. Applications

2.1 ITER (Publications I, II and III)

ITER will contain a number of ports to give access to the plasma and the interior of the machine for various purposes such as auxiliary heating and current drive, diagnostics and maintenance. These ports will be at three different levels: upper, equatorial and divertor (lower) ports, with 18 upper ports and 9 divertor ports. At the equatorial level, there will be 3 neutral beam injection (NBI) ports and 14 non-NBI (regular) ports [2, 20].

With the exception of the NBI ports, the equatorial and upper ports will be filled by plugs which contain equipment for the purpose in question. Calculations are necessary to determine the heat production in the inner part of each plug and the adequacy or otherwise of the shielding properties of the plug. The latter involves two main criteria: the heating in the superconducting coils, especially the toroidal field coils, must be limited, and so must the shutdown dose rate around the end of each port (see above). It may also be necessary to determine the fluence to which certain components, such as vacuum windows, will be exposed.

The author has been involved mainly in calculations on plugs containing non-NBI heating and current drive equipment. This heating is done by electromagnetic waves in three different frequency ranges: the ion cyclotron (IC) resonance, lower hybrid (LH) and electron cyclotron (EC) resonance ranges. Launchers for all three kinds of heating will be present in some equatorial ports, and some upper ports will contain EC launchers. The author has performed calculations on all four kinds of plugs, as described in Publications I through III. His contribution has been to model the plugs themselves, insert these models into existing models of a 10- or 20-degree sector of ITER, modifying the general ITER model as necessary (some cells had to be subdivided to allow sufficient resolution for importances or weight windows) and to perform the calculations.

These plugs contain voids, e.g., waveguides, running through them, with bends or doglegs to limit neutron and gamma streaming. To make it possible to insert and remove them, they are separated from the vacuum vessel and blanket by a

gap, which is 2 cm thick in most places according to present designs. This gap contains a dogleg at the boundary between the blanket and the vacuum vessel.

These calculations were very challenging. On one hand, the system is designed to limit the radiation reaching the outer end of the ports, and the distances and material thicknesses involved are considerable. Thus a lot of variance reduction is required, such as use of large importances. On the other hand, there are streaming paths that make it possible for a particle from a low-importance region to reach a high-importance region without passing through material-filled cells on the way. This is a recipe for “long histories” (see above) and the calculations were in fact plagued by this problem, especially in the full MODE N P (combined neutron+photon) calculations required by the DIS method. To avoid long histories, it was necessary to limit the importance variation, which meant that the variance reduction could not be as effective as desired. Thus fractional standard deviations (FSD) below 0.1 could generally not be achieved with reasonable runtimes, say a week or less. Typical FSDs were about 0.2. This, combined with the simplifications and approximations (for instance, geometric simplifications or killing neutrons and, especially, photons in the less important parts of the system) meant that the calculated results are not likely to be very accurate. They could be in error by a factor of 2 or so either way. This is not a problem where the heating of the superconducting field coils is concerned, since this was in all cases found to be well below the stipulated limits. The shutdown dose rate, on the other hand, was more problematic. The calculated dose rates were generally below 100 $\mu\text{Sv/h}$, as required, except for locations near the roots of the ports, where hands-on maintenance will probably not be needed. However, the safety margin to the 100 $\mu\text{Sv/h}$ limit was frequently less than a factor of 2.

Most of the shutdown dose rate is attributable to neutron streaming in the gap between the port plug and port walls. Flagging neutrons in this gap shows that they cause about 90% of the dose rate, whatever the interior of the plug may contain. This is therefore a generic problem, common to all non-NBI equatorial ports. Moreover, survey calculations have shown that the streaming is strongly affected by small changes in the shape and dimensions of the gap (though not by changes in the offset of the dogleg, so long as it is sufficient to prevent straight lines of sight along the gap). Thus, careful attention needs to be paid to design details affecting this gap.

In addition to heating and current drive plugs, the author has also been involved in calculations on one plug containing test blanket modules, specifically for the helium-cooled pebble bed blanket design; see Publication III. This work was shared with Petri Kotiluoto. The results were consistent with what was said above regarding equatorial ports in general.

2.2 PPCS, model C (Publication IV)

Design studies have been performed for actual fusion power plants. One such study was the Power Plant Conceptual Study (PPCS), which involved four different models of 1500 MWe power plants with progressively more advanced technology, from the “near-term” models A and B to the very advanced model D:

- Model A uses a water-cooled lithium-lead (WCLL) blanket and, in general, technology close to the present state of the art.
- Model B uses a helium-cooled ceramic breeder blanket and slightly more advanced materials, technologies and plasma physics.
- Model C is a dual-coolant lithium-lead (DCLL) design, with the lithium-lead breeder material pumped through the blanket and heat exchangers, but with helium cooling for the steel structures. The technology level can be described as intermediate.
- Model D is a self-cooled lithium-lead design with SiC as the structural material.

The author was involved in neutronics calculations on an early, incomplete design for model C. Ports and other details were not represented, only the breeding blanket, hot shield, cold shield, vacuum vessel and toroidal field coils. The blanket used a “banana segment” design, unlike that described in Publication IV.

These calculations covered the tritium breeding ratio, the neutron wall loading, the nuclear heating, and calculation near the inboard mid-plane of the fast and total neutron flux, the helium production in Eurofer steel, and the epoxy dose, copper dpa, heating and fast and total neutron fluence at the front of the toroidal field coil.

2.2.1 Geometry modeling

The geometry modeled in this work was a 10-degree sector, one half of the spacing between toroidal field coils, assuming 18 such coils which was the value used at that time. No ports were included. The divertor was modeled only very roughly, since no information about it was available, and the calculations concentrated mainly on the midplane. On the other hand, the breeding blanket was modeled in some detail, based on the drawings then available. Beyond this was a shield, divided into hot and cold parts, and then the vacuum vessel and toroidal field coils (TFCs).

The blanket, shield and vacuum vessel were modeled using cylindrical rather than toroidal surfaces; see Fig. 1.

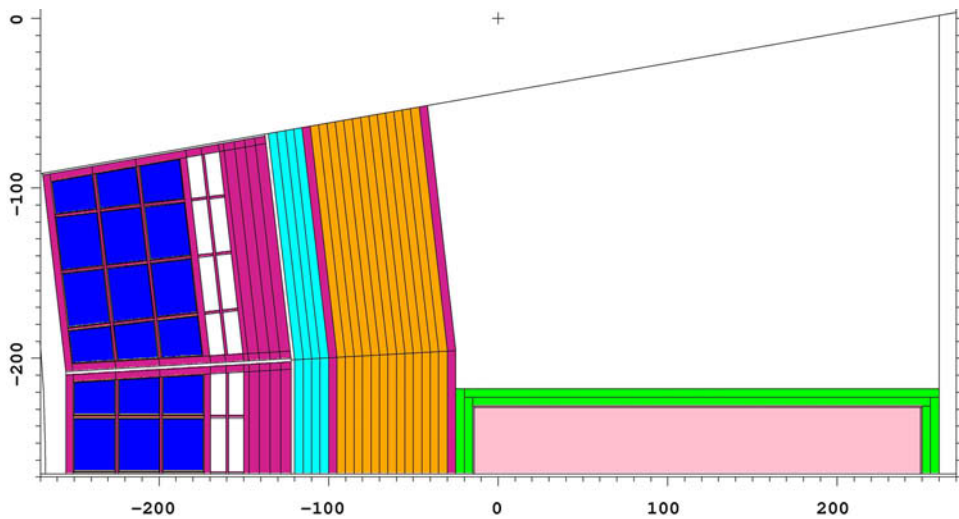


Figure 1. Plan view of the outboard part of the PPCS C model (cut near the equatorial plane). Dimensions in cm, relative to the picture origin (located at $x = 1270$ cm, $y = 268$ cm, $z = 0.1$ cm in the coordinate system centered on the machine axis). Colors: Purple = Eurofer low-activation steel, Blue = Pb-17Li (83 atomic % Pb, 17% Li enriched to 90% Li-6), Yellow = SiC (not visible in picture, present as a liner between steel and Pb-17Li), Cyan = 80 volume % Eurofer, 20% water, Orange = 60 volume % borated (2%) stainless steel ASTM-A887-89, 40% water, Green = 316-LN cryogenic stainless steel, Pink = homogenized toroidal field coil.

The curvature and locations of these surfaces were determined using the method described below (quoted from an informal memo by the author) [21]:

“If the plasma dimensions in a tokamak are given in terms of the major radius R_o , the minor radius a , the elongation κ and the triangularity δ , the separatrix has the shape

$$r = R_o + a \cos(\theta + \delta \sin \theta)$$

$$z = \kappa a \sin \theta$$

in a cylindrical coordinate system, where the poloidal angle θ runs from 0 to 2π . (In a tokamak, the poloidal direction is the one in which the toroidal field coils run.) This shape can easily be plotted using Excel.

“The above formulas are not exact, since there needs to be at least one X-point where helium and impurities can be bled off into the divertor. However, they do give at least a rough idea of the plasma shape. If no information is available on the location of the X-point, one can guess at it by drawing a pair of tangents to the separatrix defined above and calling the place where they cross the X-point, but this is obviously wildly inexact if there is no information where one should place these tangents.

“Sometimes it may be necessary to estimate the position of the first wall before the designers have decided where to locate it. Even at this stage a decision on the distance between the separatrix and the first wall will probably have been made, however. Then one can fit a series of circles to the separatrix and increase their radius by the given amount. The first wall can then be modeled as a series of toroidal or cylindrical surfaces.”

2.2.2 Neutron wall loading

One quantity that is of interest in fusion neutronics is the neutron wall loading, the rate at which neutrons transfer kinetic energy through the first wall. In addition to the average neutron wall loading, the poloidal distribution is also required. This was easy to calculate. Once the source region was modeled, it was

surrounded with the surface at which the loading should be calculated, then it was just a matter of tallying and killing all neutrons crossing that surface.

The wall loading is customarily expressed in MW/m^2 . Therefore the FM multiplier (typically used to normalize tallies to a given source strength [8], p. 3–95) should be the *neutron* power (80% of the fusion power) in MW, and the SD divider (used for areas, volumes or masses) for each segment of the tally surface should be the area in m^2 . In a complicated geometry it is most practical to determine these areas stochastically, as described in the MCNP manual. The same often applies to the volumes needed in calculating many other quantities.

In the downward direction (around bin 27 in Fig. 2) the tallying surface was not the divertor surface but a horizontal surface spanning the mouth of the divertor and touching the plasma surface.

No variance reduction was needed for this calculation.

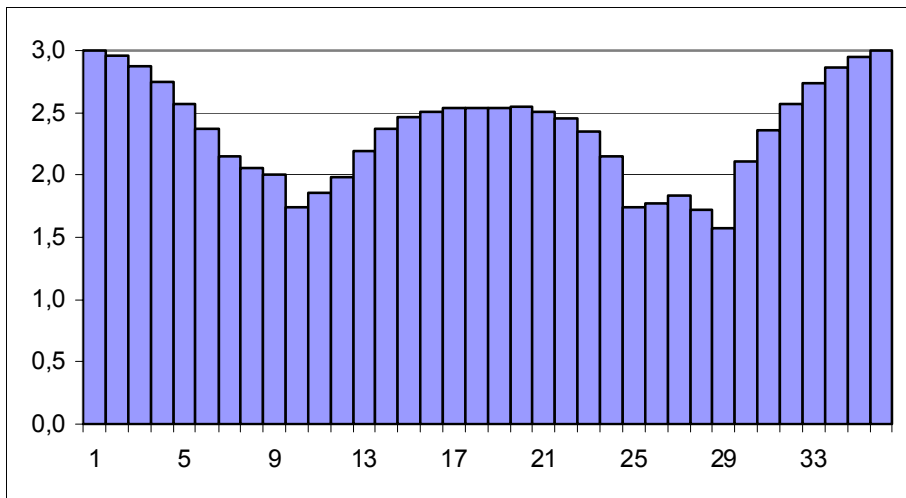


Figure 2. Poloidal distribution of neutron wall loading, unit MW/m^2 . The numbers along the x axis are the poloidal angles in units of 10 degrees at the end of each 10-degree angular bin, counting up from the outward direction, then down along the inboard wall.

2.2.3 Tritium breeding ratio

As mentioned in the introduction, large-scale use of fusion energy will require fusion reactors to produce their own tritium. For this purpose a breeding blanket will be required, containing lithium, probably enriched with respect to Li-6, and a neutron multiplier. The most famous neutron multiplier is beryllium, but lead can also be used for this purpose. In fact, the (n,2n) cross section of lead is greater than that of beryllium above ca. 2 MeV.

In PPCS model C, the breeding material was chosen to be Pb-17Li, a mixture of lead and 17 atomic percent lithium enriched to 90 percent Li-6. Note that the shielding properties of this material are poor; the neutron flux declines much more slowly with distance than in a steel-water mixture. The tritium breeding ratio (TBR, the ratio of tritium atoms produced to those consumed) was calculated using data for total tritium production (reaction number MT = 205) in the FENDL-2 library. With the geometry model believed to be most realistic, a TBR of 1.156 was obtained. A value of at least 1.06 was considered necessary to ensure tritium self-sufficiency, since in a real machine such details as ports would lower the TBR.

Several variations of the model were tried, providing a kind of sensitivity study. The main result was that the TBR is highly sensitive to any water (or, presumably, other hydrogenous material) in the hot shield. 10 volume percent of water in the hot shield is enough to lower the TBR by more than 0.05. The value of 1.156 was obtained based on the assumption that no water can be present in the hot shield, since the temperature is too high.

The total thickness of lithium-lead is also important. Increasing the inboard PbLi thickness from 37.5 cm to 67.5 cm was found to increase the TBR by 0.069.

The influence of the water content in the cold shield was not studied. A water content of 20 volume percent was assumed. Subsequent shielding calculations suggested that a higher water content may be desirable, and perhaps this will lower the TBR. However, it is expected that the composition of the cold shield will have much less influence on the TBR than that of the hot shield, and with a calculated value of 1.156 there is enough margin to accommodate some lowering of the TBR.

In later versions of PPCS model C (not covered by the calculations), a more triangular plasma shape was chosen. This might raise the TBR still further, if it means that the outer blanket, with its greater PbLi thickness, covers a greater part of the poloidal circumference. On the other hand, if the blanket is broken up into modules smaller than the large ones assumed, that will lower the TBR somewhat, since some neutrons will disappear into the gaps between the modules and into the module walls.

The TBR calculations also required no variance reduction.

2.2.4 Shielding calculations

Calculating responses beyond the shield was somewhat more demanding, but the required variance reduction was still easy due to the absence of penetrations in the model. The following quantities were calculated for the inboard midplane region (from 50 cm below to 50 cm above the midplane):

- The dose rate [Gy] to the epoxy at the front of the winding pack, tallied in F2 (surface flux) tallies multiplied by the total cross section and the average heating number (MeV/collision). These quantities are available with the FM numbers -1 and -4 for neutrons, -5 and -6 for photons.
- The fast fluence ($E > 0.1\text{MeV}$)[cm^{-2}] at the front of the winding pack. This was calculated using a simple F4 (volume flux) tally with 2 energy bins.
- The displacement damage to copper [dpa] at the front of the winding pack. An F2 tally was used, multiplied by a dpa cross section entered using E (energy) and EM (energy multiplier) cards.
- The nuclear heating [Wcm^{-3}] at the front of the winding pack, calculated the same way as the epoxy dose rate.
- The helium production [atomic fraction] at the rear of the cold shield. This was calculated for Eurofer steel and for the elements Cr, Fe, Ni and B separately using the reaction cross sections for $\text{MT} = 22$ ($n, n'\alpha$) and 107 (n, α) or, in the case of B, $\text{MT} = 207$ (total α production), in F2 (surface flux) or F4 (volume flux) tallies.

Calculations were performed for three water volume fractions in the cold shield: 20, 40 and 60%.

The results indicated that the design was adequate to keep the fast fluence and the heating density in the winding pack below the appropriate limits. The helium production, unlike the other quantities, increased monotonically with increasing water fraction, and was slightly above the limit at the higher water fractions. The epoxy dose and copper dpa had a minimum at a water volume fraction of about 40 to 50%, but even then they were well above the limits, by factors of 10 and 6, respectively. To solve this problem, the thickness of the cold shield and the vacuum vessel were increased inboard by 10 and 5 cm, respectively. Even this was not quite enough to bring the epoxy dose down to the desired level. It was thus necessary to change the material composition of the hot and cold shields so that both included 70 volume percent tungsten carbide. This finally brought down the epoxy dose to an acceptable value.

2.3 IFMIF (Publications V–VIII)

2.3.1 Background and geometry

As mentioned in the introduction, the purpose of IFMIF is to test materials exposed to neutron irradiation in a spectrum sufficiently similar to that of a fusion reactor (in terms of the primary recoil spectrum and relative transmutation rates) and in a flux sufficient to provide relevant fluences (equivalent to 150 dpa_{NRT}) in a few years. The author was involved in modeling the test cell of IFMIF and carrying out some calculations.

In the model, the test cell of IFMIF, shown in Fig. 3, consists of a space 3 m long, 2.5 m wide and 6 m deep, surrounded by walls of heavy concrete, 3 m thick. The cover, also composed of heavy concrete, has a thickness of 2.4 m except for the removable plugs where the thickness is 2.7 m. The deuterons enter through two slits with a rectangular cross section in one wall and strike a jet of liquid lithium. Beyond the backplate shaping the lithium flow lies the high-flux test module (Fig. 4), in which small metal specimens suitable for embrittlement tests are irradiated at controlled temperatures, which may be different in each of

the 12 cassettes. Next comes the medium-flux test module, which in the basic model contained a creep fatigue testing machine, also referred to as a universal testing machine, which subjected samples to mechanical stress while they were being irradiated; a tungsten spectral shifter; and an in-situ tritium release experiment. Finally the low-flux / very-low-flux module contains some vertical tubes for insertion of relatively large specimens.

Each module is connected to the space above the test cell by several ducts penetrating the cover. The cover contains four removable plugs: VTA1 (Vertical Test Assembly 1) connects to the high-flux test module, VTA2 to the medium flux module, and the VIT (Vertical Insertion Tubes) plug to the low-flux / very-low-flux module. There is also the CSP (Central Shielding Plug) with no connections to anything in the test cell.

The model has undergone many modifications through the years. Fig. 5 shows the geometry according to md39, the 39th generation of the model.

The geometry is fairly complicated (though still much simpler than ITER), and the model is correspondingly complicated. (The input file md39 is 8193 lines long without tallies.) In particular the cover is penetrated by three sets of ducts, each with a different geometry, and in addition there are also large, gas-filled coolant ducts to cool the concrete in each of the four removable shield blocks. No information was available about coolant ducts in the fixed part of the cover, so none were modeled. Even without them, there are thus seven different sets of ducts, each with its own geometry and streaming properties.

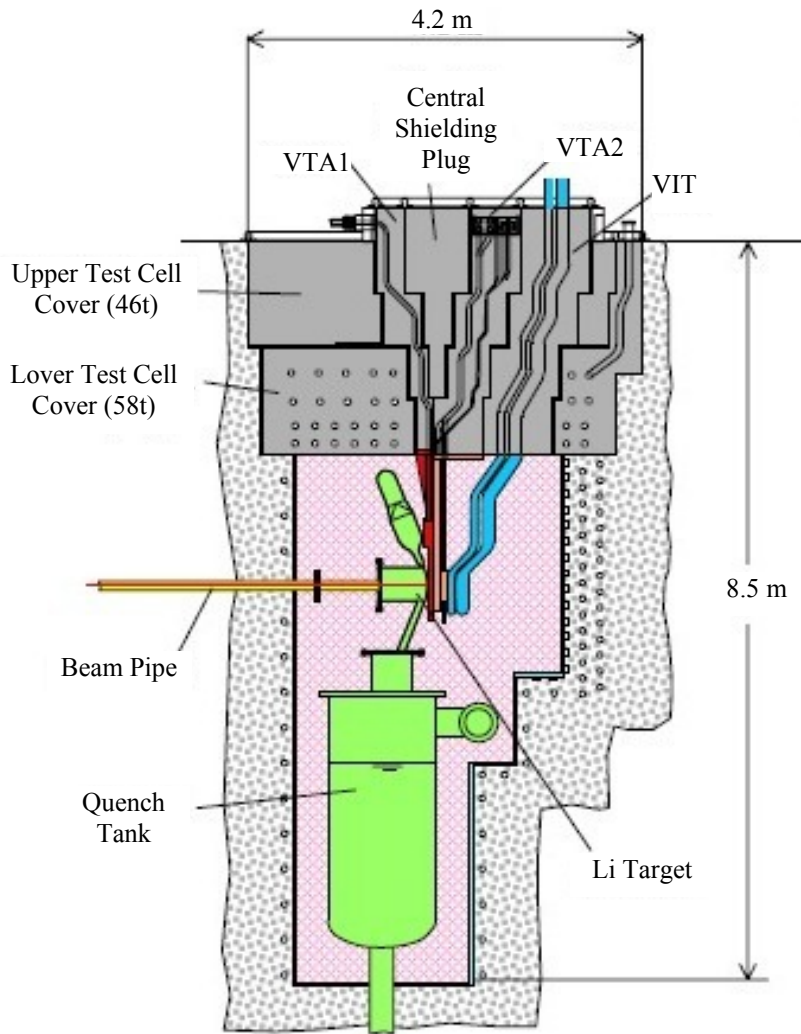


Figure 3. The test cell of IFMIF, according to A. Möslang, 7th May 2002.

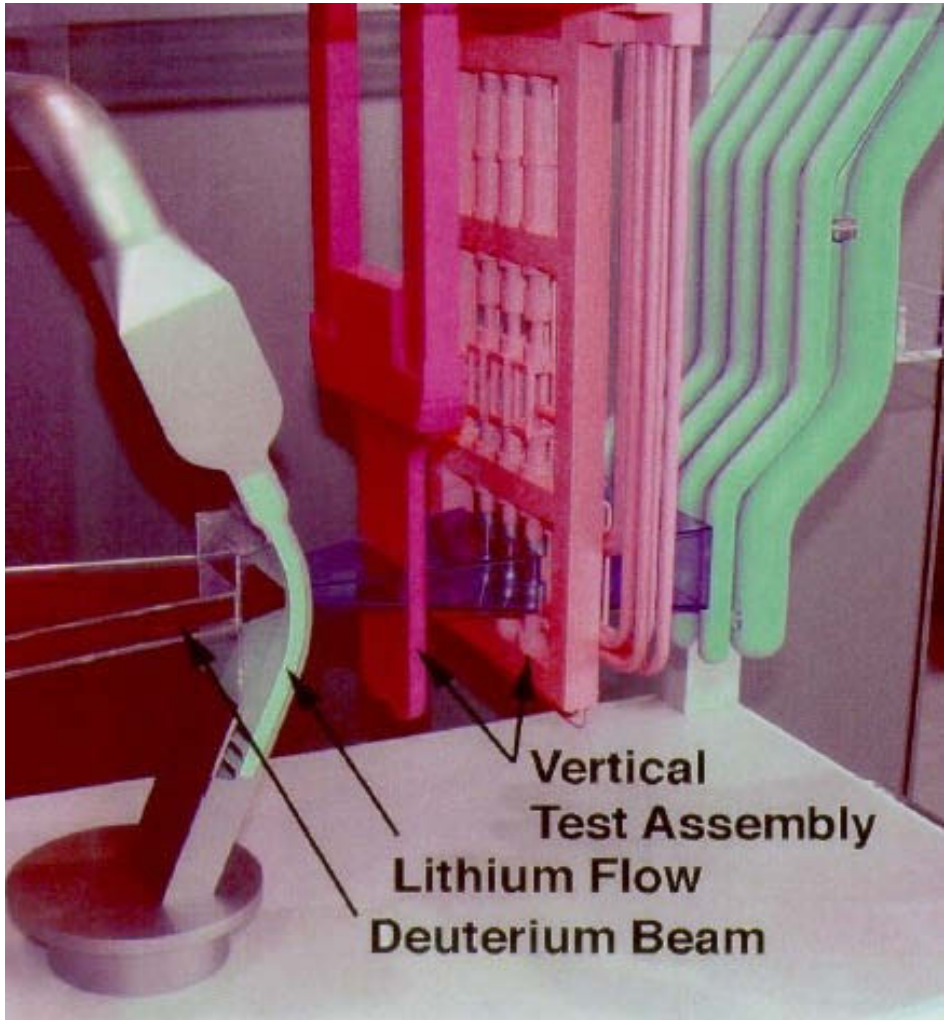


Figure 4. Exploded detail of IFMIF test cell, according to A. Möslang, 7th May 2002.

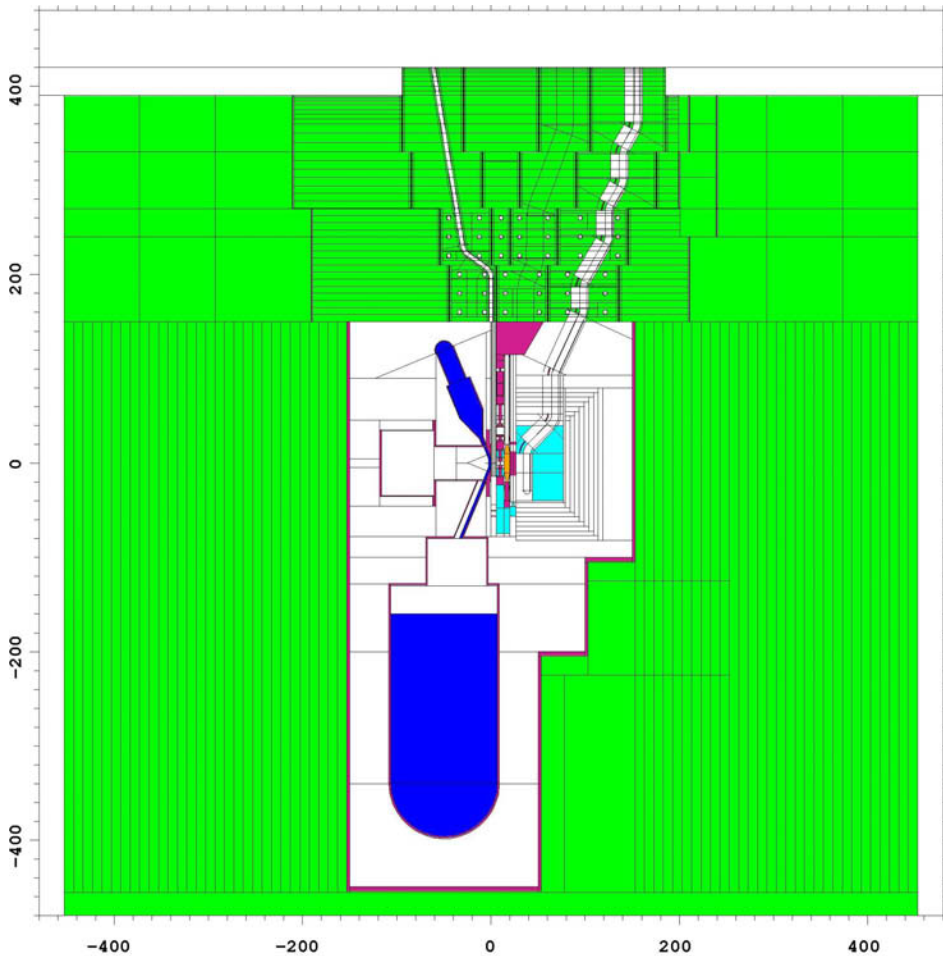


Figure 5. Elevation view of model md39 of IFMIF. Green = heavy concrete, Purple = steel (with very low density in the adapter connecting the medium flux test module to shield block VTA2), Blue = lithium, Cyan = graphite, Orange = tungsten. Certain volumes in the low-flux module and the cover are shown incorrectly as voids because the program has difficulties in plotting lattices. The cells surrounding the graphite reflector of the low-flux module are shown correctly as voids. These cells were added to model the horseshoe reflector but were voided in model md39.

The cover was modeled using universes, in such a way that the ducts were modeled in universes which were then used to fill cells that were stacked vertically to form the shield blocks. This was done before the author discovered

that the MCNP4C manual was misleading as explained in Section 1.6. It turned out to be an unfortunate choice, as described below in connection with the shielding calculations for the cover, since it precluded the use of cell-based weight windows in these calculations. However, modeling the cover in any other way would probably have been much more difficult.

Universes were also used to model the test equipment, at the request of one of the users of the model (P. Vladimirov). This makes it easier to move different parts with respect to each other. In particular, in some variants of the model the tungsten spectral shifter was moved from its original location between the creep fatigue testing machine and the in-situ tritium release experiment, to a location between the high-flux test module and the creep fatigue testing machine. In other variants, the thickness of the spectral shifter was reduced, and in one case thinner spectral shifters were placed in both locations. All this was much easier to do with universes. In this instance there was also no trouble with weight windows, because calculations on the test modules themselves do not require much variance reduction.

Most of the actual calculations were done by other people at FZK, but the author was involved in some calculations. The two most demanding sets of these calculations are described below.

2.3.2 Calculating neutron transport through the beam tubes

This work was part of the effort to determine the activation of the accelerators and adjacent structures in IFMIF. One source of activation will be the neutrons emerging from the test cell, mainly along the beam tubes. The task of the author was to calculate this neutron current in cooperation with Petri Kotiluoto, Stanislav Simakov and Ulrich Fischer. This current was then treated as a surface source and provided to Michael Loughlin at the UKAEA, who was responsible for the activation calculations. A detailed description of the calculations is given in Publication VIII, so only a summary will be provided here.

The calculations were performed using the program McDeLicious and a geometry model that was not quite up-to-date concerning the details of the cover but had a cell structure in the walls of the test cell that was more appropriate for

these calculations than that in later models. The main objective was to let the program store the neutrons emerging from the outer surface of the wall containing the beam tubes as a surface source. This could be done with the SSW (Surface Source Write) option, which records the location, direction, energy and weight of each particle crossing a specified surface. This surface source was the most important output of the calculations, but we included some tallies to check what was going on.

The neutrons emerging from the wall surface could be divided into three components:

- Neutrons coming directly from the source or scattered from the adjacent components and flying through the beam tubes without traversing any material.
- Neutrons colliding in the beam tube walls and scattering back into the beam tubes.
- Neutrons traveling, at least part of the way, through the test cell wall itself.

Since every point in the source, where the deuterons hit the lithium target, has a direct line of sight to the ends of both beam tubes without any intervening material, the first of these components is the most important. (In fact, it could be calculated analytically if the angular distribution of the source were known. It was not known to the author, however.)

The small solid angle subtended by the ends of the beam tubes means that only a small fraction of the neutrons produced will be included in this first component. This contribution cannot be emphasized through the use of importances or weight windows, nor is angular biasing of the source available in McDeLicious. DXTRAN could perhaps have been used, but would have been problematic due to the rectangular rather than circular cross section of the beam tubes, so it was not employed. That meant that the only way of reducing the variance was to use low importances to cut short the histories wandering into unimportant parts of the geometry.

The first calculation, with 7,500,000 histories, gave a quite respectable number of tracks in the surface source, namely 127,338. However, it was clear that about

99% of these were very low-weight tracks, belonging to the second and third of the components described above, and that including them in the calculation of neutron transport beyond the test cell wall (the responsibility of the UKAEA) would have been a waste of time. Thus the importances used in this calculation were poorly chosen and had to be modified in order to de-emphasize these components.

Improved importances did solve the problem of low-weight contributions. The next calculation, with 7,104,165 histories, gave 3,073 tracks in the surface source. This indicated that the low-weight tracks were much less numerous and had a higher weight, so this source was much more practical. However, the number of tracks was insufficient to get decent statistics in the next step, so longer runs were required.

This led to difficulties. Extending the number of histories beyond about 7,500,000 made the program freeze, similarly to the behavior described in Section 1.6. However, in this case it was clear that the “long history” explanation previously assumed for such behavior couldn’t be correct, since it happened even when all importances were set to 1 or 0, so that no splitting could occur. Instead, the reason was found to be a programming error in McDeLicious, which was diagnosed and corrected by Dr Simakov.

Thus, in this case the “long history” hypothesis was not a correct explanation for the hanging run problem. However, the programming error involved was specific to McDeLicious, and hanging runs occur with standard MCNP as well. Considering how widely MCNP is used, it is extremely unlikely that a similar bug would have escaped detection. Moreover, while it is not feasible to examine in detail a history that takes hours, days or longer, limited attempts to study them by dumping event logs for them have been made, and the results are consistent with the hypothesis that they are due to excessive proliferation of tracks, often combined with long survival of each track before it is terminated.

While this work was going on, Dr Fischer made a proposal to ensure that adequate numbers of tracks would be made available in the surface source without incurring excessive run times. In the full geometry calculations, many histories waste a lot of time wandering around in the complicated geometry of the test modules, and these make a relatively modest contribution to the

emerging current, while the most important contribution comes from the source neutrons emerging directly through the beam tubes. Therefore, one could save time by simply killing all neutrons except in the target, the beam tubes and a few cells between and around these. This could be considered a more radical application of the same principle embodied in setting the importances to less than 1 in the test modules. An input file based on this proposal was written by the author and then run by Dr Simakov, since the author was otherwise occupied at the time. A run with 10^9 histories created a surface source file with 122,836 tracks.

This “reduced geometry” approach did involve an error, killing some neutrons that would otherwise have made it through the beam tubes or even through the wall. By comparing surface flux tallies for the full geometry and reduced geometry calculations, the author calculated a correction factor of 2.02263, by which the results obtained with the reduced geometry source should be multiplied. This source and the correction factor were then used by Dr Loughlin at the UKAEA to calculate the contact dose rates after shutdown at the raster scanner and other accelerator components near the test cell [22].

This method is not exact. It ignores the fact that the killed neutrons would have emerged with another (probably softer) spectrum than those included in the reduced geometry source and with a different angular distribution. Nonetheless, it is able to provide a rough estimate, sufficient for a dose rate calculation.

2.3.3 Cover shielding calculations

The other main calculation activity for IFMIF in which the author was involved concerned the dose rate in the access cell above the test cell, both during operation and after shutdown. This meant evaluating the shielding effectiveness of the cover, consisting of 2.7 m (2.4 m outside the central area) of heavy concrete, penetrated by about 40 ducts with a circular cross-section and a diameter of several cm. All of these ducts contain bends to limit the streaming, but these bends are rather gentle and in some cases barely sufficient to prevent unobstructed lines of sight. Thus this is a very challenging shielding problem, for the same reasons as those mentioned in connection with ITER calculations. In fact, it turned out to be even more difficult.

The first set of calculations attempted to estimate the dose rate during operation. Originally the goal was to perform a full MODE N P (neutrons + photons) calculation, but this proved very difficult, even using the techniques described in Publication X. Runs with sufficient variance reduction to produce useful results were plagued by a consistent tendency to hang. Event logs showed that this was not only due to track proliferation in some histories; a single track could last very long before termination, due to weak absorption in concrete.

One possible remedy was to use an energy cutoff, ensuring that tracks would be terminated reasonably rapidly by dropping below the cutoff. In this way it was possible to get an estimate of the fast flux (above 0.1 MeV). This showed that, during operation, the dose rate from fast neutrons alone – ignoring the contribution from epithermal and thermal neutrons and from gammas – could approach 2 millisieverts per hour, even when averaging over a substantial area (the top of the VTA2 shield block) and ignoring local hot spots. This suggests that hands-on work in the access cell during operation cannot be recommended.

The problem of determining the dose rate after shutdown remained. This required calculating the delayed gammas resulting from neutron irradiation of the cover. It was decided that the R2S method would be used.

The first step was to calculate the total neutron flux in the cover, especially near the upper surface. This was the same task that had proven intractable when trying to calculate the dose rate during operation, and continued attempts to accomplish it were no more successful, being consistently plagued by hanging runs. Finally it was decided that a calculation of the fast flux would again have to suffice, and such a calculation was performed, with the intent of following this up with activation calculations and calculations of photon transport and dose rates.

Shortly after this decision, the author attended the RPS2006 meeting, the American Nuclear Society's 14th Biennial Topical Meeting of the Radiation Protection and Shielding Division, in Carlsbad, New Mexico, USA. At one session of this meeting he brought up the subject of how to perform shielding calculations in a geometry like this. John Hendricks, one of the developers of MCNP, agreed that this was a very difficult problem. Nonetheless, he had a suggestion. This suggestion, which the author named the "tally source" method, is described in Section 3.3 below. This method was tried in a test calculation on

one of the seven sets of ducts. It worked, although it is very laborious and involves some loss of accuracy.

By the time this test calculation had been finished, it was clear that Association Euratom-Tekes would no longer be involved in IFMIF work, so the involvement of the author in IFMIF calculations was terminated. The reports describing the work done so far and data files constituting the results of that work are available to Forschungszentrum Karlsruhe, which will presumably continue the work.

3. Method development

3.1 Background

The preceding chapter shows that there is a clear need to develop efficient variance reduction methods. The most important variance reduction method in MCNP, as described in Section 1.6, is geometry splitting / Russian roulette. Implementing this requires the user to choose importances or weight windows.

There is a weight window generator in MCNP. However, it has weaknesses, some of which are described in Section 1.6. Besides these, there are cases where weight windows are inappropriate, for instance if the use of universes precludes the use of cell-based weight windows and mesh-based weight windows will not fit the geometry adequately.

In any case, when using the weight window generator in a deep penetration problem, it is difficult to get enough particles to score to provide usable weight windows. One possible approach is to start with importances chosen to be as close to optimal as the user's engineering judgment can provide. This is the approach espoused in this work, but there are other alternatives.

For instance, Sato, Iida and Nishitani [23] recommended the stepwise method mentioned in Section 1.6. The starting importances can be set to 1, but the first calculation involves a target tally close to the source, so one gets good statistics for it. The resulting weight windows are then used in the next step, making it feasible to use a target tally located farther into the shield. The procedure is repeated, until one reaches the location where one really wants to tally the flux.

The same article also recommended a backward transport calculation to set weight windows for gammas. One puts a gamma source in the tally cell(s) and follows the gammas towards the real source. If no gammas reach a given cell, this is taken to mean that it is so far from the tally region that gammas born in that cell have a negligible probability of scoring, so they are killed in the final calculation. Where the backward calculation gives a non-zero flux, this flux can be used to calculate a weight window lower bound. Strictly speaking, this backward calculation should be an adjoint calculation, but for gammas the forward and adjoint fluxes are likely to be sufficiently similar that the forward

flux can be considered a sufficient approximation for the adjoint flux, keeping in mind that the weight windows do not need to be very accurate to be useful.

Another article by Sato and Nishitani [24] (in Japanese) took a different stepwise approach. The target tally is set at its final location, but the densities of the shield cells are reduced. Once weight windows are generated for low densities, the densities may be increased, and so on until the true densities are reached.

Hodgdon [25] applied a backward method – similar to the one Sato, Iida and Nishitani used for gammas – to the neutrons themselves, also getting useful results in this way.

Many articles have been written about the use of deterministic adjoint calculations to determine sills for Monte Carlo. Here we will consider only a few of them.

Sweezy et al. [26] used PARTISN to provide the sills, with the intention of incorporating it into MCNP. The transfer of geometry data from MCNP to PARTISN was automated, based on a weight window mesh, but the fact that the material was taken to be that at the center of each mesh cell underscores the problem that a complicated geometry cannot be represented exactly in a regular mesh. Good results were obtained for an oil-well logging problem, but for a problem involving a dogleg duct in a shield, MCNP using the standard weight window generator performed much better.

Probably the best known combination of a Monte Carlo program with a deterministic program to calculate weight windows is A³MCNP [27]. Omura et al. [28] described a version of this program, altered to model volume sources rather than just distributions of point sources. This version was tested in a cask problem and a reactor dosimetry problem and performed well even when calculating streaming through a ventilation duct in the cask problem. However, the width of this duct was 10 cm, which is rather wide compared with those described in Chapter 2.

Shahdatullah et al. [29] described calculations using the finite element code EVENT to find sills for MCNP. Good results were obtained even in a case with a dogleg duct through a shield, but again this was a duct with a width of 10 cm.

On the question of cell-based vs. mesh-based weight windows, Hendricks and Culbertson [30] wrote: “*Mesh-based windows can outperform cell-based windows. Cell-based windows are superior only if the geometry is optimally subdivided for variance reduction.*” However, the problems they treated were not much like the streaming-dominated problems common in fusion neutronics.

Murata et al. [31] described a method of biasing the scattering direction in a Monte Carlo calculation. This can be very useful in a streaming calculation. Unfortunately, MCNP does not provide such a facility. In some cases, DXTRAN [7], p. 2–156 et seq., or the tally source method described in Subsection 2.3.3 and Section 3.3 can substitute.

Freiesleben, Richter, Seidel and Unholzer [32] described a comparison between a deep penetration experiment using steel and perspex (simulating water) as shielding materials and MCNP4A calculations. The results agreed within 30 percent at the most critical position.

Serikov et al. [33] provided a recent example of ITER shielding calculations, specifically for an upper port ECRH launcher.

The brief literature review above is, of course, very far from exhaustive. But it shows that most methods of finding importances or weight windows for deep penetration Monte Carlo calculations can be grouped into 3 broad categories:

- Direct: Start with the best importances your engineering judgment can provide for the whole geometry, then use the weight window generator to calculate improved weight windows, iteratively if necessary. The main weakness of this approach is that it requires a lot of skill and knowledge to choose the starting importances well. The advantages are that, if done right, it requires only a few intermediate calculations for weight window generation and no extra programs.
- Stepwise: As in the two articles by Sato et al. mentioned above, either start with a target (for the weight window generator) near the source, or reduce the densities. Then gradually move the target toward the final location of interest or increase the densities. The disadvantage of this approach is that it requires several calculation steps, which may be quite laborious if one follows the recommendation of the MCNP5 manual to

review and correct the weight windows at each step. The advantage is that it requires little skill in setting the starting importances. Even setting them all to 1 will do the job. In this case, too, no extra programs are required.

- **Deterministic:** Perform an adjoint calculation with a deterministic program, often based on the discrete ordinates method, to find optimal weight windows. This method requires a suitable deterministic program, either a stand-alone program, which will necessitate the creation of two separate geometry models, or combined with the Monte Carlo program into one program that requires only one input file. It is likely to be quite effective for reasonably homogeneous shields. For shields containing ducts and gaps it may be less effective, for two reasons: in the first place, a deterministic program using a regular mesh may not be able to model the geometry accurately. In the second place, even if the geometry is modeled accurately, deterministic methods tend to do poorly in voids; for instance, the discrete ordinates method is notorious for ray effects.

Other methods are also conceivable. For instance, the use of backward but non-adjoint Monte Carlo calculations, as in Refs. [23] and [25], may be considered a fourth class of methods. Although theoretically unsound, in that adjoint calculations would be preferable, it may work adequately, especially for gammas. Some Monte Carlo programs have the capability for adjoint calculations, but they tend to have limitations: for instance, MCNP can perform adjoint calculations only on a multigroup basis, and not with continuous energy.

For a variety of reasons, including the unavailability of combined deterministic-Monte Carlo programs at the institutions where the work was performed, the author chose the direct approach. Therefore, the main thrust of the research described below was to develop ways of choosing appropriate starting importances and a good cell structure, though the tally source method was also tested.

In choosing importances, the user faces two contradictory requirements. On one hand, he must use sufficient biasing (in this case, importances that increase fast enough, going through the shield) to ensure that enough particles penetrate to give adequate statistics. On the other hand, heavy biasing will make the individual histories longer, slowing down the calculation. In a simple solid shield (i.e., without penetrations and with all optical path lengths through the shield reasonably similar) it is not very difficult to strike a reasonable balance.

The MCNP manual suggests choosing the importances so that the number of tracks stays roughly constant, proceeding through the shield. The work described below applies the same principle to shields with penetrations, but one must keep in mind that this may in some cases lead to high-weight particles streaming through voids to cells with very high importances, leading to extreme splitting and to the feared “long history” phenomenon. Thus, when in doubt, it is probably better to underbias rather than overbias. (The MCNP manual agrees with this.)

One point worth keeping in mind is that, fortunately, it is not necessary to determine the exact optimum importances. Doing that would be as difficult as solving the transport problem itself, but any reasonable importances are likely to improve the performance of MCNP compared with doing nothing (keeping all importances at 1), so long as one avoids serious overbiasing.

3.2 Choosing importances (Publications IX, X and XI)

Publications IX, X and XI all deal with the problem of how to choose importances or weight windows for a neutron or neutron-photon calculation on a shield with penetrations, in particular a shield penetrated by a planar slit with a dogleg, similar to the gap between a port plug and the port walls in an ITER non-NBI equatorial port. It is likely that the same principles can be applied to many different kinds of penetrations, though experience from the IFMIF cover shielding calculations suggest that having many penetrations near each other, so that particles may move from one penetration to another, will require some modification of the method presented here. Calculations of photon transport alone have not been investigated, but most likely some similar method would work for those, too.

The three publications deal with different stages of the process. Publication IX is essentially a first exploration of the problem, but it outlines a method of determining the longitudinal distribution of importances, i.e., in the direction of particle transport. It also finds that the weight window generator can give significantly improved performance, though this may partly be due to the fact that the next question had not been properly addressed. This question, the transverse importance distribution, is addressed in Publication X. No dogleg was present in

this study, but that should not detract from the applicability of the results to geometries with doglegs. In Publication XI the results of the two preceding publications are drawn together in a geometry with a dogleg and the resulting method is tested.

3.2.1 The longitudinal importance distribution: the Handy Method

In determining the longitudinal importance distribution, we follow the advice that the track density should be kept roughly constant. First we consider transport through a bulk shield. In such a case the flux and current will decline in a roughly exponential manner, so we divide the shield into layers, each with a thickness roughly similar to, or somewhat greater than, the halving distance h (the shield thickness required to decrease the flux by an additional factor of 2). The value of this halving distance will vary from case to case, but in these investigations we are concerned mainly with fusion reactor applications. In a typical fusion reactor spectrum, experience has shown that an optimum mixture of water and stainless steel (about 25 and 75 volume %, respectively) gives a halving length of about 7.5 cm. (Actually the value for a pure bulk shield might be closer to 4.5 cm, but we are not dealing with such shields here.) Thus we get importances doubling at steps of 7.5 cm.

On the other hand, we also need to consider streaming along the penetration. In a duct with a circular cross-section, we assume that the streaming component of the current, at a certain distance into the duct, is proportional to the solid angle subtended by the opening of the duct at this distance. It is not obvious exactly what the constant of proportionality should be, but it is also not very important. If the radius of the duct is r and the distance from its beginning is x , we can take the flux to be $(r/x)^2$ times the flux at the beginning of the duct (obviously only when $x > r$, otherwise use the factor 1).

If we have a planar slit of thickness d instead of a cylindrical duct, the corresponding attenuation factor could be set to d/x , again only for $x > d$. Alternatively a slightly different constant of proportionality could be used; it doesn't matter much.

In any case, the inverse of this streaming component of the current will give an alternative set of importances. Now, for each layer of the shield we simply

choose the smaller of the two importances. Usually, when r or d is small compared to h , the bulk importances will be lower near the beginning of the shield (when x is small), but the streaming importances will be smaller farther on. If the latter is not the case, this suggests that the shield is not thick enough to reduce the flux or current to the point where streaming dominates.

After a bend or dogleg, one can repeat the process, starting with the importance derived for the cells just before the bend. This issue will be considered in somewhat more detail in Subsection 3.2.3.

As a final step, it's useful to change the importance to the highest power of 2 that does not exceed the importance estimated by the above method. This will ensure that the ratios between importances are always integers, avoiding the non-conservation of weight that may arise in individual histories if this is not the case.

This method has been named the "Handy Method", because it is similar, though not identical, to a method with this name of obtaining rough flux estimates behind shields with penetrations, proposed by Iida et al [34].

Publication IX introduced and tested this method in a simple, two-dimensional test case, a shield penetrated by a slit with a dogleg. The resulting importances were found to work adequately as starting values, but generated weight windows significantly improved the performance. It is likely that much of this improvement was due to the fact that the issue of the transverse variation of the importances was almost ignored when applying the Handy Method. Only a slight transverse variation was used (reducing the importances by a factor of 2 at some distance from the slit). This issue will be considered in the next subsection.

The Handy Method is a direct method in the sense of Section 1.6, in that it determines a set of starting importances for the whole geometry. In Publication IX, the stepwise or progressive method of determining weight windows (see Section 1.6) was also tested and found to give performance comparable to the direct method. The choice between these methods is to some extent a matter of taste, but for users who lack experience at choosing importances, the stepwise method may be better.

For calculations covering the whole neutron energy range, and even more for coupled neutron-photon calculations, it is usually advisable to start with a calculation covering only fast neutrons. One can then generate weight windows, which may give improved performance. This can be iterated if necessary. Once the fast neutron weight windows (or importances) are satisfactory, they can be extended to lower energies and, if required, to photons. In Publication IX, the alternative approach of starting with a coupled neutron-photon calculation right away was also tested, and in this simple case it worked, but it is likely to work less well in more complicated cases.

Mesh-based weight windows were also tried, as were the exponential transform and forced collisions. The results obtained with mesh-based weight windows were disappointing, but it is not clear why. One cannot conclude from a single series of test calculations that mesh-based weight windows are unsatisfactory. Unfortunately, schedule and funding limits precluded an investigation of their poor performance. Both the exponential transform and forced collisions gave small improvements in performance. For this particular kind of problem it seems questionable whether this small improvement is sufficient to justify the extra work these methods require, though of course in some problems the benefit may be greater.

3.2.2 Transverse importance distribution

In Publication IX, the improvement obtained using the weight window generator did not consist of reducing the fractional standard deviations for a given number of histories. On the contrary, the fractional standard deviations increased in some cases, but the runtime decreased substantially, improving the figure of merit (defined as $1/R^2T$, where R is the fractional standard deviation and T the runtime). This means that, within a given time, one can run more histories and thus obtain better statistics.

This behavior is a sign that the generated weight windows were higher – corresponding to lower importances – than the manually determined importances, at least in some cells. This is confirmed by Figure 3 of Publication IX, reproduced below as Fig. 6.

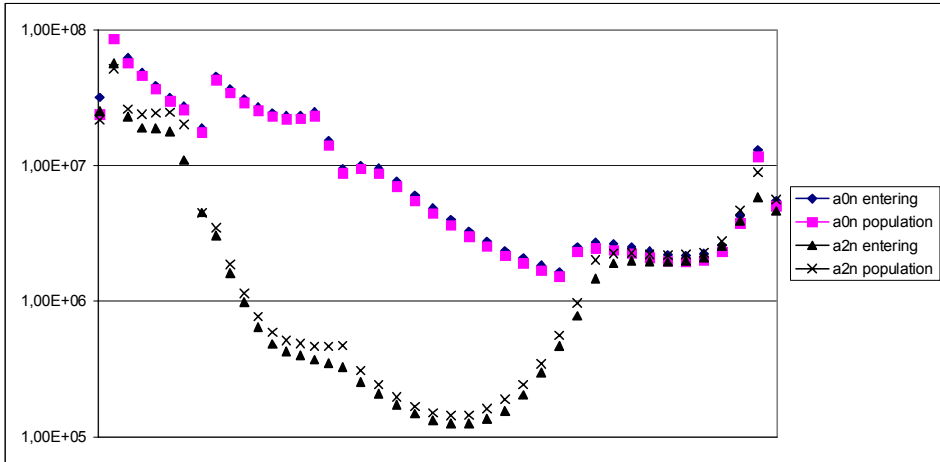


Figure 6. Fast neutron populations in two runs of the test problem described in Publication IX. $a0n$ = run with initial importances, $a2n$ = run using generated weight windows. “Entering” and “population” refer to the “tracks entering” and “population” columns of print table 126 in the MCNP output, the particle activity table. All values are summed over each transverse slice of the geometry, i.e., for all cells in a particular x interval. The horizontal axis shows x , the distance into the shield, from 0 to 302 cm.

We can see that the starting importances did a good job of keeping the number of tracks roughly constant, as recommended in the manual. (Note that the actual flux was reduced by about 7 or 8 orders of magnitude from one end of the geometry to the other.) The generated weight windows did not do this to anything like the same extent. The dip in the middle part shows that here, the weight windows were higher than what would have corresponded to the starting importances. This appears strange at first sight, but there are two things that explain this behavior.

In the first place, the importances derived using the Handy Method as described above are actually appropriate only for the slit itself. However, the cells in the slit were modeled as voids, and MCNP does not split in a void. (Doing so would, in fact, be pointless, since all the progeny of a particle would follow the same path until it entered a non-void cell.) Thus, however high the importance or low the weight window in a void cell may be, it has no effect.

Secondly, the optimal importance obviously declines as one moves away from the slit. As pointed out above, this was almost neglected in the manually-chosen importances used in Publication IX, since the author had no idea of how sharply the importances should decline. This was the subject chosen for investigation in Publication X.

In this work the author used a simple slab-type shield, 240 cm thick, with a straight penetration. The shield was divided into a number of cells, in both the longitudinal and transverse directions. The neutron current on the far side of the shield was tallied. The weight window generator was used, and the weight windows were then translated back into importances by dividing the lower boundary of the weight window in the source cell by the lower boundary for the cell in question. The resulting importance distribution was investigated and conclusions drawn.

First some sensitivity studies were performed to check which features of the model had a major influence on the results. The geometry of the penetration did not make a big difference, so a planar slit 2 cm thick was used. This is similar to the gaps between plugs and port walls in ITER. A monoenergetic 14 MeV source and a fission spectrum source were also found to give similar results, so the former was used. The energy cutoff was also not very important, so 0.1 MeV was used.

On the other hand, changing the shield material had a large influence, so calculations were made for seven different materials: water, quartz (a simplified version of concrete), light concrete, pure iron, stainless steel 316 L(N) ITER grade, stainless steel with 20 volume % water at a density of 0.9 g/cm^3 , and tungsten. The calculations showed pure iron to be a very poor shielding material, presumably due to the presence of cross section windows. The best shield materials were tungsten and the 80% steel + 20% water mixture.

The hopefully optimal importances calculated by the above method agreed well with the results of the Handy Method in the slit itself. However, that is not in important in itself, since MCNP does not split in voids. Thus these importances matter only as a scaffolding, upon which one can construct the importances to be used in non-void cells, and the results of interest concern the transverse importance distribution. The decline of this distribution with increasing distance from the slit was striking.

Two aspects of the transverse importance distribution were considered: the ratio of the importance in the cells immediately adjacent to the slit (called “wall cells” in Publication X) to that in the slit itself, and the rate at which the importance declined further as a function of distance from the slit.

In both respects, the transverse importance distribution is relatively flat at the surfaces of the shield, particularly the far surface (where the current is tallied) and much less flat in the middle. It is, in fact, obvious that the transverse importance distribution must be flat near the far side. A neutron that has made it that far has about the same chance of scoring whether it is near the slit or far from it. On the other hand, in the middle of the shield, any neutron that strays far from the slit has only a very small chance of reaching the far side.

Even a neutron in a wall cell has a much smaller chance of scoring than one that is streaming through the slit, which is illustrated by Fig. 7. With increasing distance from the slit, this chance quite rapidly declines further in good shield materials; see Fig. 8.

From these figures, one can conclude that the following recipe should give reasonably good importances in a thick shield of some good shielding material (unlike pure iron) with a straight penetration:

- 1) The ratio of the importances adjacent to the penetration to those in the penetration itself, derived from the Handy Method, should be about 0.1 at the beginning of the shield, declining to about 0.01 one quarter of the way through the shield, remaining close to that value up to three quarters of the thickness and finally rising to 1 at the end.
- 2) In the best shielding materials, it is appropriate to make the cells adjacent to the penetration about 1 mm thick or less in the transverse direction. In the next layer of cells, the importances should be lower by a factor of 4 (except near the end, and perhaps the beginning) of the shield, and these cells should extend some millimeters further from the penetration. Beyond that, a further reduction by a factor of 4 or more is appropriate. For shielding materials that are not so good, a somewhat flatter transverse importance distribution is appropriate, maybe increasing the thickness of the second cell layer to several centimeters.

Of course, a more detailed subdivision would give a better fit to Fig. 8, but it is doubtful whether the benefits would be worth the added complexity in the geometry modeling.

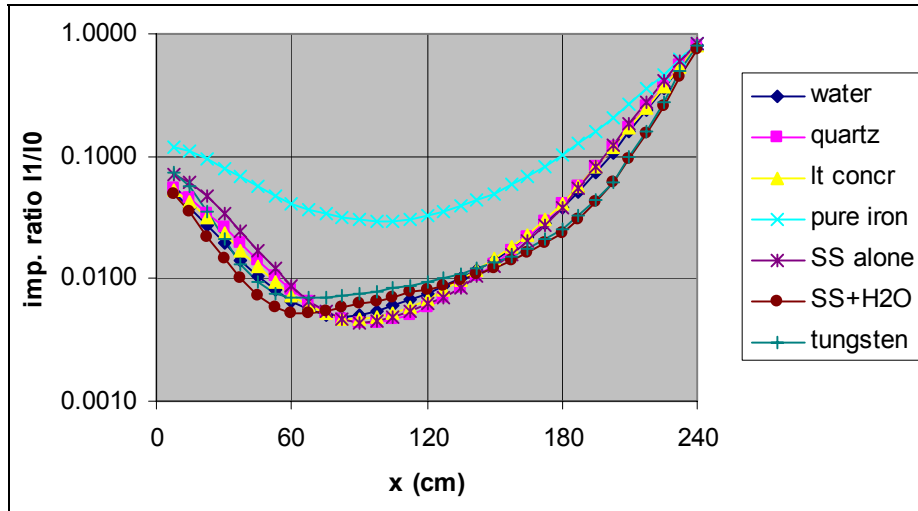


Figure 7. Ratios of importance in the first 0.001 cm of the wall (I_1) to that in the slit (I_0) as functions of the longitudinal coordinate x .

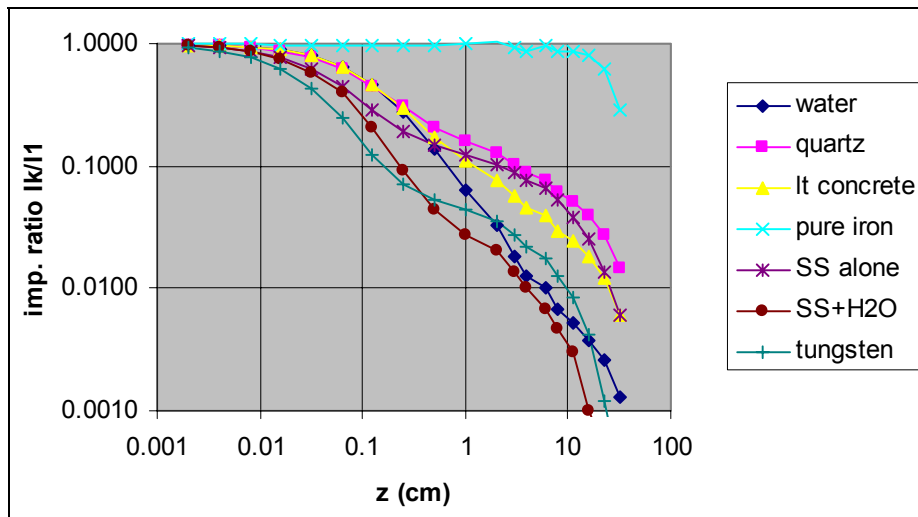


Figure 8. Ratios of importance in the k 'th cell (I_k) to that in the first 0.001 cm of the wall (I_1) as functions of the lateral coordinate z in the interval $112.5 \text{ cm} < x < 120 \text{ cm}$ (in the middle of the shield).

3.2.3 Testing the methods

In Publication XI the author tested the methods described above in a geometry representing a very simplified version of an ITER non-NBI equatorial port, shown in Fig. 9. The calculations simulated a shutdown dose rate calculation, though they were performed for prompt rather than delayed gammas.

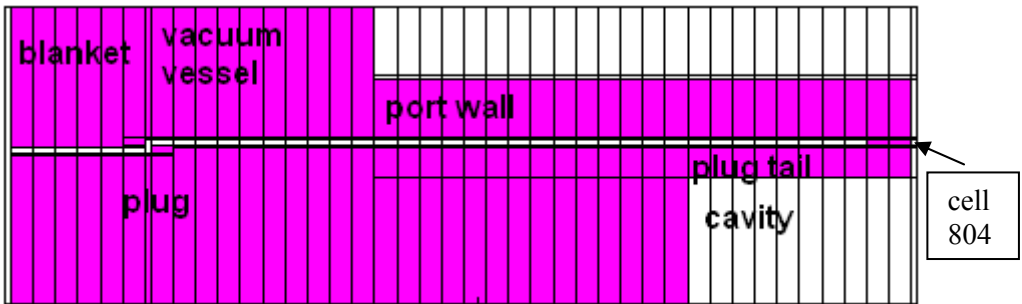


Figure 9. Geometry used in Publication XI (homogeneous version).

Starting importances for the fast flux were estimated using the Handy Method and transverse distributions based on the work described in the preceding subsection. These gave good results for the fast flux at the end of the port wall, but the fact that one also needs to calculate the dose rate around the port walls complicated the issue. It necessitated the use of quite different transverse importance distributions in the outer parts of the geometry, where particles traveling upward through the port wall or downward through the plug tail could contribute to the score. Once this was done and the tally used for the weight generator was modified correspondingly, good results for the fast flux and good weight windows were obtained.

The next step was then to extend the calculation to epithermal and thermal neutrons and to gammas. This necessitated extending the weight windows to these particle types, which was done by multiplying the fast neutron weight windows by appropriate factors, called weight factors in Publication XI. Since it was not known what values might be suitable for these weight factors, they were initially mostly set to 1, and in some cases to 0.1. A calculation using the resulting weight windows was then performed and new weight windows were generated.

The generated weight windows were then analyzed to find improved values for the weight factors. To reduce the stochastic noise, the cells in the model were divided into classes. In each cell, the weight factors needed to obtain the weight windows for epithermal and thermal neutrons and for gammas from the fast neutrons were calculated, and then these factors were averaged over each class. Geometric rather than arithmetic averages were used to limit the influence of excessively large values caused by undersampling. The resulting averages were then rounded, and the rounded weight factors were used to calculate new weight windows, which were then tested in a new calculation.

This calculation gave reasonably good results for the photon flux on the top surface of the port wall, but at the end of the wall the results were very poor. The fractional standard deviation in cell 804, the tally cell in the footprint of the gap, was about 5.5 times as high as in the previous calculation in spite of a doubling of the number of histories.

It is plain that the composite tally cell used in generating the weight windows, consisting of cells both on top of the port wall and at the end of the wall, was not well suited for this application. For fast neutrons it worked well, presumably because the collimated flux at the end of the gap ensured that enough fast neutrons reached cell 804 so that the tally was not excessively dominated by the cells on the top surface. The gammas, on the other hand, were emitted isotropically from wherever they were born, so that many more of them reached the top surface of the port wall than the end. Thus, the weight windows generated with the composite tally cell emphasized upward transport through the tally wall to such a degree that these weight windows did not work well for the gamma flux at the end of the port.

Some minor adjustments of the weight factors were tried first but proved inadequate. Then a new set of weight windows was generated using a tally cell covering only the end of the port wall⁸. The weight factors obtained in this way were compared with the previous ones, and a set of compromise weight factors was worked out. These factors are shown in a table in Publication XI. When used to determine weight windows for the next calculation, they worked well.

⁸ The weight windows were generated on the basis of a photon energy tally. They were derived for three neutron energy groups, with boundaries at 1 eV and 0.1 MeV, and one photon group.

Usually one can expect further improvements from using the weight window generator to obtain new and better weight windows, iterating the process as far as necessary. In this problem, however, it would then be necessary to use two different sets of weight windows, which one could perhaps combine somehow, for instance by using the lower weight window for each cell. It would probably be more practical to perform separate calculations for the top and end surfaces of the port wall if one wishes to iterate the weight windows.

In the last calculation described in Publication XI, a lower limit was imposed on the weight windows so that extremely low values for the sills were not permitted. The motivation for this was that such a measure may help avoid hanging runs due to long histories. No hanging runs had occurred in this work, but they are a common problem, so testing a measure intended to protect against them was considered justified. It turned out that this actually improved the performance. There was some slight increase in the fractional standard deviations, but the run went more than twice as fast, so the figure of merit improved. This means that the procedure outlined above seems to lead to some degree of overbiasing, so imposition of such a limit appears to be a good idea.

3.3 The “tally source” method (Publication XII)

Even with the methods described above, some problems remain intractable. One example, mentioned in Subsection 2.3.3, was the cover shielding calculation for the IFMIF test cell. As noted in that subsection, John Hendricks made a suggestion, which can be described as follows:

Tally the neutron current at a suitable location, specifically at the beginning of a long straight stretch of duct, taking care to ensure sufficient resolution in space, angle and energy. Then define a surface source based on this tally, biasing it in angle to favor neutrons streaming along the duct. Use this source to calculate the neutron transport to the next such location and repeat until the end of the shield is reached.

This should not be confused with writing and reading a surface source using the SSW and SSR options in MCNP, since that provides no opportunity for angular

biasing. The advantage of this method is specifically that it provides a way of biasing the flux in angle. This ensures that the neutrons that matter most, those that stream along the ducts, will be better sampled.

If weight windows rather than importances were used, it would also alleviate the risk of long histories, since the neutrons most likely to reach cells with low weight windows would already have low weights and would thus undergo less splitting. Unfortunately, the use of cell-based weight windows was impractical in the cover shielding problem due to the way universes were used in modeling the cover, and revising the model was also considered unfeasible. Modeling the cover in a different way would probably have required much more work than the original modeling. Mesh-based weight windows might have been usable, but they would have fit the geometry poorly.

A test calculation was performed for one of the seven sets of ducts in the test cell cover, as described in Publication XII. The through-going VTA1 ducts were chosen as a test case, because they are relatively simple. These 8 ducts consist of three straight stretches of duct, two of them relatively short and the third long, connected by bends. One such duct can be seen in Fig. 10, where it is the leftmost duct in the cover.

The first tally source was deployed at the entrance of the ducts, at the bottom surface of the cover. The neutrons striking the cover were tallied in space, energy and angle bins. The tallies were analyzed to find a way to represent the current as a surface source, within the limitations imposed by the SDEF source description in MCNP4C. It turned out that the angular distribution depended on the spatial location and the energy spectrum depended on the angle. However, MCNP4C did not allow more than one level of dependence. Since the most important angle bins of the source in this location are the ones closest to the upward vertical, and since the spectrum was reasonably constant for these bins, this spectrum was used, ignoring the softer spectrum in the tally bins farther from the upward vertical. The resulting source was biased in space, angle and energy, to emphasize the most important particles. One obvious drawback of this is a large weight variation among the particles.

The second tally source was deployed on the inclined plane delimiting the bottom end of the topmost straight segment of the ducts (surface 4773 in the

model). In this case the angular distribution was independent of location. Thus the location and angle could be treated as independent variables, while the spectrum was modeled as dependent on the angle bin. The need to use areas of different shapes in modeling the location dependence of the source caused some difficulties, which were resolved by treating a rectangle as a circle, from which the excess parts were trimmed by using cookie cutter cell rejection. The resulting source was then used in a calculation extending to the upper surface of the cover.

Following this, a sequence of three calculations was needed: from the source in the lithium jet to the lower surface of the cover, from that surface to surface 4773, and finally from there to the upper surface of the cover. In each of the first two calculations the parts of the geometry beyond the tally surface had their importances set to zero, killing all neutrons passing the tally surface. Thus, neutrons reflected back and forth across this surface were not included in the tally source. On the other hand, in each subsequent calculation, the full geometry of the preceding calculation was retained, so reflected neutrons were taken into account at this stage.

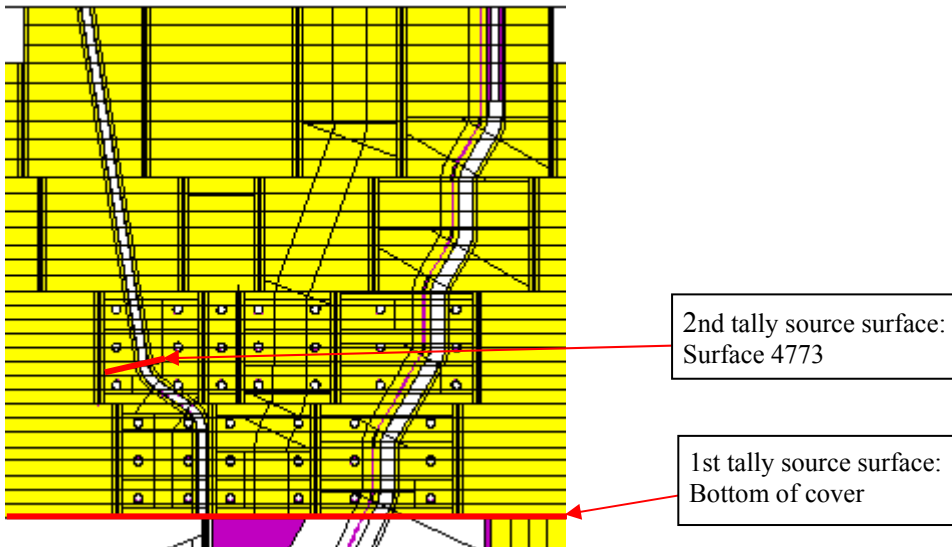


Figure 10. Tally source surfaces.

The result desired from this sequence of calculations was the neutron flux near the ducts, which is required for activation calculations. This was tallied using an F4 tally. In the part of the cover below surface 4773 it was necessary to tally the neutrons in both the second and third calculations. The second gave the contribution from neutrons which had not passed surface 4773, the third the contribution from those which had passed this surface and then been reflected. These two contributions had to be added to get the total flux. Since the auxiliary programs used to prepare the flux data for a FISPACT calculation take this data from MCTAL files, another auxiliary program was written to add fluxes from two or more such files.

As we see, this method involves far more work than an ordinary MCNP shielding calculation. Each duct type has to be treated separately, and several calculation steps are needed, each requiring a substantial amount of work. Moreover, the discretization involved in tallying the current and then defining a source on the basis of this tally involves some loss of accuracy. However, against this one must set the fact that the tally source method can solve otherwise intractable problems.

4. Summary and conclusions

This dissertation describes some experience of using MCNP, mostly MCNP4C, for fusion neutronics calculations, especially shielding calculations for ITER and IFMIF, as detailed in Publications I through VIII. There are good reasons why the Monte Carlo method is used for such problems. In particular, deterministic programs have difficulties in dealing with the mixture of voids and thick shields. On the other hand, it is not easy for Monte Carlo calculations to handle either. Since the whole point of shielding is to reduce the neutron and gamma flux radically, heavy splitting is required in order to get useful results. Conversely, the presence of narrow penetrations means that, once in a while, a particle emanating from a low-importance cell will reach a high-importance cell without splitting on the way. It may then split into an excessive number of tracks, so that a prohibitive amount of time is spent on a single history.

It is therefore essential to choose the importances or weight windows well. The weight window generator in MCNP is useful, but it has limitations. There is consequently a need for some way of choosing good starting importances. In addition, it is also necessary to choose the cell structure of the geometry model in a way that provides sufficient resolution for importances or weight windows, without making the cells so small that the weight window generator is hampered by unacceptably poor statistics. (If one uses mesh-based weight windows, a similar issue arises for the mesh.)

Much of this dissertation addresses this issue. The method espoused here is first to determine an importance distribution in the longitudinal direction (the direction of streaming) in whatever penetration is the most important streaming path. The Handy Method is used for this. This importance distribution is not important in itself, since MCNP does not split in voids, but it constitutes a scaffolding on which one can hang the importances in the non-void cells. This is done using the transverse distributions determined in Publication X. It is notable that they drop off very rapidly with increasing distance from the penetration. Thus, unless the shielding material is very poor, the non-void cells immediately adjacent to the penetration should be quite thin, on the order of 1 mm. The next layer of cells should be somewhat thicker, but only about 2.5 mm for good shielding materials.

Of course this depends on the geometry and on what quantities one is interested in tallying. For instance, the example of Publication XI demonstrates that thicker cells are appropriate when particle transport at right angles to a penetration is of interest.

Sometimes such, relatively conventional, techniques are not enough, and the absence of provisions in MCNP for biasing the flux not only in space and energy but also in angle becomes a serious problem. Then one should consider the tally source method proposed by Hendricks and described and tested in Publication XII. This does provide a kind of angle biasing capability. This method has its drawbacks, being laborious and inexact, but it can be used to solve problems that do not yield to more direct methods.

One issue that has not been explicitly addressed in this text is the accuracy of the calculations. It should be noted that they were generally best estimate calculations rather than aiming for conservatism, so the errors may go in either direction.

MCNP provides estimates not only of fluxes and reaction rates, but also of the stochastic error in the form of fractional standard deviations. These are themselves evaluated stochastically, so the larger the stochastic uncertainty is, the less reliably is it estimated. In addition there are other sources of error, which may often be greater, such as the uncertainties in the cross sections and simplifications in the modeling.

In the easier cases, requiring only calculation of the flux near the plasma, the errors are likely to be small, of the order of a few percent. Examples of such cases are calculations of the wall loading or the tritium breeding ratio. However, as one goes deeper into the materials surrounding the plasma, it becomes more difficult to get good statistics. When estimating the shutdown dose rate at the end of an ITER port, calculated fractional standard deviations of about 0.2 were commonplace. In addition, with increasing depth of penetration the uncertainties of the total cross sections also become more significant. In the strictly intuitive opinion of the author, a factor of 2 might be a reasonable estimate of the uncertainty in such calculations. For the IFMIF test cell cover described in Publication XII, an even greater uncertainty factor, maybe 10, should be used, due to the approximations involved in the tally source method. On the other hand, high accuracy is generally not needed in shielding calculations. The

uncertainties estimated here are reasonably acceptable in such applications, considering that the shutdown dose rate in the IFMIF access cell (above the test cell) are likely to be well below the limit of what can be allowed.

References

1. Shimomura, Y. The present status and future prospects of the ITER project. *Journal of Nuclear Materials*, 2004, Vol. 5–11, pp. 329–333.
2. Shimomura, Y. Preparation of ITER construction and operation. *Fusion Engineering and Design*, 2006, 2, Vol. 81, No. 1–7, pp. 3–11.
3. Cozzani, F. Status and possible prospects of an international fusion materials irradiation facility. *Fusion Engineering and Design*, 1999, 11, Vol. 46, No. 2–4, pp. 413–421.
4. Andreani, R., Diegele, E., Gulden, W., Lässer, R., Maisonnier, D., Murdoch, D., Pick, M. & Poitevin, Y. Overview of the European Union fusion nuclear technologies development and essential elements on the way to DEMO. *Fusion Engineering and Design*, 2006, 2, Vol. 81, No. 1–7, pp. 25–32.
5. LA-12625-M, Version 4B. Briesmeister, J.F. (Ed.) MCNP – A General Monte Carlo N-Particle Transport Code, Version 4B. 1997.
6. LA-13709-M. Briesmeister, J.F. (Ed.) MCNP – A General Monte Carlo N-Particle Transport Code, Version 4C. 2000.
7. LA-UR-03-1987. X-5 Monte Carlo Team MCNP – A General Monte Carlo N-Particle Transport Code, Version 5. Volume I: Overview and Theory. 2003, revised 2005.
8. LA-CP-03-0245. X-5 Monte Carlo Team MCNP – A General Monte Carlo N-Particle Transport Code, Version 5. Volume II: User's Guide. 2003, revised 2005.
9. X-5 Monte Carlo Team MCNP – A General Monte Carlo N-Particle Transport Code, Version 5. Volume III: Developer's Guide. 2003, revised 2005.

10. Fischer, U., Simakov, S.P., von Möllendorff, U. & Pereslavytsev, P. Validated computational tools and data for IFMIF neutronic calculations. Proceedings of the ANS Annual Meeting AccApp'03. San Diego, California, USA, June 2003.
11. Simakov, S.P., Fischer, U., von Möllendorff, U., Schmuck, I., Konobeev, A.Y., Korovin, Y.A. & Pereslavytsev, P. Advanced Monte Carlo procedure for the IFMIF d-Li neutron source term based on evaluated cross section data. Journal of Nuclear Materials, 2002, 12, Vol. 307–311, Part 2, pp. 1710–1714.
12. Waters, L.S. (Ed.) MCNPX User's Manual, version 2.1.5.
13. FENDL-2.1. Fusion Evaluated Nuclear Data Library (Dec. 2004) [Homepage of IAEA], [Online] Available: <http://www-nds.iaea.org/fendl21/>.
14. Sato, S., Iida, H., Plenteda, R., Valenza, D. & Santoro, R.T. Evaluation of biological dose rates around the ITER NBI ports by 2-D S/activation and 3-D Monte Carlo analyses. Fusion Engineering and Design, 2000, 1, Vol. 47, No. 4, pp. 425–435.
15. Chen, Y. & Fischer, U. Rigorous MCNP based shutdown dose rate calculations: Computational scheme, verification calculations and applications to ITER. 6th Int. Symp. Fusion Nuclear Technology. San Diego, California, USA, 2002.
16. UKAEA FUS 514. Forrest, R.A. & Gilbert, M.R. FISPACT-2005: User manual. 2004.
17. Petrizzi, L., Batistoni, P., Chen, Y., Fischer, U., Iida, H. & Morimoto, Y. Advanced Methodology for Dose rate Calculation of ITER-FEAT. 12th Biennial Topical Meeting of the Radiation Protection and Shielding Division of the American Nuclear Society. Santa Fe, New Mexico, USA, 2002.
18. Iida, H., Valenza, D., Plenteda, R., Santoro, R.T. & Dietz, J. Radiation Shielding for ITER to allow for Hands-on Maintenance inside the Cryostat. Journal of Nuclear Science and Technology 1999, 19 Oct. 1999.

19. Valenza, D., Iida, H., Plenteda, R. & Santoro, R.T. Proposal of shutdown dose estimation method by Monte Carlo code. *Fusion Engineering and Design*, 2001, 9, Vol. 55, No. 4, pp. 411–418.
20. ITER Technical Basis document G A0 FDR 1 01-07-13 R1.0.
21. Wasastjerna, F. Experience of Fusion Neutronics Calculations, version 3. VTT memo ed.
22. Loughlin, M.J. Final Report, TW6-TTMI-001: IFMIF accelerator facilities. Dose rate evaluation in the IFMIF accelerator. 2007.
23. Sato, S., Iida, H. & Nishitani, T. Evaluation of shutdown gamma-ray dose rates around the duct penetration by three-dimensional Monte Carlo decay gamma-ray transport calculation with variance reduction method. 2002. 1237 p.
24. Sato, S. & Nishitani, T. A study on variance reduction of Monte Carlo calculation with weight window generated by density reduction method. 2007. 5 p.
25. Hodgdon, A.D. A Variance Reduction Management Algorithm for MCNP. *Transactions* 2003, Iss. 89, pp. 373–374. ISSN 0003-018X.
26. Sweezy, J., Brown, F., Booth, T., Chiaramonte, J. & Preeg, B. Automated variance reduction for MCNP using deterministic methods. *Radiation Protection Dosimetry*, 2005, Vol. 116, No. 1–4, pp. 508–512.
27. Haghghat, A. & Wagner, J.C. Monte Carlo variance reduction with deterministic importance functions. *Progress in Nuclear Energy*, 2003, Vol. 42, No. 1, pp. 25–53.
28. Omura, M., Miyake, Y.1., Hasegawa, T., Ueki, K., Sato, O., Haghghat, A. & Sjuden, G.E. Performance of the improved version of Monte Carlo code A³MCNP for large-scale shielding problems. *Radiation protection dosimetry*, 2005, Vol. 116 (2), No. 1–4, pp. 493–497.

29. Shahdatullah, M.S., Ziver, K., Eaton, M.D., Pain, C.C. & Goddard, A.J.H. Monte Carlo variance reduction using finite element adjoint weight windows. Vol. 2006. 2006.
30. Hendricks, J.S. & Culbertson, C.N. Assessment of MCNP Weight Windows. 2000.
31. Murata, I., Yamamoto, H., Miyamaru, H., Goldenbaum, F. & Filges, D. Scattering direction biasing for Monte Carlo transport calculation. Nuclear Instruments and Methods in Physics Research, 2006, A 562, pp. 845–848.
32. Freiesleben, H., Richter, D., Seidel, K. & Unholzer, S. Fusion neutronics-streaming, shielding, heating, activation. The CAARI 2000: Sixteenth international conference on the application of accelerators in research and industry. AIP Conference Proceedings, Volume 576. 2001. Pp. 763–767. ISSN 0094-243X.
33. Serikov, A., Fischer, U., Heidinger, R., Henderson, M.A., Spaeh, P. & Tsige-Tamirat, H. Radiation shield analyses in support of the FS design for the ITER ECRH launcher. SOFT-24 Symposium on Fusion Technology, No. 24, Warsaw, POLOGNE (11/09/2006), 2007, Vol. 82, No. 5–14. Pp. 736–743.
34. Iida, H., Santoro, R.T., Valenza, D. & Khripunov, V. A handy method for estimating radiation streaming through holes in shield assemblies. Fusion Engineering and Design, 1998, 10, Vol. 43, No. 1, pp. 1–13.
35. Leppänen, J. Development of a new Monte Carlo reactor physics code. VTT Publications 640, Espoo 2007. 228 p. + app. 8 p.
<http://www.vtt.fi/inf/pdf/publications/2007/P640.pdf>.

Appendix B: Publications I, II, III, V, VI, XI, XII are not included in the PDF version. Please order the printed version to get the complete publication (<http://www.vtt.fi/publications/index.jsp>)

Appendix A: An Analytic Estimate of the Spatial Discretization Error in the Rigorous Two-Step Method for Calculating Shutdown Dose Rates

Two competing methods of calculating shutdown dose rates with Monte Carlo programs such as MCNP are known as the Direct One-Step (D1S) and Rigorous Two-Step (R2S) methods, respectively. Each has its own advantages and disadvantages. Perhaps the most obvious disadvantage of the R2S method is the spatial discretization error. Instead of each delayed gamma being born at the exact location where the neutron producing it was absorbed, as in the D1S method, the neutron flux is averaged over each cell and then the resulting activation is calculated in a separate program, such as FISPACT. In the gamma transport calculation, the gamma source is taken to be constant in each cell, losing the detailed spatial information within the cell. The aim of the work described here was to obtain at least a rough estimate of the magnitude of this discretization error and its dependence on the cell size, with a view to choosing cell sizes appropriately, for instance in IFMIF shielding calculations.

To make the problem tractable, we make some simplifying assumptions. Take a purely one-dimensional shielding problem in slab geometry, with a shield extending from $x = 0$ to $x = a$, embedded in a void on both sides. Neutrons impinge on the shield on the left side ($x = 0$), and the quantity of interest is the delayed dose rate on the right side. We assume that the neutron flux in the shield follows an exponential distribution,

$$\phi(x) = Ce^{-\kappa x}. \quad (1)$$

The delayed gamma source in the shield is proportional to the neutron flux,

$$Q(x) = S\phi(x). \quad (2)$$

A gamma photon born at x will reach the far side of the shield with a probability of

$$e^{-\lambda(a-x)}. \quad (3)$$

Thus the gamma flux (or dose rate) beyond the shield is

$$\psi = \int_0^a KQ(x)e^{-\lambda(a-x)} dx = \int_0^a KSCe^{-\kappa x} e^{-\lambda(a-x)} dx = \frac{KSCe^{-\lambda a}}{\lambda - \kappa} (e^{(\lambda-\kappa)a} - 1). \quad (4)$$

We now divide the shield into layers, $i = 1, \dots, I$, each layer extending from x_{i-1} to x_i ($x_0 = 0$, $x_I = a$). Let the thickness of each layer be Δx_i . The exact contribution to the dose rate from each layer (within the assumptions we have made here) is

$$\psi_i = \int_{x_{i-1}}^{x_i} KSCe^{-\kappa x} e^{-\lambda(a-x)} dx = \frac{KSC}{\lambda - \kappa} e^{-\lambda a} e^{(\lambda-\kappa)x_{i-1}} (e^{(\lambda-\kappa)\Delta x_i} - 1). \quad (5)$$

In the R2S method, however, the neutron flux is treated as constant within each layer,

$$\tilde{\phi}_i = \frac{C}{\Delta x_i} \int_{x_{i-1}}^{x_i} e^{-\kappa x} dx = \frac{C}{\kappa \Delta x_i} e^{-\kappa x_{i-1}} (1 - e^{-\kappa \Delta x_i}). \quad (6)$$

Accordingly, the gamma flux at the shield surface caused by activation in layer i will be

$$\tilde{\psi}_i = \frac{KSC}{\kappa \Delta x_i} (e^{-\kappa x_{i-1}} - e^{-\kappa x_i}) \int_{x_{i-1}}^{x_i} e^{-\lambda(a-x)} dx = \frac{KSC}{\kappa \lambda \Delta x_i} e^{-\lambda a} e^{(\lambda-\kappa)x_{i-1}} (e^{\lambda \Delta x_i} - 1) (1 - e^{-\kappa \Delta x_i}). \quad (7)$$

For the sake of legibility, let us introduce the symbols $K = \kappa \Delta x_i$ and $L = \lambda \Delta x_i$. Then the ratio between the discretized and non-discretized gamma flux contributions from layer i is

$$\frac{\tilde{\psi}_i}{\psi_i} = \frac{L - K}{LK} \frac{(e^L - 1)(e^K - 1)}{e^L - e^K}. \quad (8)$$

When $\kappa = \lambda$, the above formula breaks down, but then it reduces to

$$\frac{\tilde{\psi}_i}{\psi_i} = \frac{(e^L - 1)(e^K - 1)}{LKe^K}. \quad (9)$$

Suppose we set as an objective that the discretization error of the most important layer should be less than 10%. This is a fairly tight criterion, in that the total effect of other sources of error in an ITER or IFMIF shielding calculation will usually exceed this by a large margin. Then Table A.1 (see the yellow cells) shows that this is achieved if

$$\Delta x_i < \frac{1}{\sqrt{\kappa\lambda}}. \quad (10)$$

Moreover, when κ and λ are very different, the allowable layer thickness becomes greater than that allowed by the above inequality.

In practice, the thickness allowed by this reasoning may be about 1 cm. However, we do not need to use this cell thickness throughout the system. If we assume that photons are attenuated more sharply than neutrons, i.e., $\lambda > \kappa$, the layer thickness limit need only apply to the cell layer at the end of the shield ($i = I$). For cell layers farther back, their relative contribution will be decreased by the factor

$$e^{-(\lambda-\kappa)(a-x_i)}. \quad (11)$$

It is also conceivable that the neutron attenuation may exceed that of photons, so that $\lambda < \kappa$. In that case the dominant cell layer will be the first one, not the last, and the following layers will have their contributions attenuated by a factor

$$e^{-(\kappa-\lambda)x_{i-1}} \quad (12)$$

caused by the attenuation of the neutron rather than photon flux.

Tables A.2 and A.3 show how one can use the above results in practice. Table A.2 shows the relative error, $|\tilde{\psi}/\psi| - 1$, caused by discretization as a function of κ , λ and Δx , using a value of κ corresponding to a halving length of 7.5 cm and values of λ appropriate for photons with energies of 2.4, 1.2, 0.6 and 0.3 MeV in heavy concrete. In Table A.3 a discretization scheme is shown, together with the resulting contributions to the dose rate error, relative to the dose rate from the last x interval (-1 to 0 cm), taking into account the attenuation correction. We see that in this example the discretization error remains small. Of course, the theory on which this result is based is in itself inexact, but it probably gives an idea of the order of magnitude of the discretization error.

Table A.1. $\tilde{\psi}/\psi$ values for selected $K = \kappa\lambda xi$ and $L = \lambda\Delta xi$. The largest K and L values for which $\tilde{\psi}/\psi < 1.1$ are highlighted in yellow, the cells where $K = L$ in green.

K \ L	0.100	0.126	0.158	0.200	0.251	0.316	0.398	0.501	0.631	0.794	1.000	1.259	1.585	1.995	2.512	3.162	3.981	5.012	6.310	7.943	10.000
0.100	1.001	1.001	1.001	1.002	1.002	1.003	1.003	1.004	1.005	1.007	1.008	1.010	1.013	1.016	1.019	1.023	1.027	1.031	1.035	1.039	1.041
0.126	1.001	1.001	1.002	1.002	1.003	1.003	1.004	1.005	1.007	1.008	1.010	1.013	1.016	1.020	1.024	1.029	1.035	1.040	1.045	1.049	1.052
0.158	1.001	1.002	1.002	1.003	1.003	1.004	1.005	1.007	1.008	1.010	1.013	1.016	1.020	1.025	1.031	1.037	1.044	1.051	1.057	1.062	1.066
0.200	1.002	1.002	1.003	1.003	1.004	1.005	1.007	1.008	1.011	1.013	1.017	1.021	1.026	1.032	1.039	1.047	1.056	1.064	1.072	1.079	1.085
0.251	1.002	1.003	1.003	1.004	1.005	1.007	1.008	1.011	1.013	1.017	1.021	1.026	1.033	1.040	1.050	1.060	1.071	1.082	1.092	1.101	1.108
0.316	1.003	1.003	1.004	1.005	1.007	1.008	1.011	1.013	1.017	1.021	1.026	1.033	1.041	1.051	1.063	1.076	1.090	1.105	1.118	1.130	1.139
0.398	1.003	1.004	1.005	1.007	1.008	1.011	1.013	1.017	1.021	1.027	1.033	1.042	1.052	1.065	1.080	1.097	1.116	1.134	1.152	1.167	1.179
0.501	1.004	1.005	1.007	1.008	1.011	1.013	1.017	1.021	1.027	1.034	1.042	1.053	1.067	1.083	1.103	1.125	1.149	1.174	1.197	1.217	1.233
0.631	1.005	1.007	1.008	1.011	1.013	1.017	1.021	1.027	1.034	1.042	1.054	1.068	1.085	1.106	1.132	1.161	1.193	1.226	1.256	1.283	1.306
0.794	1.007	1.008	1.010	1.013	1.017	1.021	1.027	1.034	1.042	1.054	1.068	1.086	1.108	1.136	1.169	1.208	1.251	1.296	1.338	1.375	1.406
1.000	1.008	1.010	1.013	1.017	1.021	1.026	1.033	1.042	1.054	1.068	1.086	1.109	1.138	1.175	1.219	1.271	1.330	1.391	1.450	1.503	1.547
1.259	1.010	1.013	1.016	1.021	1.026	1.033	1.042	1.053	1.068	1.086	1.109	1.139	1.177	1.226	1.285	1.357	1.439	1.526	1.611	1.687	1.751
1.585	1.013	1.016	1.020	1.026	1.033	1.041	1.052	1.067	1.085	1.108	1.138	1.177	1.228	1.292	1.373	1.473	1.590	1.718	1.846	1.962	2.060
1.995	1.016	1.020	1.025	1.032	1.040	1.051	1.065	1.083	1.106	1.136	1.175	1.226	1.292	1.379	1.492	1.634	1.807	2.002	2.203	2.390	2.550
2.512	1.019	1.024	1.031	1.039	1.050	1.063	1.080	1.103	1.132	1.169	1.219	1.285	1.373	1.492	1.650	1.858	2.121	2.434	2.772	3.096	3.379
3.162	1.023	1.029	1.037	1.047	1.060	1.076	1.097	1.125	1.161	1.208	1.271	1.357	1.473	1.634	1.858	2.167	2.583	3.112	3.722	4.341	4.897
3.981	1.027	1.035	1.044	1.056	1.071	1.090	1.116	1.149	1.193	1.251	1.330	1.439	1.590	1.807	2.121	2.583	3.255	4.194	5.390	6.713	7.968
5.012	1.031	1.040	1.051	1.064	1.082	1.105	1.134	1.174	1.226	1.296	1.391	1.526	1.718	2.002	2.434	3.112	4.194	5.900	8.408	11.600	14.949
6.310	1.035	1.045	1.057	1.072	1.092	1.118	1.152	1.197	1.256	1.338	1.450	1.611	1.846	2.203	2.772	3.722	5.390	8.408	13.760	22.221	32.920
7.943	1.039	1.049	1.062	1.079	1.101	1.130	1.167	1.217	1.283	1.375	1.503	1.687	1.962	2.390	3.096	4.341	6.713	11.600	22.221	44.608	83.588
10.000	1.041	1.052	1.066	1.085	1.108	1.139	1.179	1.233	1.306	1.406	1.547	1.751	2.060	2.550	3.379	4.897	7.968	14.949	32.920	83.588	220.245

Table A.2. The relative error, $|\tilde{\psi}/\psi|-1$, for a given κ and selected values of λ and Δx .

	kappa	lambda			
	0.092	0.114	0.165	0.235	0.331
delta-x (cm)					
1	0.000874	0.001266	0.001802	0.002538	
2	0.003501	0.005068	0.007218	0.010153	
3	0.007890	0.011428	0.016271	0.022853	
4	0.014061	0.020376	0.029003	0.040648	
5	0.022037	0.031957	0.045472	0.063560	
10	0.090439	0.131885	0.187179	0.256424	

Table A.3. A cell subdivision scheme (with $x = 0$ at the end of the shield), showing the contribution to the total error (as a multiple of the dose rate contribution from the last layer), including the attenuation factor.

	kappa	lambda			
	0.092	0.114	0.165	0.235	0.331
x	delta-x				
0	1	0.000874	0.001266	0.001802	0.002538
-1	2	0.003425	0.004712	0.006256	0.007995
-3	3	0.007386	0.009180	0.010595	0.011157
-6	4	0.012322	0.013149	0.012297	0.009689
-10	5	0.017685	0.015400	0.010882	0.005824
-15	5	0.015843	0.010691	0.005323	0.001763
-20	10	0.058246	0.030629	0.010720	0.002153
-30					

Appendix B: Publications I–XII

PUBLICATION IV

**Conceptual design of the EU
dual-coolant blanket (model C)**

20th IEEE/NPSS Symposium on Fusion Engineering
(SOFE). San Diego, CA, USA 2003. 4 p.
Copyright IEEE, 445 Hoes Lane, P.O. Box 1331,
Piscataway, NJ 08855-1131, USA.
Reprinted with permission from the publisher.

Conceptual Design of the EU Dual-coolant Blanket (Model C)

P. Norajitra, L. Bühler, A. Buenaventura^a, E. Diegele, U. Fischer, S. Gordeev, E. Hutter, R. Kruessmann, S. Malang, D. Maisonnier^b, A. Orden^a, G. Reimann, J. Reimann, G. Vieider^c, D. Ward^d, F. Wasastjerna^e

Forschungszentrum Karlsruhe, P.O. Box 3640, D-76021 Karlsruhe, Germany

^aEFET/IBERTEF, Spain; ^bEFDA CSU Garching, Germany; ^cVR, Sweden; ^dUKAEA, UK; ^eVTT Processes, Finland

Abstract. Within the framework of the EU Power Plant Conceptual Study (PPCS), also the design of the Dual-coolant Blanket (the so-called model C) was assessed technologically. A brief summary of the results shall be given below, starting with some very important design requirements to be fulfilled and a general description of the concept. This work is performed under the coordination of Forschungszentrum Karlsruhe in co-operation with CEA, EFET/IBERTEF, UKAEA, VR, and VTT.

I. INTRODUCTION

As a strategy of the EU PPCS, four different power plant models are investigated: Model A: Based on a water-cooled lead-lithium (WCLL) blanket using a ferritic/martensitic steel EUROFER as structural material and a water-cooled divertor with a CuCrZr alloy as structural material; Model B: Based on a helium-cooled ceramics/beryllium pebble bed (HCPB) blanket using EUROFER as structural material and a He-cooled divertor with W alloys as structural material; Model C: Based on a dual-coolant (DC) blanket (bulk self-cooled lead/lithium + He-cooled structures) using EUROFER as structural material and SiC_f/SiC as thermal and electrical insulators, and a He-cooled divertor made of W alloys and EUROFER as structural materials; Model D: Based on a self-cooled lead/lithium (SCLL) blanket and lead-lithium-cooled divertor, both made of SiC_f/SiC structural material.

Model C [1] is a compromise of the “near-term” models A and B with their limited attractiveness and the “very advanced” model D which is characterized by very attractive features, but considerable development risks. It offers the following advantages related to the DC design: a) Simple construction, i.e. less complexity, smaller heat transfer area, leading to a high reliability, b) a higher coolant temperature than that of the structure is attainable by circulating the liquid metal coolant with internal heat sources and by the use of SiC_f/SiC flow channel inserts (FCIs), c) less permeation safety issues due to the possibility of using the gas turbine cycle. Further advantages which are typically related to the use of liquid-metal breeders are: a) No nuclear damage of the liquid-metal breeder, b) replenishment of the Li-6 breeder material can be done easily online, c) only the structures and inserts have to be exchanged or recycled, d) relatively small thickness of shielding for vacuum vessel (VV) and magnet coils is required when using a water-cooled low-temperature shield.

The PPCS refers to a standardized commercial power plant with a unit size of 1500 MWe.

II. THE CONCEPTUAL DESIGN OF MODEL C

A. Physics of the Reactors and Design Requirements

Models C and D are based on advanced physical assumptions characterized by: a) high β and high confinement, with realistic plasma pressure gradients, b) MHD stabilization

by strong plasma shaping, c) high bootstrap current fraction, d) low divertor power loads and low Z_{eff} , no ELMs are foreseen in reactor operation. Analysis with the PROCESS code [2], [3] shows that, indeed, the above assumptions lead to a high Q, reduced-size reactor, high bootstrap current fraction, and reduced plasma current when compared to models A and B, with nuclear loads limited to $< 2.5 \text{ MW/m}^2$. Also, the heat load to the divertor could be reduced to 5 MW/m^2 (model D). In all cases, the net power plant output to the grid is 1500 MWe and the D-T fuel mix is 50-50.

The following overall design requirements and criteria are imposed: a) Easy replacement of blanket and divertor modules, b) sufficient shielding of VV (for reasons of reweldability) and magnets to make them to life-time components, c) low volumetric fraction of steel to enhance the breeding ratio ($\text{TBR} > 1$), d) use of oxide dispersion-strengthened (ODS) steel limited to the plasma-facing zone of the first wall with highest temperature, e) sufficiently high coolant inlet temperature to avoid material embrittlement (DBTT) under irradiation, and sufficiently high coolant outlet temperature to allow the use of a BRAYTON cycle power conversion system, f) to minimize the tritium permeation loss, purification and tritium extraction systems for liquid metal have to be foreseen.

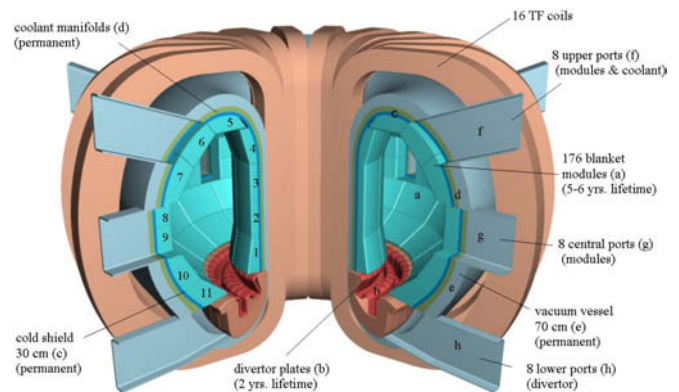


Fig. 1. Fusion reactor with DC blanket modules (model C).

B. Brief Design Descriptions of the Blanket and Divertor

Blanket: The DC concept which is based on the study in [4] and the ARIES-ST study [5] is characterized by the use of self-cooled breeding zones with the eutectic lead-lithium alloy Pb-17Li serving as breeder and coolant at the same time, the use of a helium-cooled reduced-activation ferritic/martensitic (RAFMs) steel structure like EUROFER, and the use of SiC_f/SiC FCIs serving as electrical and thermal insulators. The plasma-facing surface of the first wall is plated with a small layer of ODS. Instead of the “banana segments” adopted in earlier studies [6], [7], the blanket segmentation now consists of “large modules” [8], which helps to reduce thermal stresses and to better cope with the forces caused by disruptions, while

maintenance is facilitated. A total of 11 modules, five of them at the inboard and six at the outboard (Fig. 1), form a 7.5° segment of the torus. They are large, stiff boxes with a helium-cooled grid structure inside forming flow channels for the Pb-17Li (Fig. 2). The modules are divided into a lifetime part (cold shield, coolant manifold, and vacuum vessel) and a breeding and hot shield part which will be exchanged at 6-years' intervals. For cooling the entire blanket structure, high-pressure (8 MPa) helium gas is used. Two separate He systems provide for a redundancy of decay heat removal. Counter-flow manifolds ensure a uniform temperature distribution to minimize thermal stresses. The inlet temperature of the helium amounts to 300 °C, the outlet temperature to 480 °C. Moreover, the liquid-metal breeder Pb-17Li also serves as a coolant. It enters the modules at 460 °C and leaves them at 700 °C, a value that is maximized for efficiency reasons. Primary coolant loop and manifold are provided with concentric tubes, with the "hot outlet coolants" being in the inner tube (for the Pb-17Li coolant in particular, this tube is thermally insulated with SiC_p/SiC inserts), and the "cold inlet coolants" flowing through the annular channels.

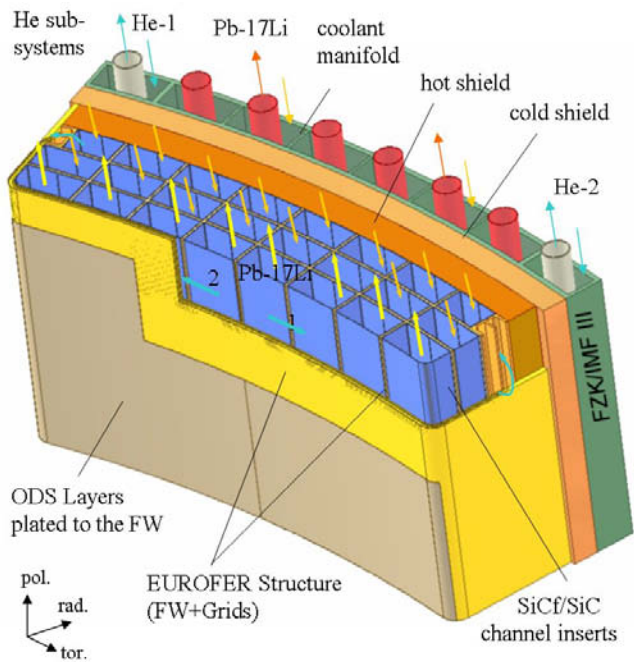


Fig. 2. DC equatorial outboard blanket module (radxtorxpol: 1.5x3.0x1.6 m³).

Divertor: About 15% of the heat energy are released into the divertor which also serves as a trap for plasma impurities. A high heat flux of 10 MW/m² at least is assumed to hit the divertor target plates. For divertor cooling, helium gas is preferred, because it is compatible with other materials, which is of major relevance with respect to safety, and, therefore, ensures a good integration of the divertor in the power conversion system. A high helium outlet temperature is favorable to increase thermal efficiency. A modular design and small temperature gradients are recommended to reduce thermal stresses. The main design criteria are: a) The lower boundary of the divertor operation temperature window has to be higher than the ductile-brittle transition temperature (DBTT), and b) the temperature at the upper boundary has to be lower than the recrystallization limit of the structural components made of refractory alloys under irradiation, c)

high heat transfer coefficients must be ensured, while the coolant mass flow rate and, therefore, the pressure loss as well as the pumping power have to be as low as possible. The proposed design of a He-cooled modular divertor with integrated pin array (HEMP) consists of target plates divided into small modules. Underneath each tile of tungsten used as thermal shield, a finger-like heat transfer module (thimble) is brazed on. A pin array as flow promoter is integrated at the bottom of the thimble to increase the cooling surface. Helium at 10 MPa and 700 °C enters the pin array at high velocity to cool the target plates and is heated up to about 800 °C. Main neutronic and thermohydraulic data as well as the power balance of the DC blanket concept are summarized in Tab. I.

C. Neutronic Analysis and Shielding Efficiency

Distribution of neutron wall loading was calculated with the MCNP code. More than 90% of the fusion neutron power are loaded on the blanket modules, while the remainder flows through the divertor opening. Concerning volumetric heating, a major fraction of $\cong 80\%$ of the volumetric heat power is generated in the blanket segments, including the first wall. With the DC reference design, $\approx 4\%$ are generated in the water-cooled low-temperature (LT) shield. This power may not be utilized for electricity production and, therefore, must be minimized, e.g. by enhancing the shielding capacity of the high-temperature shield. Regarding the shielding efficiency, there are two essential requirements that must be fulfilled: a) Reweldability of lifetime components made of steel and b) sufficient protection of the superconducting toroidal field (TF) coils. Based on existing data, the current assumption is that rewelding of stainless steel should be successful at helium concentrations below 1 appm. Calculations to estimate the helium production in EUROFER steel show that even after a lifetime cycle of 40 years, reweldability is achieved. Hence, the LT shield may be designed as a lifetime component, if welded joints are placed on its rear. The TF coil, on the other hand, is protected from the penetrating radiation by the blanket, the shield, and the vacuum vessel. An efficient neutron moderator (water or a hydride) is required to this end, combined with a good neutron absorber (steel, tungsten, etc.). The radiation loads of the TF coils were calculated for the inboard mid-plane, where the shielding requirements are highest due to the minimum space available between the plasma and the TF coil. It is noted that the design limits are met by the DC reference design.

D. Thermohydraulic, Thermomechanic, and MHD Analyses

The layout of the blanket and the divertor requires iterations between system code analysis and blanket layout concerning neutronic, thermohydraulic, thermomechanical, MHD, and velocity field calculations to determine a set of reactor parameters. For the ODS layer on the first wall, the maximum temperature should stay below 650 °C due to creep rupture, while the interface temperature of the EUROFER structure and Pb-17Li should be below 500 °C due to corrosion. For thermomechanical calculations, data of T91 were used instead of ODS data. The results show that the requirements can be fulfilled.

Also for the divertor, an assessment of temperatures and stresses was undertaken. Structural design criteria as required by the ITER structural design code are met, i.e. mechanical stresses do not exceed design limits under any operation

condition. From these values, it is expected that fatigue of some anticipated 100-1000 cycles of reactor shutdown with cooling down from operation conditions to RT is permissible. In a first thermohydraulic assessment of the divertor, a heat transfer coefficient of approx. 60 kW/m²K related to the surface area of the basis plate was determined with a corresponding pumping power of about 5.5% related to the heat removal.

MHD analysis shows that SiC_f/SiC inserts with a wall thickness of 5 mm already ensure a sufficient electric insulation, resulting in a small pressure drop in the Pb-17Li channels and, thus, a small pumping power for the liquid-metal coolant.

E. Power Conversion System

For safety reasons (chemical reaction between water and liquid metal) and to attain a high thermal efficiency, a Brayton cycle (closed-cycle helium gas turbine) is considered as the reference concept. Thus, tritium permeation losses to the environment can be minimized. Four parallel closed three-compression-stage Brayton cycles are used leading to a thermal net efficiency of about 43%.

F. Tritium Recovery and Purification Systems for Pb-17Li and He Cooling Loops

The requirements on the tritium removal and recovery system are to keep the tritium inventory low in the total blanket system and to limit the tritium losses to the environment to an acceptable value. This mainly refers to the tritium which permeates through the walls of the heat exchanger and intercoolers into the water. These losses may easily be limited to acceptable values due to the low temperatures (maximum helium temperature ≈ 300 °C, water temperature ≈ 30 °C) in these components.

Several methods were proposed and assessed for tritium removal from Pb-17Li. During the breeding process, also helium is produced. Due to its low solubility in Pb-17Li, bubbles will be formed. It might be straightforward to combine helium bubble removal with the tritium removal system discussed, since some of the methods might be also efficient for helium bubble removal. Finally, liquid-metal purification systems are also required in general to control the oxygen content of the system and remove corrosion products. For irradiated Pb-17Li, additional removal of heavy metal isotopes (Po, Hg, Ti) will be necessary.

Several helium loops cool the different systems of the plant. Helium gas has to be cleaned regularly so as to remove gaseous and radioactive impurities (especially tritium). The coolant purification system will also serve as a means of pressure control.

G. Balance of Plant and Fusion Power Plant Layout

This section deals with additional components to set up an entire operational and functioning plant for generating electric power. The following main systems were considered: a) Primary heat transport system, b) power conversion cycle, c) service water system for cooling auxiliary systems, d) component cooling water system to supply selected auxiliary components with cooling water. The component cooling water system acts as an intermediate barrier between the circulating water system and potentially radioactive cooling loads. Thus, the possibility of radioactive leakage to the environment is

reduced, e) circulating water system: The circulating water system provides for a continuous supply of cooling water to the heat rejection heat exchanger, the intercoolers, the component cooling water heat exchanger, and the service water system, f) water treatment plant, g) compressed-air system, h) fire protection, i) electrical power, j) HVAC system: The HVAC system provides for the ventilation and air conditioning of different plant buildings.

The whole site of the power plant (Fig. 3) consists of several buildings to house the reactor, auxiliary systems, the power supply, and the turbines, but also workshops and offices. The design of the tokamak building (Fig. 4) and the hot cell building will be further evaluated, based on the design of the ITER site.

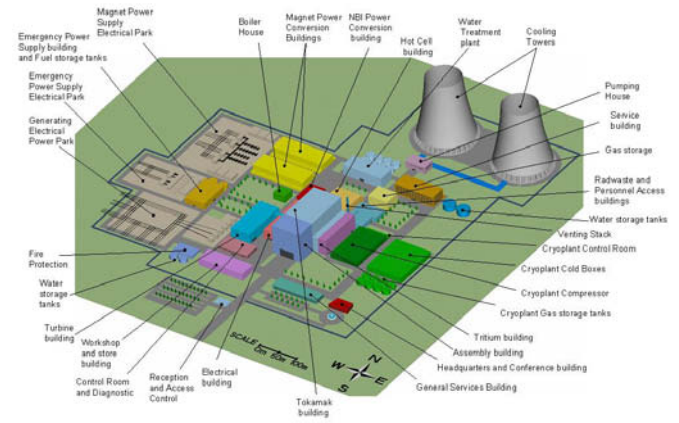


Fig. 3. Fusion power plant, general layout.

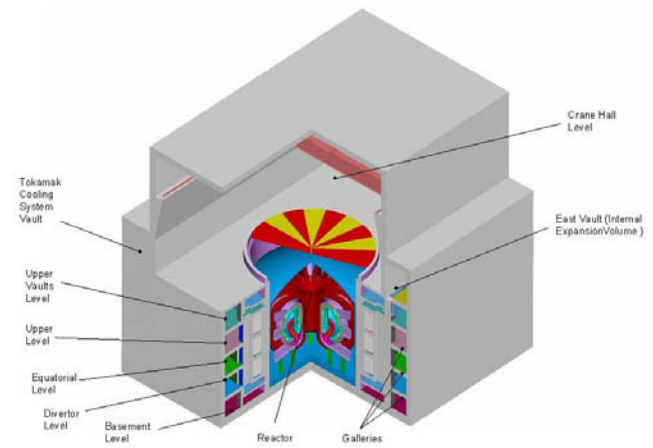


Fig. 4. Tokamak building, general view.

III. Conclusions and Outlook

The technologies and plasma physics models employed for model C represent a compromise of the “near-term” models A and B with their limited attractiveness and the “very advanced” model D with its very attractive features, but considerable development risks. Model C is based on a self-cooled lead-lithium breeding zone and a helium-cooled structure made of the reduced-activation ferritic steel EUROFER as well as on a helium-cooled divertor. Flow channel inserts made of SiC_f/SiC composite in the lead-lithium channels serve as thermal and electrical insulators in

order to minimize magneto-hydrodynamic (MHD) pressure loss and obtain high coolant exit temperatures and, thus, a high efficiency of the power conversion system, for which the BRAYTON cycle (closed-cycle helium gas turbine) is used. The modular designs of the DC and the He-cooled divertor are addressed. Within the framework of this study, a self-cooled liquid-metal breeder blanket is assessed for a standardized commercial power plant with a typical unit size of 1500 MWe. The overall results of this study lead to the conclusion that the plant model C has a high potential of meeting the goal of fusion research, i.e. to develop an economically and environmentally attractive energy source.

TABLE I
MAIN DATA OF THE DC BLANKET CONCEPT

	Overall plant	
Electrical output [MW]	1500	
Fusion power [MW]	3410	
	Blanket	Divertor
Average neutron wall load [MW/m ²]	2.27	1.7
Max. neutron wall load [MW/m ²]	3.0	
Average surface heat load [MW/m ²]	0.45	0.67
Max. surface heat load [MW/m ²]	0.59	10
Alpha-particle surface power [MW]	546	136
Heating power [MW]		112
Neutron power [MW]	2445	283
Energy multiplication	1.17	1.17
Thermal power [MW]	3408	583
Surface area [m ²]	1077	69.3 (target)
Helium coolant:		
- Inlet temperature [°C]	300	700 (target)
- Outlet temperature [°C]	480	800 (target)
- Pressure [MPa]	8	10 (target)
- Mass flow rate [kg/s]	1528	473 (bulk) 477 (target)
- Pumping power, $\eta = 0.8$ [MW]	30	3.4
Pb-17Li coolant:		
- Inlet temperature [°C]	480	
- Outlet temperature [°C]	700	
- Mass flow rate [kg/s]	46053	
Secondary helium loop:		
- Inlet temperature [°C]	285	
- Outlet temperature [°C]	700	
- Pressure [MPa]	15	
Net efficiency (blanket/divertor cycle)	0.43	

Key Issues and R&D Needs

Blanket: a) MHD - modeling and computations of 3D inertial flows in expansions, b) tritium recovery: The experience gained so far from the use of components for tritium recovery is not sufficient to reliably design such a system. More work on liquid/gas contactors is recommended, which should also include other volatile radioactive isotopes, c) Pb-17Li purification: Uncontrolled precipitation of corrosion products in liquid-metal loops must be avoided by using efficient purification systems. The aim should be to keep

these products in solution and to trap them in cold traps, thus preventing them from depositing, especially on the surfaces of the heat exchangers. Much more work is required for removing radioactive isotopes from the liquid metal. In particular, the radiotoxic α -emitter Po-210 formed from Bi-209 is considered to be a critical issue. Techniques to remove thallium and mercury are not yet available, d) SiC_f/SiC FCIs: Fabrication routes, compatibility with Pb-17Li flow at high temperatures above 700 °C, irradiation experiments, e) investigation of electromagnetic forces caused by disruptions.

Divertor: a) Material issues: In the long term, a development of W alloys is needed, which broadens the operational temperature window from the today's range of 800 – 1200 °C to 600 – 1300 °C by increasing the recrystallization temperature and simultaneously lowers the DBTT. Potential use of graded materials should be considered, b) choice of appropriate materials to reduce activation and widen the design options: Replacement of TZM as thimble material by tungsten or tungsten alloy and use of ODS EUROFER as structural material for the plate structure instead of TZM, c) development of fabrication routes and joining technology, in particular joining of steel to W, surviving frequent temperature cycles between RT and the operating temperature of about 600 °C, d) alternative: Development of transition pieces. The large mismatch in the thermal expansion coefficients of steel and refractory alloys, which are 10 - 14 x 10⁻⁶/K and 4 – 6 x 10⁻⁶/K, respectively, will cause very high local plastic strains at edges and corners.

ACKNOWLEDGMENT

This work has been performed within the framework of the Nuclear Fusion Program of Forschungszentrum Karlsruhe and is supported by the European Union within the European Fusion Technology Program.

REFERENCES

- [1] P. Norajitra, L. Bühler, A. Buenaventura, E. Diegele, U. Fischer, S. Gordeev, E. Hutter, R. Kruessmann, S. Malang, A. Orden, G. Reimann, J. Reimann, G. Vieider, D. Ward, and F. Wasastjerna, "Conceptual Design of the dual-coolant blanket within the framework of the EU power plant conceptual study (TW2-TRP-PPCS12), Final report," FZKA 6780, May 2003.
- [2] DJ Ward, "Assessment of economics of PPCS plant models A and B," PPCS/UKAEA/PPCS6-2, July 2002.
- [3] DJ Ward, "Assessment of economics of PPCS plant models C and D," PPCS/UKAEA/PPCS16-2, August 2003.
- [4] M.S. Tillack and S. Malang, "High-performance PbLi blanket," Proc. of the 17th IEEE/NPSS Symposium on Fusion Energy, San Diego, California, pp. 1000-1004, 1997.
- [5] D.K. Sze, M. Tillack, and L. El-Guebaly, "Blanket system selection for the ARIES-ST," Fusion Engineering and Design, vol. 48, pp. 371-378, 2000.
- [6] P. Norajitra, L. Bühler, U. Fischer, K. Klefeldt, S. Malang, G. Reimann, H. Schnauder, L. Giancarli, H. Golfier, Y. Poitevin, and J.F. Salavy, "The EU advanced lead lithium blanket concept using SiC_f/SiC flow channel inserts as electrical and thermal insulators," Fusion Engineering and Design, vol. 58-59, pp. 629-634, 2001.
- [7] P. Norajitra, L. Bühler, U. Fischer, S. Malang, G. Reimann, and H. Schnauder, "The EU advanced dual coolant blanket concept," Fusion Engineering and Design, vol. 61-62, pp. 449-453, 2002.
- [8] P. Norajitra, L. Bühler, U. Fischer, S. Gordeev, S. Malang, and G. Reimann, "Conceptual design of the dual-coolant blanket in the frame of the EU power plant conceptual study," Fusion Engineering and Design, vol. 69, pp. 669-673, 2003.

PUBLICATION VII

**Tungsten spectral shifter: neutronics
analysis (dpa evaluation, H, He
and other impurities generation,
recoil spectrum, etc) of different
positions and geometries**

Final report on the EFDA task TW5-TTMI-003,
Deliverable 8. FZK (Forschungszentrum Karlsruhe)
report, 2006. 11 p. Copyright 2006 by
Forschungszentrum Karlsruhe.
Reprinted with permission from the publisher.

REPORT for TASK of the EFDA Technology Programme			
Reference:	Field: Tritium Breeding and Materials Area: IFMIF Task: TW5-TTMI-003 Task Title: IFMIF Test Facility Subtask Title: Tungsten spectral shifter: neutronics analysis (dpa evaluation, H, He and other impurities generation, recoil spectrum, etc) of different positions and geometries		
Document:	Final report on the EFDA task TW5-TTMI-003, Deliverable 8: "Tungsten spectral shifter: neutronics analysis (dpa evaluation, H, He and other impurities generation, recoil spectrum, etc) of different positions and geometries"		
Level of confidentiality	Free distribution <input checked="" type="checkbox"/>	Confidential <input type="checkbox"/>	Restricted distribution <input type="checkbox"/>
Author(s):	S.P. Simakov, P. Vladimirov, U. Fischer, V. Heinzl, A. Möslang, F. Wasastjerna* Forschungszentrum Karlsruhe, Postfach 3640, D-76021, Karlsruhe, Germany *Euratom-Tekes, VTT Processes, P.O. Box 1608, FIN-02044 VTT, Finland		
Date:	1 October 2006		
Distribution list:	Rainer Laesser (CSU Field Coordinator) Angel Ibarra (Responsible Officer) A. Möslang (Project Leader) V. Heinzl (Coordinator Task TTMI-003) U. Fischer (Coordinator Task TTMI-004) W. Bahm (FZK, Fusion Programme Management) K. Hesch (FZK, Fusion Programme Management)		
Abstract:	<p>The objective of this task is the optimization of (i) the tungsten irradiation conditions in IFMIF to closer represent those in the divertor of the power fusion reactors and (ii) the tungsten spectral shifter plates position in front and behind the Creep-Fatigue testing machine (CFTM) to adjust the primary knock-on atom spectrum in the in situ creep-fatigue samples.</p> <p>For the comparative tungsten irradiation conditions analyses the nuclear responses in the W tiles covering the divertor of 4000 MW fusion power reactor with helium cooled lithium lead blanket were calculated.</p> <p>In the case of IFMIF they were calculated at several locations around Li target using McDeLicious code and latest deuteron-lithium and neutron evaluated cross sections files. It was found that in the neutron downstream direction (High Flux Test Module, its lateral neutron reflector, Universal Test Machine) the displacement damage rate (dpa) and the gas-to-dpa production ratios for tungsten exceeds that of the fusion power reactor divertor several times. In backward direction (inside deuteron beam tube) the gas-to-dpa ratio is comparable whereas atom displacement rate is much less than in the fusion reactor divertor. It means that a compromise could be found in the flange of lithium target located in perpendicular direction to the deuteron beam.</p> <p>The optimization of the location and thickness of tungsten neutron spectral shifter near Creep Fatigue and Tritium Release Modules was performed, considering as a criterion the damage rates, neutron and nuclei recoil spectra. It was found that the variant with half-width (3.2 cm) tungsten plate located behind CFTM would be the most preferable one. It provides similar damage level at CFTM as the previous variant with full-width (6.4 cm) plates and the highest damage rate in beryllium irradiated at TRM.</p>		
Revision No: 0	Changes: none		
	Written by:	Revised by:	Approved by:
	S.P. Simakov, P. Vladimirov		

Tungsten spectral shifter: neutronics analysis (dpa evaluation, H, He and other impurities generation, recoil spectrum, etc) of different positions and geometries

*Final report on the EFDA task
TW5-TTMI-003, Deliverable 8*

S.P. Simakov¹, P. Vladimirov², U. Fischer¹,
V. Heinzl¹, A. Möslang², F. Wasastjerna³

¹*Institut für Reaktorsicherheit,*

²*Institut für Materialforschung I,*

*Association FZK- Euratom, Forschungszentrum
Karlsruhe, Programm Kernfusion*

³*VTT Processes,*

Association Euratom-Tekes, Finland

October 2006

1. Introduction

The IFMIF facility is projected to reproduce irradiation conditions of fusion power reactors and to study the radiation properties of the fusion structural materials [1, 2]. So far many efforts have been undertaken for developing the computational tools and data and predicting the nuclear responses mainly in the low activated steel and tritium breeder materials [3 - 7]. It was shown that IFMIF irradiation conditions can perfectly meet helium, hydrogen and displacement production rates relevant for fusion reactor.

The objective of this task is the optimization of (i) the tungsten irradiation conditions in IFMIF to closer represent those in the divertor of the power fusion reactors and (ii) the tungsten spectral shifter plates position in front and behind the creep-fatigue testing machine (CFTM) to adjust the primary knock-on atom spectrum in the in situ creep-fatigue samples.

2. Tungsten nuclear response parameters in power fusion reactor divertor

PPCS/HCLL Fusion Reactor (vertical cut)

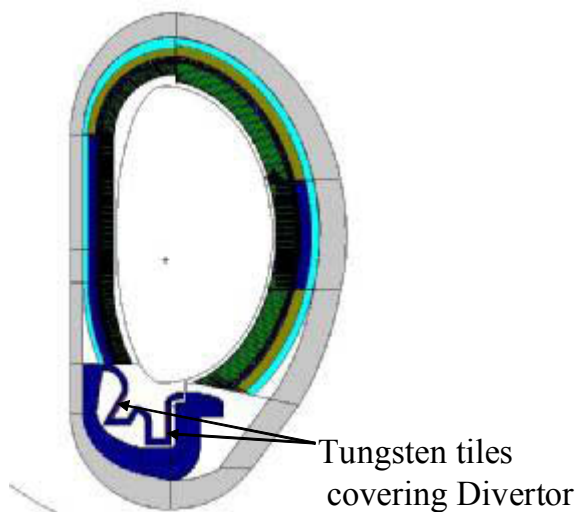


Fig.1. Vertical cut of the PPCS fusion power reactor with HCLL blanket

For the comparative tungsten irradiation conditions analyses the nuclear responses in the W tiles covering the divertor of fusion power reactor (Fig. 1) were calculated. This was done for a 4000 MW power reactor with helium cooled lithium lead blanket (HCLL) investigated in the Power Plant Conceptual Study (PPCS) [8]. The tungsten nuclear responses were calculated by the MCNP4C Monte Carlo code using a three-dimensional 20 degrees torus sector model and FENDL-2 cross section data for the neutron transport.

The results presented in Table 1 show that each tungsten atoms will be displaced 2.4 times from its lattice node during 1 full power operation of fusion reactor. The gas generation in tungsten will be dominated by hydrogen and helium production caused by neutrons at the levels of 2.3 appm and helium 0.7 appm, that give the gas to dpa ratios 1.0 and 0.3, correspondingly.

3. Tungsten irradiation parameters in IFMIF

The aim of this subtask is a search of location for the tungsten specimens in the IFMIF test modules or close to them, where the atom displacement rate and gas production ratio will optimally reproduce the ones expected in fusion power reactor.

3.1. Optimization of the tungsten specimens location

In the IFMIF facility the High, Medium and Low Flux Test Modules (HFTM, MFTM, LFTM) are located just behind Li-jet target to house the specimens for long term irradiations.

As a first step we have estimated nuclear responses in the tungsten specimens located there, supposing that they will partly replace the steel samples in the HFTM or can be easily allocated between pull-push rods of Universal Test Machine (UTM), which is a front part of MFTM (see Fig. 2). To perform such neutronics calculations the McDeLicious code [5] with recently updated and validated d-Li cross sections data (task TW4-TTMI-003, Deliverable D9) [6] were employed. For the representation of current IFMIF test cell design the global MCNP model developed in the frame of task TW4-TTMI-003, Deliverable D5a (TEKES, Finland) was used.

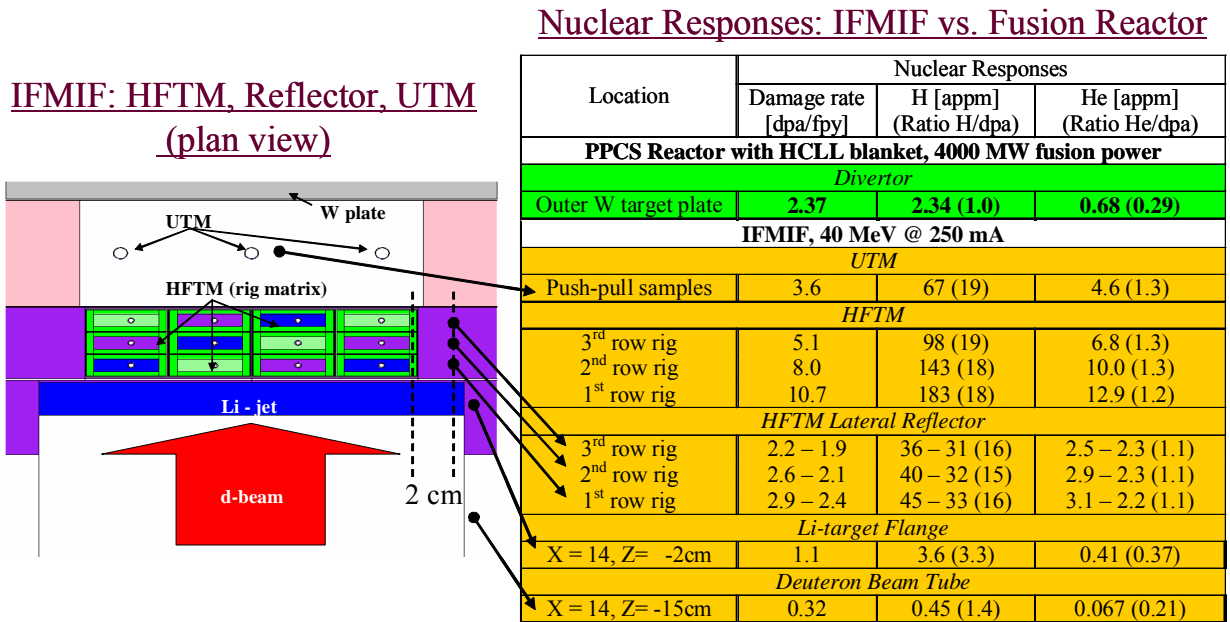


Fig. 2. Horizontal cut of the IFMIF test cell fragment: Li-jet, HFTM, neutron reflector, UTM and W plate.

Table 1. Tungsten nuclear responses in the divertor of fusion power reactor and at different locations inside IFMIF as indicated in Fig. 2.

The results listed the Table 1 show that atom displacement rate 3.6 dpa/fpy in tungsten could be achieved in UTM, if the specimens will be located between the push-pull rods. This already exceeds the dpa rate in the fusion power divertor. On other hand for the proper representation of the fusion reactor radiation conditions one needs to have the gas production to dpa ratios 1.0 for hydrogen and 0.3 for helium. As Table 1 shows during irradiation near UTM rods these ratios will amount 20 and 1.3, hence 20 - 4 times exceeding the fusion levels.

In the HFTM, even higher tungsten atom displacement rates (5 to 11 dpa/fpy) could be reached depending on the rig and row housing the specimens. But the gas-to-dpa ratios will also exceed fusion level by same large factor as in UTM.

The reasons of that are the difference of energy neutron spectra inside the fusion and IFMIF facilities and sensitivity of gas production reactions to the high energy neutrons. The fusion neutron spectra cut off at 15 MeV, whereas IFMIF ones produced by d-Li reaction extends up to 55 MeV (Fig. 3). The gas productions cross sections on tungsten such as (n,xp) and (n,xα) have thresholds around 10 MeV and increases one-two orders of magnitude as neutron energy goes up from 14 to 55 MeV (Fig. 4). The dpa cross section increases only two times in this energy range, being the same time non threshold reactions.

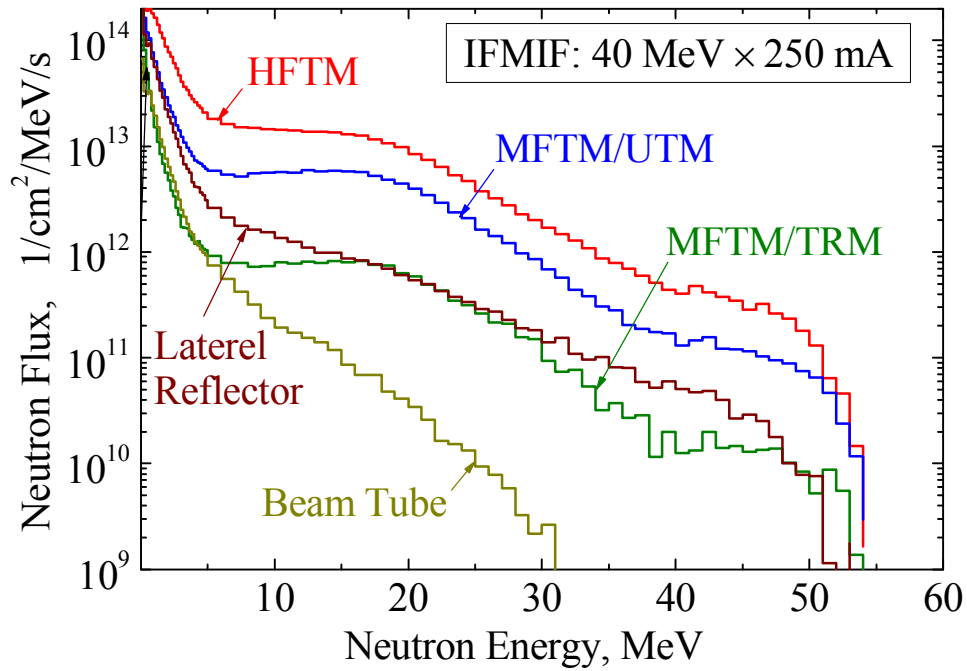


Figure 3. Energy differential neutron flux in the HFTM, MFTM, HFTM Lateral reflector and deuteron beam tube.

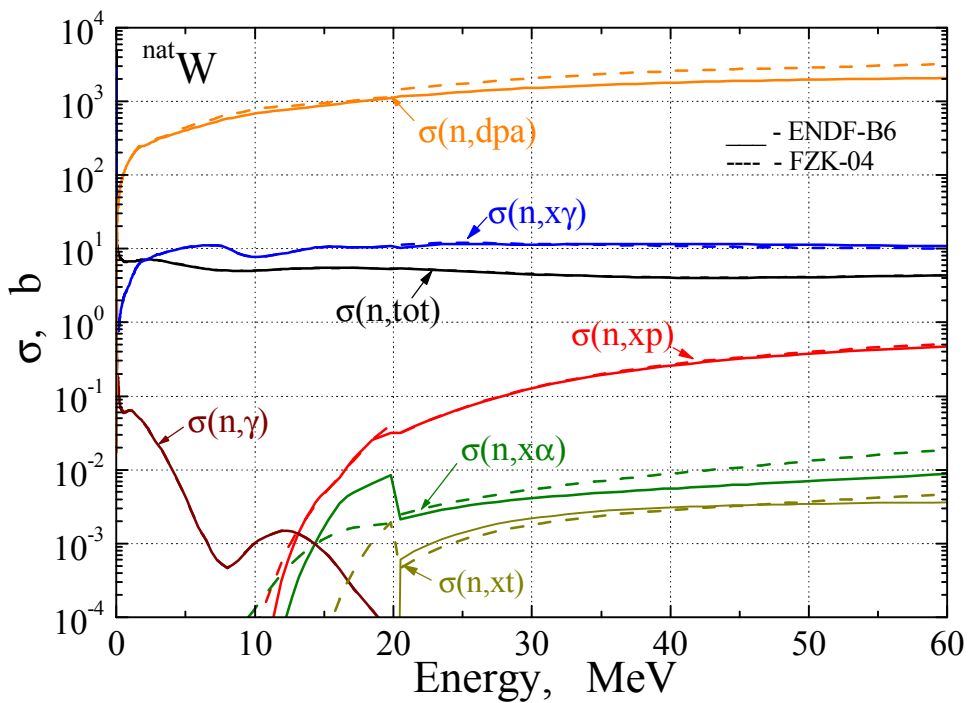


Figure 4. Neutron reactions cross sections for natural tungsten from ENDF/B-VI (solid curves) and FZK-04 (dash curves) libraries.

Principally, for the reproduction the fusion gas-to-dpa ratios in the IFMIF the tungsten specimens should be shifted in sideward or even backward directions relative to the deuteron beam direction, where the fraction of neutrons with energy more than 15 MeV essentially decreases (Fig. 3). We considered following geometrically possible spots for the samples as indicated in Fig. 2: the HFTM lateral reflector, lithium target flange and deuteron beam tube (inside the vacuum system).

Results of calculations are summarized in Table 1:

- location of the tungsten specimens inside the HFTM lateral reflector gives the acceptable dpa rate but the gas-to-dpa ratio as large as in HFTM and UTM;
- practically the same gas-to-dpa ratios as in the fusion reactor divertor could be achieved inside the deuteron beam tube, but at 0.3 dpa/fpy displacement rate which is 10 times less than fusion one;
- location of the W specimens in the flange of Li-target exhibits the intermediated option with dpa rate half of fusion one and gas-to-dpa ratios 3-2 times larger.

Further study is needed to clarify the possibility of the housing the tungsten specimens there regarding all engineering issues.

3.2. Dependence of results of calculations on nuclear data base

The results of estimation of nuclear responses in the tungsten depend on the neutron induced reactions cross section used in the calculations. As Fig. 4 shows, the agreement between ENDF/B-VI library and recent new evaluation FZK'04 [9] are quit reasonable up to 60 MeV. Nevertheless the differences for some specific reactions are visible and reach in the case of helium production even a factor of 5.

Table 2. Dependence of tungsten nuclear responses on nuclear data used in calculations.

Location	Nuclear Responses			Neutron cross section Data
	Damage rate [dpa/fpy]	H [appm]	He [appm]	
PPCS Reactor with HCLL blanket, 4000 MW fusion power				
<i>Divertor</i>				
Outer W target plate	2.37	2.34	0.68	ENDF-B6 FZK-04 Difference
	2.45	2.26	0.72	
	3.3%	3.5%	5.7%	
IFMIF, 40 MeV @ 250 mA				
<i>HFTM</i>				
3 rd row rig	5.1	98	6.8	ENDF-B6 FZK-04 Difference
	5.8	105	5.7	
	13%	6.7%	18%	
2 nd row rig	8.0	143	10.0	ENDF-B6 FZK-04 Difference
	9.0	150	8.3	
	12%	4.7%	19%	
1 st row rig	10.7	183	12.9	ENDF-B6 FZK-04 Difference
	9.0	150	8.3	
	17%	20%	43%	

To estimate the influence of nuclear data base on final results we calculated tungsten nuclear responses with these two evaluations. The results listed in the Table 2. show that dependence of W nuclear responses on nuclear data amounts 3 to 6% for the case of fusion reactor calculations and 5 to 40% for IFMIF. The largest difference appears for gas production in tungsten, that emphasizing the necessity for experimental validation of the relevant cross sections in the IFMIF energy range.

4. Optimization of the Tungsten spectral shifter for reproduction fusion irradiation conditions in Medium Flux Test Module

Previous Monte Carlo simulations has shown that for the properly selected geometry IFMIF irradiation conditions can perfectly meet helium, hydrogen and displacement production rates relevant for DEMO reactor. Additional spectral shifter allows also fitting primary recoil spectrum so that the fraction of damage produced by recoils with the energy greater than given is very close to that of DEMO reactor.

Spectral shifter materials should withstand significant radiation and thermal loads being able to effectively modify neutron spectrum. Tungsten was selected as a spectral shifter material due to its high melting temperature, good thermal conductivity as well as good neutronics properties such as high scattering ability. The further sections describe the selection of the optimal geometry of spectral shifter plates (position, width) with the aim to reproduce DEMO irradiation conditions at creep-fatigue testing machine and tritium release module as close as possible (details are available in [10]).

4.1. Various positions of spectral shifter plates

Two tungsten spectral shifter plates positioned in front and behind the creep-fatigue testing machine (CFTM) were proposed for the adjusting of the primary knock-on atom spectrum at in situ creep-fatigue samples. Previous neutronics calculations showed that an adjusted spectrum perfectly matches that of the DEMO reactor at the first wall position.

Later during preliminary engineering design it was recognized that two plates would require too much design efforts and space for their cooling and temperature monitoring. Therefore designers suggested placing one plate of double width behind the CFTM. This part of the task is aimed at the study of consequences of such disposition for the change of irradiation conditions at CFTM and tritium release module (TRM).

Several geometry variants differing by the width and placement of tungsten spectral shifter plates were considered (see Figs. 5 - 9 and Table 3).

Table 3. Description of geometry variants.

Variant	Position relative to CFTM	Width, cm	Figure
md39	behind	6.4	5
md40a	in front	6.4	6
md40b	in front	3.2	7
md40c	behind	3.2	8
md40d	in front & behind	3.2	9

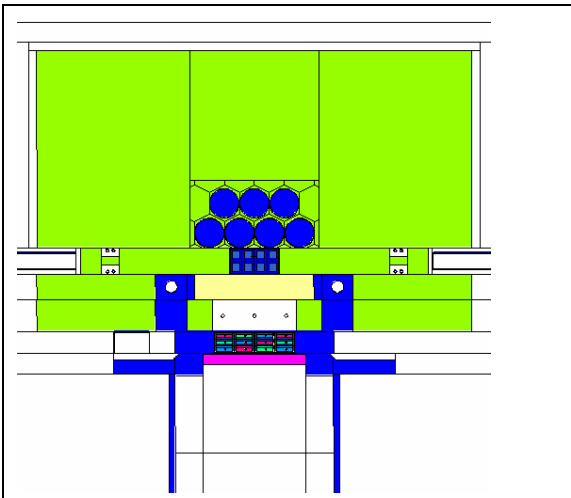


Figure 5. Double width plate (6.4 cm) behind CFTM: md39

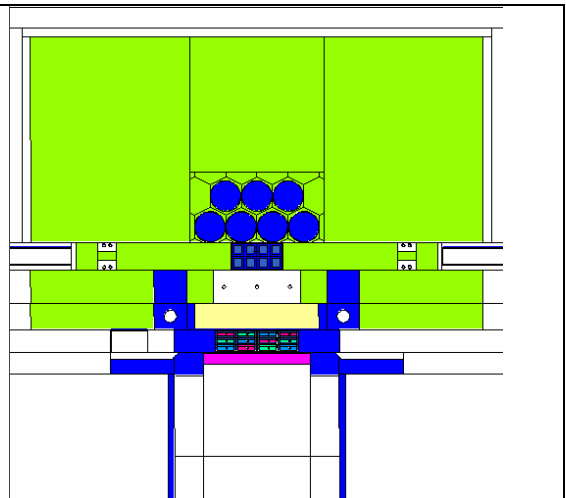


Figure 6. Double width plate (6.4 cm) before CFTM: md40a

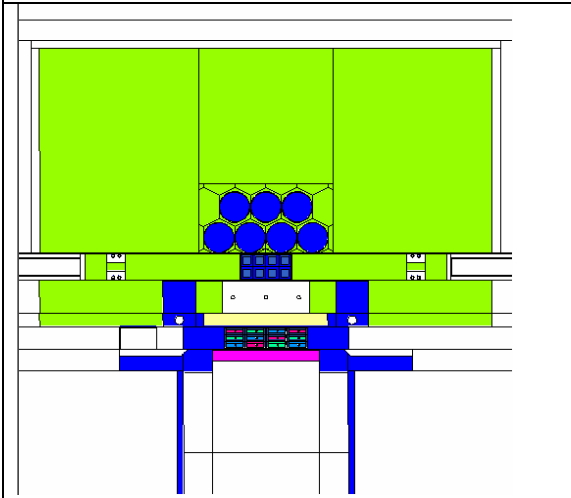


Figure 7. Half width plate (3.2 cm) before CFTM: md40b

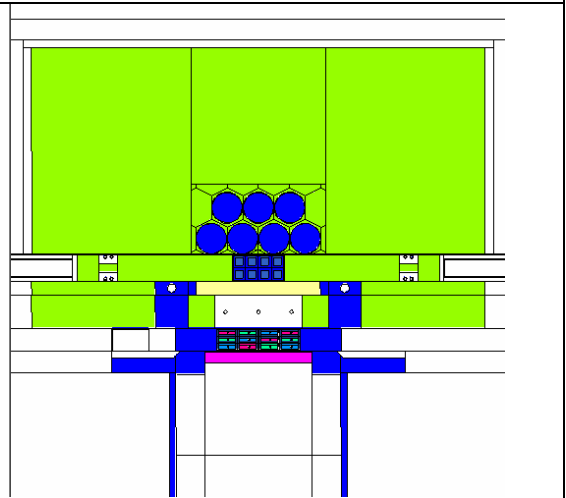


Figure 8. Half width plate (3.2 cm) behind CFTM: md40c

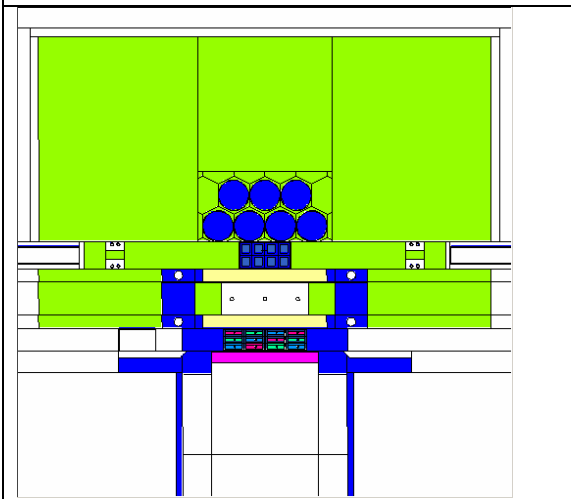


Figure 9. Two half width plates (3.2 cm) before and behind CFTM: md40d

Comments to Figures 5 - 9:
 plot origin (0, 0, 24.5 cm)
 plot scale (60, 60 cm).

4.2. Neutron spectra, damage and gas production at CFTM

Neutron transport calculations were performed using McDeLicious-05 code with an updated version of the evaluated d-Li reaction cross sections. The obtained neutron spectra for the discussed above IFMIF geometry variants and DEMO reactor are presented in Figure 10. The effect of the width of the spectral shifter plate positioned in front of CFTM is clearly visible as a change of the shoulder height in the range 1 - 20 MeV. This part of the neutron spectrum is effectively shifted to the low neutron energy by the tungsten plate.

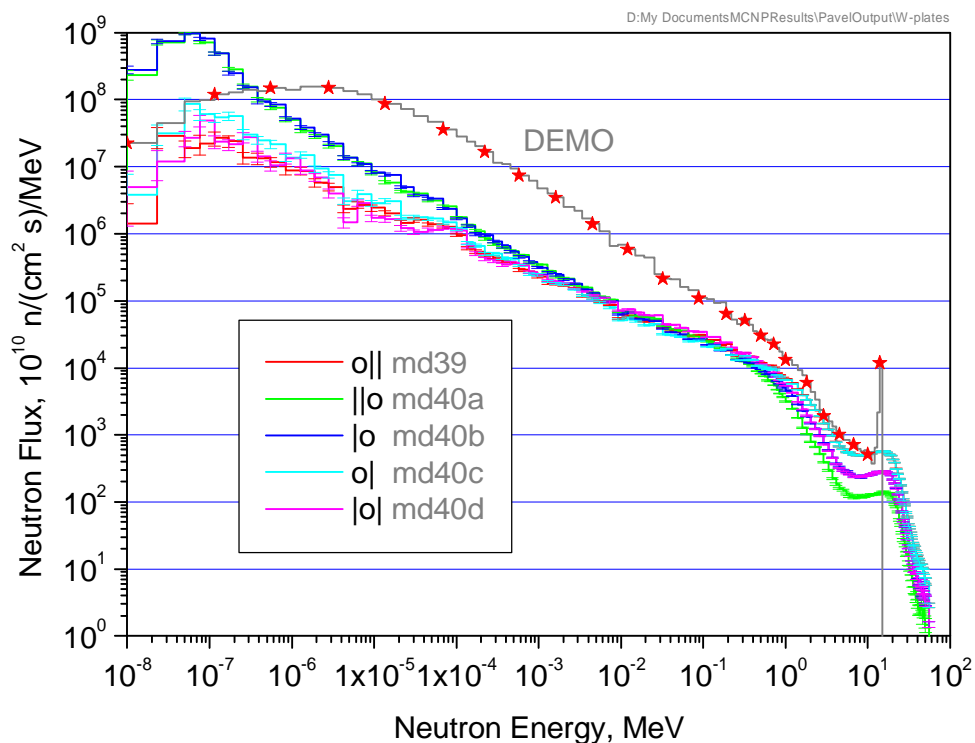


Figure 10. Differential neutron spectra at CFTM position in comparison with the DEMO First Wall spectrum.

The plate placed behind the CFTM reflects neutrons back further decreasing neutron flux available at TRM. The efficiency of thermal neutron absorption slightly increases with the plate thickness (cf. md39 and md40c). Damage and gas production rates in iron located inside the central creep-fatigue specimen are collected in Table 4.

Table 4. Iron irradiation conditions for the central creep-fatigue specimen (cell 5021) at CFTM.

Variant	Flux, 10^{14} n/cm ² /s	Damage, dpa/fpy	He appm/fpy	H, appm/fpy
md39	3.33	11.76	75.4	215.2
md40a	1.81	3.50	18.4	52.3
md40b	2.30	6.26	37.2	106.0
md40c	3.16	11.64	75.4	215.1
md40d	2.53	6.48	37.2	105.9

As could be expected very similar results were obtained for the variants with full (md39) and half-width (md40c) W-plates behind CFTM. The plates placed in front of the CFTM gradually decrease damage and gas production rates with increasing plate thickness. Qualitatively similar results were obtained during preliminary study performed before the availability of the global geometry IFMIF model [Report TW0-TTMI-003-D10, 2002]. The results of damage rate in beryllium placed at TRM are presented in Table 5.

Table 5. Beryllium irradiation conditions at the first row of TRM.

Variant	Flux, n/cm ² /s	Damage, dpa/fpy
md39	9.73×10^{13}	3.23
md40a	1.33×10^{14}	2.76
md40b	1.69×10^{14}	3.74
md40c	1.81×10^{14}	4.22
md40d	1.32×10^{14}	2.91

Differential primary recoil spectra are qualitatively similar to that for DEMO First Wall (see Fig. 11). Considerable difference is observed only at energies lower than 300 eV.

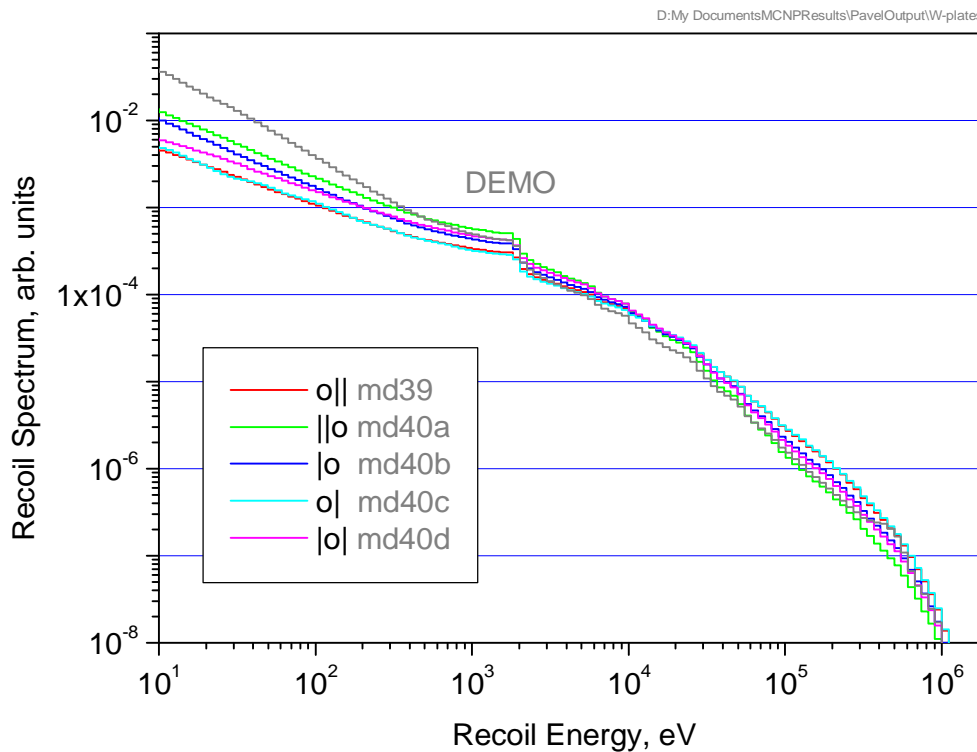


Figure 11. Differential recoil spectra at CFTM position for various geometry configurations versus DEMO First Wall recoil spectrum.

However, even a small difference in the high-energy portion of the spectrum could result in substantial change of radiation damage rates. For example, damage produced at the central creep-fatigue sample varies in the range from 3.5 up to 11.8 dpa/fpy. It can be seen from

Table 3 that maximum damage rate at CFTM is obtained for the variants (md39, md40c) where tungsten plates are placed behind CFTM. For the plate of full-width the damage rate is slightly larger than that for the half-width due to the more effective neutron backscattering from the thicker plate.

It is expected that damage at TRM decrease with the width of W-plates placed in front of TRM. Indeed, thick tungsten plate noticeably reduces damage rate at TRM (cf. 3.50 dpa/fpy for the full-width plate (md40a), 6.26 dpa/fpy for the half-width plate (md40b) and 11.64 dpa/fpy for the half-width plate placed behind CFTM (md40c)). In contrary, damage rate for the variant with half-width plate behind CFTM (md40.c) is even slightly higher than for the variant without W-plates (fw21.6) from our previous study. It might be related to the presence of the extended carbon reflector in variants considered in the present report.

Fraction of damage produced by recoils with an energy greater than given energy T , so called $W(T)$ function, is plotted in Figure 12. It can be seen from the Figure that good approximation to the DEMO curve is provided by the variants md39, md40c and md40b.

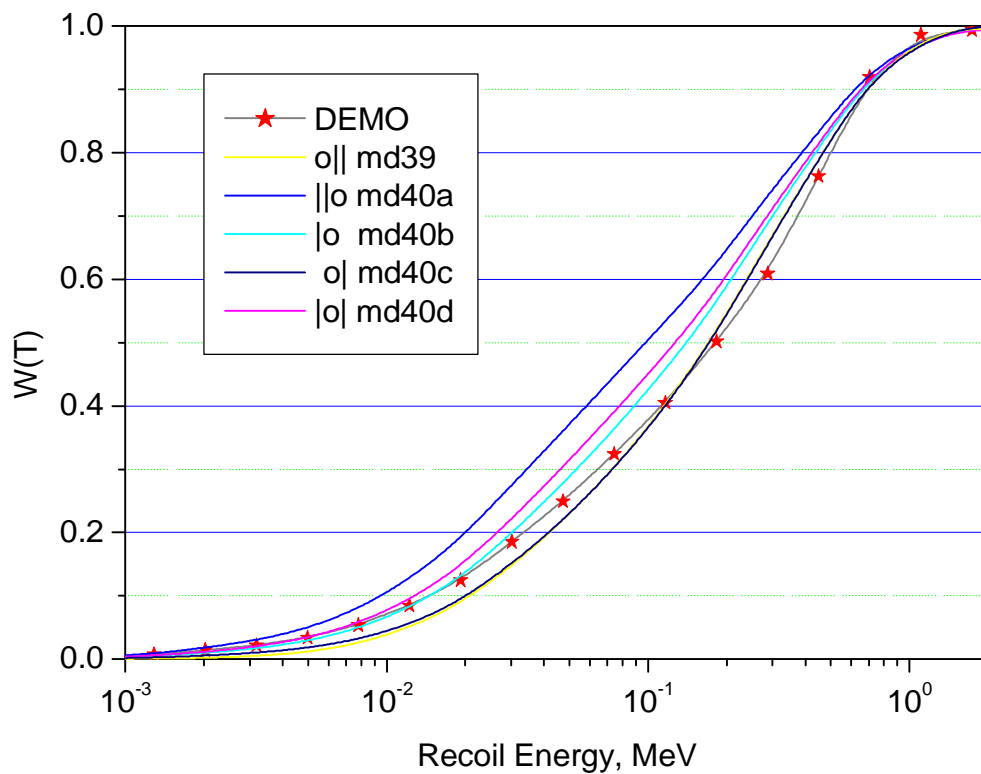


Figure 12. Fraction of damage produced by recoil with energy greater than given for various geometry configurations.

Conclusions

The nuclear responses in the tungsten under irradiation parameters for 4000 MW power reactor with helium cooled lithium lead blanket have been calculated. To reproduce them in the IFMIF facility the relevant calculations have been performed at several locations: inside the High Flux Test Module (HFTM) and its lateral neutron reflector, between the pull-push rods of the Universal Test Machine (UTM), in the lithium target flange and inside deuteron beam vacuum tube. The calculations have been performed by the McDeLicious code using a detailed 3-d geometrical model of the entire IFMIF test cell. In this approach the recently

updated d-Li evaluated cross section data and high energy neutron transport cross sections from LA-150, ENDF/B-VI and FZK/INPE-50 libraries were employed.

The comparison of the tungsten nuclear responses has shown that the atom displacement damage rate (dpa) inside UTM and HFTM is 1.5 - 4.5 times higher than for the fusion power reactor divertor and is comparable in the cases of the HFTM lateral reflector. The gas-to-dpa production ratio for tungsten irradiated there, however, exceeds that of the fusion power reactor divertor by several times due to the IFMIF neutron spectrum which extends above 14 MeV. Desirable ratio could be obtained in deuteron beam tube, but dpa rate there drops by one order of magnitude below fusion one. Some kind of compromise could be reached in the lithium target flange, where dpa under- whereas gas-to-dpa ratio over-rate the fusion levels by factor of 2-3.

The comparison of the nuclear responses calculated with different evaluated cross sections files (ENDF-B6 and FZK-04) reveals the spread of 3 - 40%.

If a degree of approximation of $W(T)$ is considered to be the major criterion for recoil spectra optimization together with the damage rates at CFTM and TRM, than the variant with half-width tungsten plate located behind CFTM (md40c) seems to be the most preferable one. It provides similar damage level at CFTM as the variant with full-width plates and the highest damage rate in beryllium irradiated at TRM.

Literature:

1. IFMIF Comprehensive Design Report by IFMIF International Team, The International Energy Agency, January 2004.
2. A. Moeslang, V. Heinzl, H. Matsui, M. Sugimoto, The IFMIF test facilities design, *Fus. Eng. Des.*, 81 (2006) 863-871.
3. U. Fischer, Y. Chen, S.P. Simakov, P.P.H. Wilson, P. Vladimirov, F. Wasastjerna, Overview of recent progress in IFMIF neutronics, *Fus. Eng. Des.* 81 (2006) 1195-1202.
4. S.P. Simakov, U. Fischer, A. Möslang, P. Vladimirov, F. Wasastjerna, P. Wilson, Neutronics and activation characteristics of the International Fusion Material Irradiation Facility, *Fus. Eng. Des.* 75-79 (2005) 813-817.
5. S.P. Simakov, U. Fischer, U. von Möllendorff, I. Schmuck, A. Konobeev, P. Pereslavl'tsev, Advanced Monte Carlo Procedure for the D-Li Neutron Source Term Based on Evaluated Cross-Section Files, *J. Nucl. Mat.* 307-311 (2002) 1710-1714.
6. U. Fischer, M. Avrigeanu, P. Pereslavl'tsev, S.P. Simakov, I. Schmuck, Evaluation and Validation of D-Li Cross-Section Data for the IFMIF Neutron Source Term Simulation, *Proc. of ICFRM-12* (in print).
7. Yu. Lizunov, A. Möslang, A. Ryazanov and P. Vladimirov, New evaluation of displacement damage and gas production for breeder ceramics under IFMIF fusion and fission neutron irradiation, *Journ. Nucl. Materials* 307-311 (2002) 1680-1685.
8. U. Fischer, P. Pereslavl'tsev, Neutronic Analyses for the Conceptual Design of a HCLL Reactor, Final report on the EFDA Task TW4-TRP-002, Deliverable 2a, Karlsruhe, March 2005.
9. P. Pereslavl'tsev, U. Fischer, Evaluation of n + W cross section data up to 150 MeV neutron energy., *AIP Conference Proceedings* v. 769 (2005) 215.
10. S. Gordeev, V. Heinzl, A. Möslang, S. Simakov, E. Stratmanns, P. Vladimirov, IFMIF - Design study for the in situ creep fatigue tests, Symposium on Fusion Technology (SOFT-24), Warsaw, September 2006.

PUBLICATION VIII

**Calculating the neutron current
emerging through the beam tubes
in IFMIF**

(EFDA Task TW6-TTMI-001-D3a).
VTT Research Report 2006. 9 p.
Reprinted with permission from the publisher.



Calculating the neutron current emerging through the beam tubes in IFMIF (EFDA Task TW6-TTMI-001-D3a)

Authors Petri Kotiluoto, Frej Wasastjerna

Confidentiality: Public



Report's title Calculating the neutron current emerging through the beam tubes in IFMIF	
Customer, contact person, address Tekes, National Technology Agency, Juha Linden, Kyllikinportti 2, P.O. Box 69, FI-00101 Helsinki, Finland	Order reference 40480/05
Project name Neutroniikkalaskut IFMIF/ITER	Project number /Short name 3074 / NEUT06
Author(s) Petri Kotiluoto, Frej Wasastjerna	Pages 7
Key words fusion, IFMIF, neutronics, beam tubes	Report identification code VTT-R-06720-06
<p>Summary</p> <p>This is a report on behalf of the Association Tekes for the EFDA task TTMI-001-D3, sub-deliverable 3a “Neutron field and dose rate evaluation in the components of the raster beam scanner system (mainly magnets) as a function of their distance to the Target. Neutron field evaluation.” This task is in connection with further analysis of the raster beam scanning of the IFMIF accelerator facilities. The work has been carried out in collaboration with Association UKAEA, whom will be responsible for the deliverable 3b “Dose rate evaluation.”</p> <p>In this work we have aimed at calculating the neutron current in the form of a surface source at the outer surface of the IFMIF “near wall”, the wall containing the beam tubes. This surface source can then be utilised by UKAEA to calculate the neutron flux and activation in the accelerators and their surroundings, using MCNP. Our calculations have been based on earlier McDeLicious model md34 of the IFMIF, which is not the latest model, but differences were estimated to have only marginal and at least conservative effect to the neutron field distribution along the beam tubes. The results and a data path to the created surface source file have been delivered to UKAEA.</p>	
Confidentiality:	Public
Espoo 06.09.2006 Signatures	
Timo Vanttola, Technology Manager	Petri Kotiluoto, Principal Investigator
VTT's contact address Otakaari 3 A, Espoo, P.O. Box 1000, FI-02044 VTT, Finland	
Distribution (customer and VTT): Juha Linden (Tekes), Angel Ibarra (EFDA), Rainer Lässer (EFDA), Michael Loughlin (UKAEA), Ulrich Fischer (FZK), Elizabeth Surrey (JET), Seppo Karttunen (VTT)	
<p><i>The use of the name of the Technical Research Centre of Finland (VTT) in advertising or publication in part of this report is only permissible by written authorisation from the Technical Research Centre of Finland.</i></p>	

Contents

Introduction	3
Model	3
Full Geometry: Variance Reduction	4
Full Geometry: Runs	5
Reduced Geometry	6
Summary of Results	6
Conclusions	8
Acknowledgements	8

Introduction

This work is part of the effort to determine the activation of the accelerators and adjacent structures in IFMIF. One source of activation will be the neutrons emerging from the test cell, mainly along the beam tubes. Thus we aimed at calculating the neutron current in the form of a surface source at the outer surface of the “near wall”, the wall containing the beam tubes. This surface source can then be utilised to calculate the neutron flux and activation in the accelerators and their surroundings, using MCNP.

The source was accumulated at surface 8099, defined as pz -453.0 in the model.

For reasons which will be described below, two series of calculations were performed, which we will call the full geometry and reduced geometry calculations. In the former, most of the test cell was included, with neutrons killed only in the outer parts of the floor, cover and the walls other than the near wall. In the latter, only a small part of the geometry was included, consisting mainly of portions of the target and the beam tubes, with neutrons killed everywhere else.

All tallies were normalized to a beam current of 250 mA using an fm card, but the surface sources are normalized to a single incident deuteron.

Model

Our calculations were performed using the program McDeLicious, a variant of MCNP4C developed at FZK with a source routine capable of calculating the neutrons emerging from the interaction of deuterium beams with a lithium target.

The geometry model we used was that contained in the McDeLicious input file md34. This is not the latest model for IFMIF, but the only respect in which it is not up to date is that certain dimensions of the shield blocks in the cover have been modified since md34 was prepared. This cannot influence the current emerging through the beam tubes significantly. Since the later models have a different cell structure at the edges where the cover meets the walls, a cell structure that is more appropriate for shielding calculations on the cover but less appropriate for calculations on the walls, we decided that md34 was more suitable for this work.

The horseshoe shield is present in md34. It is not known to us whether it will actually be included in IFMIF, so we could either have kept it in the model or omitted it. Keeping it was adjudged to be the more conservative assumption, since this was expected to reflect slightly more neutrons in the direction of the near wall. Therefore we kept it, using a design with 30 cm W and 10 cm B-Cd mixture. In any case, the presence or absence of the horseshoe shield is unlikely to make a significant difference (it makes none at all in the reduced geometry calculations).

For this work, the details of the beam tubes are much more important. In md34, the beam tubes are assumed to be rectangular in cross section, with an inside height of 7.5 cm and an inside width of 28 cm. The walls are modelled as 3 cm thick Eurofer steel, with a density of $2/3$ of nominal. This is a homogenized version of an assumed structure of 1 cm steel + 1 cm void + 1 cm steel. The tube walls are surrounded by heavy concrete.

The homogenization of the tube walls ignores the possibility of neutrons streaming along the gap between the two wall layers. However, this streaming is bound to be a minor effect compared to the streaming through the tube. A much more important question than this gap streaming is the accuracy of the underlying assumptions about the beam tube geometry. We have not succeeded in obtaining reliable information about this, which probably reflects the fact that the IFMIF design is not final but may still change. Thus we have to base our calculations on what seems plausible, and this rectangular beam tube geometry does seem plausible. In any case it makes much better sense from a neutronics viewpoint than a circular cross section, since it's important to minimize neutron streaming by making the beam tube walls fit as snugly around the beams as possible.

The input files used in this work (having names beginning with nw34, nw standing for "near wall") specify that a surface source be written at the outer surface of the near wall. The tallies include two current tallies at the same surface. One is segmented to separate the current emerging from the beam tubes from that emerging from their surroundings and is also subdivided into 211 energy bins and 5 cosine bins. The other lacks cosine bins and has only 3 energy bins, but all neutrons entering the tube walls are flagged. There is also a volume flux tally showing the flux in the beam tubes themselves as a function of position.

Full Geometry: Variance Reduction

We have two straight beam tubes, pointing directly at the neutron source. Moreover, they are large enough that every point in the beam footprint in the lithium jet can see the outer end of the tube directly, without intervening material. Thus one can expect neutrons coming directly from the source and streaming through the beam tubes to be the dominant component of the outgoing current. Other contributions will come from neutrons scattered in the test modules or other components, neutrons hitting the beam tube walls and scattering in the outgoing direction, and neutrons passing through the concrete wall (at least partway, perhaps also streaming along the beam tubes for part of their trajectory).

Accordingly, we needed to emphasize transport through the beam tubes. Angular biasing of the source or DXTRAN might have been the most effective ways of doing this, but both would have required modification of McDeLicious, so we preferred to try other means. Thus we had to rely mainly on importances.

Since MCNP, and consequently McDeLicious, doesn't split particles in voids (which would be pointless), importances could not be used to emphasize uncollided transport through the beam tubes directly, only indirectly by rouletting neutrons in regions far from the near wall. Consequently we used decreasing

importances with increasing distance from the near wall: 1 in the source region and High-Flux Test Module, 0.5 in the Universal Testing Machine, 0.25 in the Spectral Shifter, 0.125 in the In-Situ Tritium Release Experiment and the low-flux and very low flux module and 0.025 on the insides of the walls and cover, other than the near wall. Neutrons venturing more than a short distance into the walls and cover (about 20 to 40 cm, depending on location) were killed.

In addition, importances increasing in the outward direction were used in the tube walls to ensure that neutrons colliding in them would contribute to the surface source and tallies. In the concrete surrounding the beam tubes we sometimes used importances lower than in the tube walls, typically by a factor of 4, but also increasing outward. At the edges where the walls join the cover, the neutrons were mostly killed, since in this area it is especially difficult to devise satisfactory importance schemes, and these neutrons do not make a significant contribution.

In short test runs (60 minutes CPU time), several different importance schemes worked, and the differences in efficiency were fairly small. The best schemes increased the figure of merit by about a factor of 2.5 over setting the importance to 1 everywhere.

Full Geometry: Runs

When we tried to perform production runs, we kept encountering a situation where the program hangs, running for hours or days without producing any output, including dumps. We have encountered such behavior many times before and attributed it to “long histories”, in which a single history can sometimes proliferate into a very large number of tracks, taking essentially unlimited amounts of time. We initially assumed that that was the cause in this case too, though we did have some doubts.

In an attempt to avoid occurrence of long histories, cell-by-cell energy cut-offs with the ELPT card were tried, in order to kill those thermal or epithermal neutrons further away from the region of interest with no probability to contribute to the tallies. Also analog capture was tried instead of implicit capture. However, neither of these methods solved the problem and they were therefore abandoned.

Shorter runs worked in some cases. One run with 7,500,000 histories gave a surface source file containing 127,338 tracks, but we suspect that most of these are low-weight tracks, due to neutrons splitting in the tube walls or concrete. Probably the most important component is neutrons coming directly from the source or colliding near it and then flying out through the beam tubes without further collisions. Both analytical estimates and an investigation of the tally probability density function plot for tally 1 suggest that there may have been about 1,200 to 1,500 of these tracks, with the remaining 99% of the tracks giving just a minor contribution.

A new run was made with the importances adjusted to minimize this worthless fuzz. 7,104,165 histories gave 3,073 tracks, probably a more useful source file in spite of the small number of tracks.

The statistics of these semi-successful runs are fairly decent, with the results in the tally fluctuation chart bins passing most statistical tests. However, a much larger number of high-weight tracks in the surface source file would be desirable.

Reduced Geometry

In the full geometry calculations, many histories waste a lot of time wandering around in the complicated geometry of the test modules, and these make a relatively modest contribution to the emerging current, while the most important contribution comes from the source neutrons emerging directly through the beam tubes. This had already been taken into account to some extent in the choice of importances, but Dr Ulrich Fischer proposed something more radical: including only this direct source contribution and ignoring the scattered neutrons, for the sake of getting as many histories as possible in reasonable time. Consequently we prepared an input file with the importances set to zero – killing all neutrons – everywhere except in the target, the beam tubes and a few cells between and around these.

In such a geometry, with all importances set to 0 or 1, there was no way of getting the proliferation of tracks we had assumed to be the cause of hanging runs. Nonetheless we were plagued by hanging runs, even worse than before. Dr Stanislav Simakov found that the cause lay in the source subroutine of McDeLicious. He then corrected this subroutine and kindly performed a run with 10^9 histories, resulting in a surface source of 122,836 tracks.

Summary of Results

We believe that the surface source file resulting from Dr Simakov's calculation is the most useful one. 122,836 high-weight tracks may be sufficient to provide useful results, while 3,073 would most likely be too few and the original 127,338 track file is believed to contain mostly useless low-weight tracks. However, we must take into account that the reduced geometry calculation accounts for only the unscattered, direct contribution from the source plus neutrons scattered in the target or beam tube walls but not elsewhere.

We recommend applying two correction factors to the results obtained using Simakov's surface source. These factors are based on a comparison of tallied currents emerging from the near wall in the full geometry and reduced geometry cases. Even in the full geometry case, the statistics of this tally were good enough to permit reasonably accurate calculations of such correction factors.

The scattering factor accounts for the contribution from neutrons scattered both in the test cell internals (test modules etc.) and in the near wall outside the beam tubes. This is calculated as the ratio of the average outgoing current at the mouth of the beam tubes as calculated in a full geometry run (row 3 of Table 1) to that from a reduced geometry run (row 4). The appropriate value to use is that for the average of both beam tubes, 1.81442.

Table 1: Outgoing neutron current ($\text{cm}^{-2}\text{s}^{-1}$) at the mouth of the beam tubes, cosine bin -1 to -0.879, all energies

	Left beam tube		Right beam tube		Average
	tube	fsd	tube	fsd	
Analytical estimate					5.14125E+10
Full geometry, run 1	6.72721E+10	0.0369	6.80305E+10	0.0369	6.76513E+10
Reduced geometry	3.71981E+10	0.0042	3.73725E+10	0.0042	3.72853E+10
Ratio full / reduced	1.80848		1.82034		1.81442

Note that, although the currents in Table 1 are totals over energy, only one cosine bin, from -1 to -0.879 (-1 is the outgoing surface normal for the near wall) is included. However, the contributions from other bins are small, totaling about 2% of the contribution from the -1 to -0.879 bin.

Table 1 also shows an analytical estimate of the current, as a sanity check. This is based on the assumption that the source is isotropic and no neutron scattering occurs. The latter assumption also applies in the reduced geometry calculation, so we can see that the anisotropy of the source reduces the current by somewhat more than a quarter. The presence of scattering more than compensates for this.

The other correction factor is the wall penetration factor, which accounts for the fact that some neutrons emerge elsewhere than the beam tube mouths. Transforming the currents from tally 1 in the full geometry case into integrals rather than averages over the spatial segments and dividing the sum of these integrals by the sum over the beam tube mouths gives a factor of 1.11475.

Multiplying these two correction factors together gives a factor of **2.02263** which should be applied to responses calculated using Simakov's surface source. Multiplying this by the beam current factor, 1.56055×10^{18} deuterons per second, gives a total normalization factor of 3.15641×10^{18} .

These correction factors only account for the difference in the total current, they do not consider the differences in the spectrum or angular or spatial distribution, which would be more difficult to take into account. The true spectrum is softer than in the reduced geometry case, due to scattering. (In the full geometry calculation, 89% of the outgoing neutrons had energies above 0.1 MeV vs. 97% for the reduced geometry case. In both cases, neutrons above 20 MeV were rare.) The true angular distribution is likely to be slightly more spread out. So is the spatial distribution of the points where the neutrons emerge from the wall. Whether these effects will increase or decrease the responses to be calculated can be estimated only with knowledge of the accelerator design, the reactions of interest and the energy dependence of their cross sections, and other matters which we do not know. It may be advisable to carry out a calculation with the 3,073-history full geometry surface source as well as Simakov's reduced geometry source and compare the two.

Experience from ITER calculations suggests that in order to keep the dose rate 10^6 seconds (about 11.5 days) after shutdown below the limit of 100 $\mu\text{Sv/h}$ the flux above 0.1 MeV should not exceed about 10^7 $\text{n/cm}^2\text{s}$ during operation. The flux at the outer ends of the beam tubes is about 4 orders of magnitude higher, suggesting

a dose rate of **1 Sv/h**, 10,000 times what is considered permissible for hands-on maintenance in ITER. However, it must be realized that this dose rate would apply only at local hot spots. The dose rate averaged over some large volume will be substantially lower, and it may be possible to shield workers from the radiation emitted by the hot spots.

Conclusions

We have attempted to provide a surface source for calculations of activation and other phenomena caused by neutrons exiting the IFMIF test cell through the beam tubes. These attempts have been plagued by difficulties that we first believed to be caused by long histories. However, it was finally realised that there seemed to be a bug in McDeLicious, related to a problem of neutron birthplace identification. This bug was fixed by Dr. Stanislav Simakov, who also performed the final reduced geometry production run with $1.0 \cdot 10^9$ deuteron histories, producing 122,836 neutron tracks for the surface source file. Results derived using this file need to be corrected by a factor of about 2.02, however. Moreover, a comparison of results obtained with the reduced geometry surface source file (with the correction factor) and one or more of the full geometry source files (without a correction factor) is desirable, although the full geometry sources have poor statistics.

While calculating dose rates falls outside the scope of the work reported here, the high flux at the outer ends of the beam tubes is a cause for concern.

Acknowledgements

We are very grateful for the prompt and competent measures taken by Dr. Simakov to correct the bug found in McDeLicious. He also kindly performed the final production run for us.

This work, supported by the European Communities under the contract of Association between EURATOM/Tekes, was carried out within the framework of the European Fusion Development Agreement. The views and opinions expressed herein do not necessarily reflect those of the European Commission.

PUBLICATION IX

**A study of variance reduction
methods in MCNP4C in a slot
with a dogleg**

12th Biennial Topical Meeting of the Radiation
Protection and Shielding Division of the American
Nuclear Society. Paper 14. Santa Fe, NM, USA 2002.
11 p. Copyright 2002 by the American Nuclear
Society, La Grange Park, Illinois 60526, USA.
Reprinted with permission from the publisher.

A STUDY OF VARIANCE REDUCTION METHODS IN MCNP4C IN A SLOT WITH A DOGLEG

Frej Wasastjerna
VTT Processes
P.O. Box 1604
FIN-02044 VTT, FINLAND
+358 9 456 5021
frej.wasastjerna@vtt.fi

SUMMARY

Streaming calculations may be very challenging. This paper studies the performance of various methods of generating weight windows in a particular kind of streaming problem that is common in fusion neutronics work, involving a planar gap or slot with a dogleg. The weight window generator of MCNP4C is found to be useful, even when manual adjustment of the generated weight windows is impracticable. The exponential transform and forced collisions are also studied and found to help a little.

I. INTRODUCTION

The current design of the ITER experimental fusion reactor includes a large number of ports

in which various kinds of plugs will be inserted. For technical reasons, there must be a gap of a few centimeters between these plugs and the surrounding port walls. Even though there is a dogleg in this gap, streaming through it is the dominant contributor to the radiation at the end of many ports. Calculating radiation levels at these locations is very difficult and time-consuming, so there is an incentive to study ways of making these calculations as efficient as possible. This paper describes an attempt to study the efficacy of various variance reduction methods in MCNP4C.¹

A simple two-dimensional model was set up, see Fig. 1.

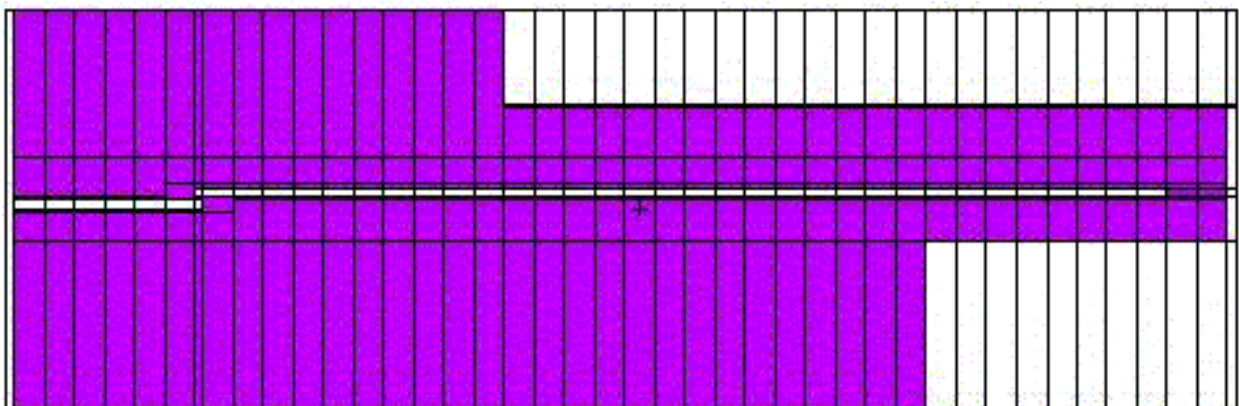


Figure 1. PY cut of geometry.

This is a two-dimensional geometry, homogeneous in the y direction and with reflecting boundary conditions at the y boundaries. In the z direction

(vertical in the figure) the extent is 99 cm; in the x direction the material, a mixture of 80% stainless steel and 20% water, extends for 302 cm with a 2

cm void, containing a source of 14 MeV neutrons, on the left and another 2 cm void for tallying purposes on the right. The gap running through the geometry is 2 cm thick, with an offset of 3 cm at the dogleg. In addition to the y boundaries, reflecting boundary conditions were also used at the left x boundary and at the bottom, with vacuum at the right and top.

This geometry, partly based on a model developed by H. Iida, is much easier to calculate than actual ITER port geometries but is nonetheless

sufficiently similar to actual equatorial ports to be useful for studies of streaming.

The geometry shown in Fig. 1 has a cell subdivision designed to be used with cell-based weight windows and possibly other variance reduction techniques such as forced collisions. Since Fig. 1 is smeared by the file conversions required to include it in this paper, Fig. 2 is included to show the geometry at the right end in more detail, clarifying the tally cell structure. This figure shows the geometry used in calculations with mesh-based weight windows.

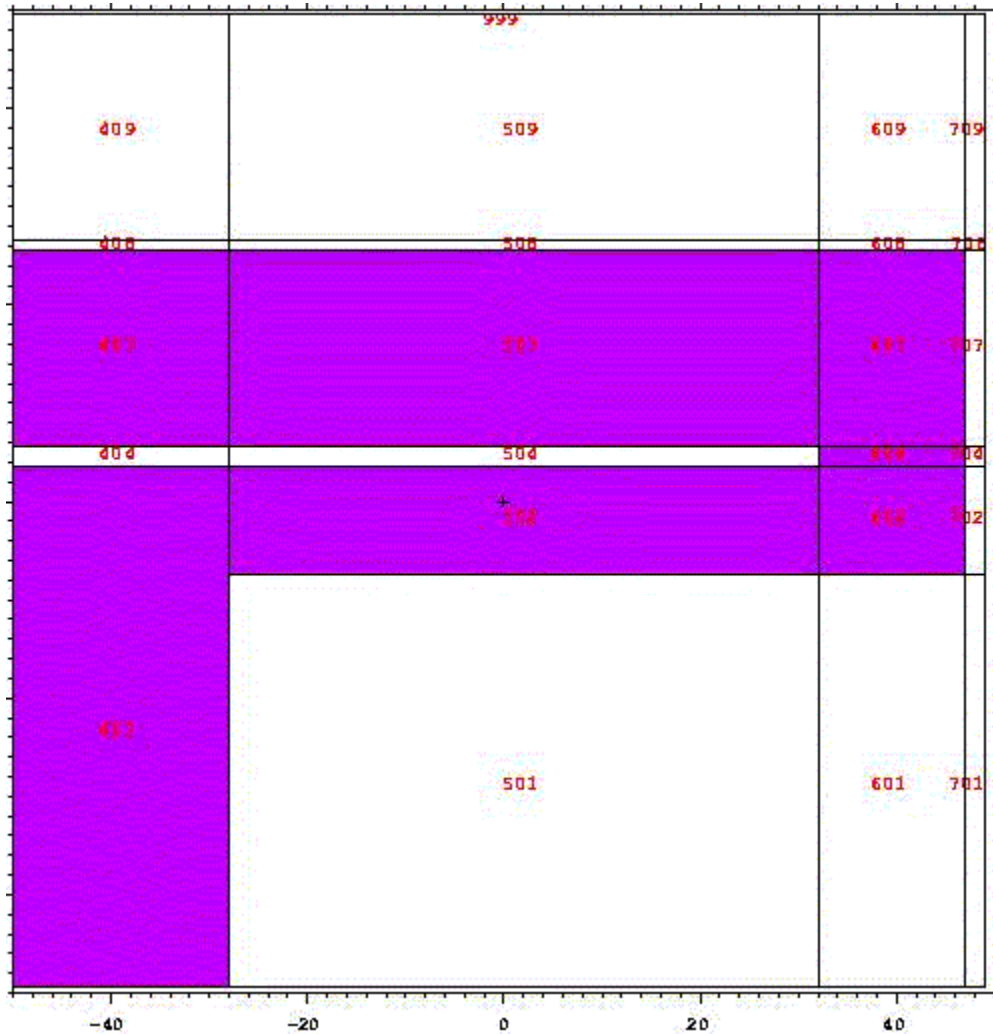


Figure 2. Detail of the right part of the geometry.

Fluxes were tallied in the following locations:

- In the flange at the end of the gap (cell 604 in Fig. 2; this is the thin cell right of cell 504)
- In the cavity at the right end of the plug: cells 501 and 601
- Above the port: cells 408 (which extends all the way to the vacuum vessel, the solid zone at the top in Fig. 1), 508 and 608
- At the right end: cells 701, 702, 704, 707, 708 and 709

Since the critical quantity driving the shield design for ITER is the gamma dose rate 1,000,000 seconds after shutdown, the ultimate goal in the calculations here was to calculate the gamma flux. In this work it was the prompt gamma flux, but presumably the performance of the variance reduction methods used would be the same in calculations on delayed gammas, regardless of whether the “direct 1-step method” of Iida et al.^{2,3} or the “rigorous 2-step method” of Fischer et al.⁴ is used.

Therefore we were primarily interested in the precision of the gamma flux, but since this requires quite lengthy calculations and is primarily determined by the neutron flux above 1 MeV, we also paid attention to the fast neutron flux, which is much easier to calculate.

The main interest here is concentrated on estimating appropriate weight windows. The use of the exponential transform and forced collisions is also explored, but this is shown to give only minor benefits.

In most cases we first tried to establish weight windows for fast neutrons and then to extend these to slower neutrons and photons. The alternative method of starting directly with coupled n,p calculations was also tried. Both cell-based and mesh-based weight windows were used, though with more emphasis on cell-based methods.

The weight window generator of MCNP4C was used heavily in these calculations. The user’s manual stresses that the generated weight windows should not be used uncritically, since they are stochastic in nature and often based on poor statistics, but should be examined and corrected. This advice is well justified, but unfortunately it is often impracticable. In a calculation with many thousands of cells, examining and adjusting the weight windows requires many days of work, which may moreover have to be repeated, since weight windows may have to be generated in many steps. Thus it may be necessary to rely on unadjusted weight windows. For that reason the weight windows were used without manual adjustments in these calculations.

II. CELL-BASED WEIGHT WINDOWS, FAST NEUTRONS

The first calculations were performed in the geometry shown in Fig. 1, where the material zones were subdivided by splitting planes at

intervals of about 7.5 cm, in the expectation that this would be the approximate halving length of the fast neutron flux. First we tried to estimate weight windows in a single step, below called the “direct” method, choosing starting importances on the basis of engineering judgment and putting the tally cell for the weight generator in or near the part of the geometry where the tallies of interest are located. We also tried the alternative “progressive” method of starting with constant importances and first generating weight windows for a tally cell fairly near the source, then using these to reach a tally cell slightly farther on and so on until the region of interest is reached.

A. Direct Weight Window Generation

In the direct method, the starting importances were chosen with the objective of keeping the track density approximately constant with increasing distance from the source. Near the source this involved a doubling of the importance for each cell layer. For use farther from the source, where streaming becomes dominant, we also calculated importances inversely proportional to the solid angle subtended by either the entrance to the gap or the entrance to the part of it lying beyond the dogleg. For each x interval, the smaller of these importances was used, rounding downward to the nearest power of 2. These importances were then modified in the z direction to emphasize streaming along the gap, then to drive the neutrons out towards the tally cells, but these modifications were rather modest.

Based on this calculation of the fast neutron flux, weight windows were generated either for a tally cell located at the end of the gap (the left half of cell 604 in Fig. 2) or for a composite cell comprising all the **other** tally cells. The resulting weight windows were then used in further calculations. The results are given in Table 1, where the original calculation is denoted a0, the calculation with weight windows based on the left half of cell 604 in Fig. 2 is called a1 and the one with weight windows derived for the composite cell is a2.

Since the real quantity of interest is the fractional standard deviation (**fsd**) and the figure of merit (**fom**), the actual fluxes have been omitted to avoid cluttering up the tables. The outcomes of the numerous statistical tests included in MCNP4C have also not been included, though they were studied. The conclusions from them were broadly consistent with those that can be drawn from the fractional standard deviations. The figures of merit

shown are in each case for the first tally cell in the mentioned part of the geometry, i.e., for cells 604, 501, 408 and 701.

All cases shown in Table 1 involved 20,000,000 histories.

Table 1. Fractional Standard Deviations and Figures of Merit for Fast Neutron Calculations, Direct Method; 20,000,000 Histories

	case	a0	a1	a2
	cell	fsd	fsd	fsd
flange	604	0.0215	0.0160	0.0159
cavity	501	0.0182	0.0273	0.0152
	601	0.0187	0.0199	0.0148
above port	408	0.0115	0.6505	0.0158
	508	0.0371	0.0912	0.0478
	608	0.0350	0.0387	0.0381
at end of pt	701	0.0189	0.0203	0.0149
	702	0.0228	0.0189	0.0181
	704	0.0257	0.0221	0.0217
	707	0.0232	0.0190	0.0183
	708	0.0413	0.0724	0.0502
	709	0.0181	0.0486	0.0215
		fom	fom	fom
flange		10.7	60.6	59.2
cavity		14.9	20.9	64.5
above port		37.2	0.04	59.7
end of port		13.9	37.6	67.3
time, min		202.07	64.44	66.75

We can see that case 1, based on weight windows calculated for cell 604 at the end of the gap,

performs very poorly in cell 408 above the port, giving an fsd above 0.5 (highlighted in red). This is not surprising, since this choice of a target cell is intended to give good results for cells near the end of the port, while cell 408 is close to the root of the port.

However, even for the other tally cells the weight windows based on the composite target cell perform better. It is notable that in some cases, shown in boldface, the fsd is actually worse than with the original importances, but the calculation runs substantially faster, leading to superior figures of merit. The reason for this is illustrated by Fig. 3, which shows the fast neutron population and tracks entering for successive layers, perpendicular to the x axis, of the geometry.

In the central part of the system the population is much smaller with the weight windows (case a2n) than with the original, manually estimated, importances (a0n). This means that less time is spent on tracking neutrons in this region.

Note that in case a0 the importances were based on the advice in the manual: "A good rule is to keep the population of tracks traveling in the desired direction more or less constant", and, in fact, they do a reasonably good job of this, considering that the total reduction of the flux from the source cell to the tally cells (except cell 604) is about 7 to 8 orders of magnitude. The weight windows do much worse at keeping the population constant, but that doesn't seem to do any harm.

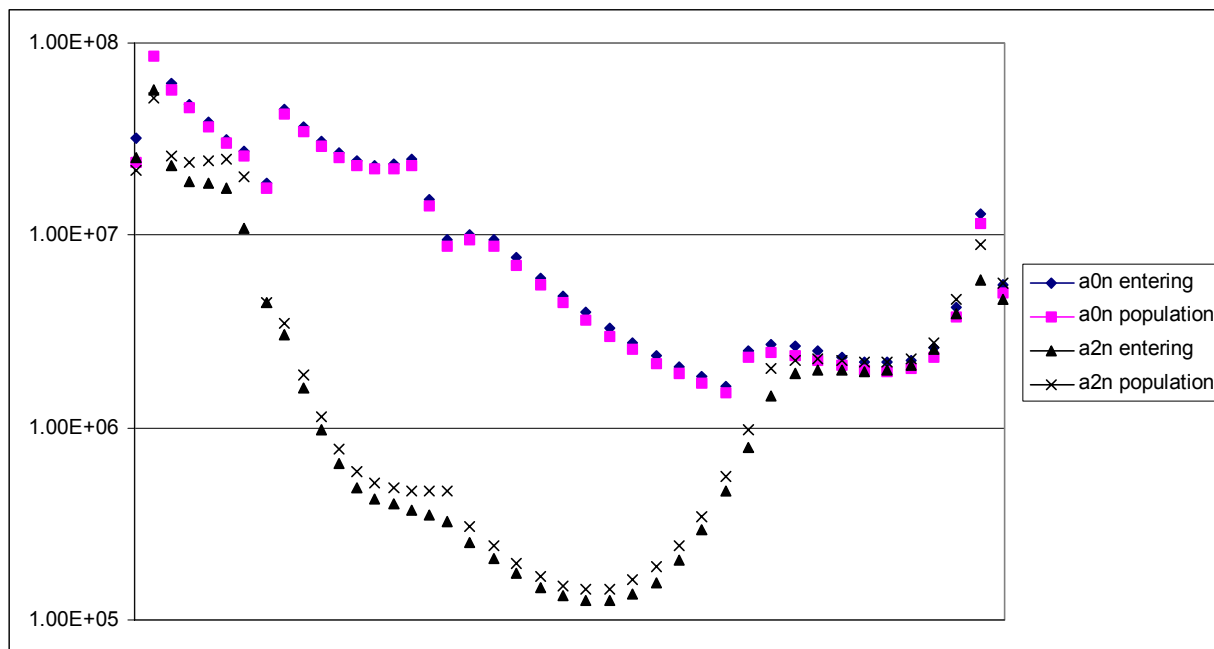


Figure 3. The neutron population with manually chosen importances (a0n) and with generated weight windows (a2n). Horizontal axis = x coordinate axis.

As one can guess from Fig. 3, the weight windows in the central region are higher than what would correspond to the original importances. It is also worth noting, though it cannot be seen from Fig. 3, that the variation in the z direction of the weight windows is substantially greater than that of the importances. Apparently the importances were underbiased in this respect, allowing too many neutrons far from the gap.

It should be emphasized that the use of a composite target cell of large extent for the weight window generator involves an obvious danger. If particles reach one part of that cell much more easily than other parts, the total score in the composite cell and thus the generated weight windows will be dominated by the easily reached part, and subsequent calculations may not sample the other parts adequately. In this case, however, the composite cell worked satisfactorily in spite of its size, presumably because all its parts are approximately equally difficult to reach, as shown by the fact that the calculated fluxes were not drastically different in different parts of it. Specifically, the highest flux, in cell 704, was about 100 times the lowest flux, and since 704 is a small cell, the integral score in it did not dominate the total score to an unhealthy degree.

The use of 20,000,000 histories made it possible to get fairly good statistics, which should make the weight window generator work well. This does not resemble the real situation for the ITER port analysis, in which the much larger and more complex geometry makes it impossible to get so good statistics with runs of reasonable length, at least before very good weight windows are available. For this reason we next performed calculations similar to a0 and a2 but with only 200,000 histories, calling them A0 and A2. The results are shown in Table 2.

Table 2. Fractional Standard Deviations and Figures of Merit for Fast Neutron Calculations, Direct Method; 200,000 Histories

	case	A0	A2
	cell	fsd	fsd
flange	604	0.2016	0.1728
cavity	501	0.1754	0.1294
	601	0.1901	0.1485
above port	408	0.0989	0.1296
	508	0.3285	0.6768
	608	0.2511	0.5291
end of port	701	0.1858	0.1471
	702	0.2158	0.1848
	704	0.2367	0.2106
	707	0.2207	0.1895
	708	0.2521	0.6362
	709	0.1968	0.2009
		fom	fom
flange		11.9	40.1
cavity		15.7	71.5
above port		49.4	71.3
end of port		14.0	55.4
time, min		2.07	0.83

Here we get large fsd's, similar to those from real ITER port calculations. In fact three of the fsd's obtained using weight windows, highlighted in red, exceed 0.5, meaning that the results are garbage, according to Table 2.3 of the manual. The trend is nonetheless similar to the a series: The use of weight windows doesn't bring any major improvement in the fsd's for a given nps (number of histories), but it speeds up the calculation, making larger nps values feasible. In this case perhaps a further iteration of the weight windows, with a longer run, or manual corrections would be advisable before one tries to get final results.

B. Progressive Weight Window Generation

An alternative way of obtaining weight windows was as follows: First find weight windows to steer neutrons to a cell near the source but in the streaming path. Then, using these weight windows, calculate weight windows for a target cell somewhat further on, and repeat until the final tally cells are reached. In this case the first target cell was set at the bottom of the dogleg, the second at the top of the dogleg, the third halfway down the post-dogleg section of the gap, and the fourth at the end of the gap, in cell 604. Finally weight windows were calculated for the composite tally cell as above.

This was done with 200,000 histories per run. The first steps worked well, with run times of less than a minute and fsd's in the target cells below 0.2.

The final step, from cell 604 to the composite tally cell, worked less well. In this run the fsd in the target was 0.4484. This was not surprising, considering the problems in going from cell 604 to, especially, cell 408 at the root of the port. However, iterating the weight window generation process gave gradually improved results, as shown in Table 3.

Table 3. Fractional Standard Deviations and Figures of Merit for Fast Neutron Calculations, Progressive Method; 200,000 Histories (B5 and B6) or 20,000,000 Histories (b7)

	case	B5	B6	b7
	cell	fsd	fsd	fsd
flange	604	0.1453	0.1520	0.0160
cavity	501	0.3988	0.1405	0.0156
	601	0.2230	0.1460	0.0155
above port	408	0.2456	0.2704	0.0442
	508	0.3466	0.2442	0.0906
	608	0.3500	0.2110	0.0612
end of port	701	0.2244	0.1460	0.0156
	702	0.1599	0.1558	0.0178
	704	0.1930	0.2028	0.0222
	707	0.1686	0.1740	0.0185
	708	0.4549	0.3071	0.0693
	709	0.4561	0.2592	0.0555
		fom	fom	fom
flange		62.1	56.0	49.4
cavity		8.2	65.5	51.5
above port		21.7	17.7	6.5
end of port		26.0	60.7	52.1
time, min		0.76	0.77	79.31

Cases B5 and B6 are successive iterations with 200,000 histories. There is at least a slight improvement in most tally bins, but the fsd's remain rather high. Finally a run with 20,000,000 histories, b7, was made to get better results. This hope was fulfilled in the sense that the fsd's were low, though no further improvement in the fom's was seen. There was, in fact, some apparent deterioration, but this probably merely reflects more realistic fsd's based on the larger number of histories.

The fsd's of cases A2 and B6 or a2 and b7 are broadly similar, suggesting that the direct and progressive methods of finding weight windows give comparable results. The progressive method requires a greater number of calculations, but at

least in this test case the calculations were fast, so their greater number was not a major problem. The direct method requires more work to find realistic starting importances.

The figures of merit were slightly better for a2 than for b7, indicating that the direct method may have a small advantage in performance. However, this is probably only the case if the starting importances are fairly good.

Our recommendation is that the direct method of weight window generation may be appropriate for users capable of choosing good importances manually. For users without sufficient experience to do this, the progressive method is probably better.

III. CELL-BASED WEIGHT WINDOWS, GAMMAS

The “a” series calculations (direct weight window generation, 20,000,000 histories per run) was continued with calculations for slow neutrons and photons. In run a3 the generated weight windows for neutrons above 1 MeV were extended manually to neutrons between 1 MeV and 1 eV, below 1 eV and to photons in such a way that, the lower the energy of a neutron and the farther from the tally cells it was, the higher was the ratio of the lower bound of the weight window to that for fast neutrons. Photons far from the tally cells were killed. Using these weight windows, new ones were generated and then used in run a4. The results are shown in Table 4.

Table 4. Fractional Standard Deviations and Figures of Merit for Photon Calculations with Initial Weight Windows Established by Fast Neutron Calculations; 20,000,000 Histories

	case	a3	a4
	cell	fsd	fsd
flange	604	0.0106	0.0144
cavity	501	0.0084	0.0108
	601	0.0085	0.0111
above port	408	0.0078	0.0170
	508	0.0113	0.0296
	608	0.0115	0.0260
end of port	701	0.0084	0.0111
	702	0.0095	0.0134
	704	0.0106	0.0158
	707	0.0099	0.0145
	708	0.0171	0.0484
	709	0.0091	0.0202
		fom	fom
flange		5.3	8.7
cavity		8.3	15.5
above port		9.7	6.2
end of port		8.4	14.7
time, min		1685.17	554.17

As expected, these calculations were considerably slower than those involving only fast neutrons. It is also interesting to note that the weight windows produced by the weight window generator for intermediate and thermal neutrons and for photons gave fsd's inferior to those obtained with weight windows estimated manually. However, the generated weight windows gave a much faster run, so that the figures of merit improved. Thus, the deterioration in fsd's for a given number of histories can be more than compensated by increasing the number of histories treated in a given time.

One can also start directly with a coupled neutron-photon calculation. We tried this option in run D0, and the resulting weight windows were then used in a new run, D2. The results are shown below. Note that only 200,000 histories were run in D2, compared with 20,000,000 in a4, so to take this into account, the fsd's for a4 have been multiplied by 10. With this adjustment they are similar for both cases, as are the figures of merit. Note that the run times have not been adjusted, and they differ by the expected factor of 100. We can thus conclude that in this test problem going straight to coupled n,p is a workable option. However, it should be noted the run time for D0, the run in which the weight windows were generated, was 60.94 minutes, a long time for a run of 200,000 histories

in this simple test problem. Therefore this method might not be practicable in more complicated problems.

Table 5. Comparison of Results in Photon Calculations Obtained by Starting with Fast Neutron Calculations (a4) and by Going Directly to Coupled Calculations (D2); 20,000,000 and 200,000 Histories, Respectively

	case	a4	D2
	cell	fsd*10	fsd
flange	604	0.144	0.165
cavity	501	0.108	0.115
	601	0.111	0.118
above port	408	0.170	0.132
	508	0.296	0.252
	608	0.260	0.244
end of port	701	0.111	0.118
	702	0.134	0.166
	704	0.158	0.189
	707	0.145	0.172
	708	0.484	0.365
	709	0.202	0.197
		fom	fom
flange		8.7	6.59
cavity		15.5	13.6
above port		6.2	10.3
end of port		14.7	12.9
time, min		554.17	5.57

IV. MESH-BASED WEIGHT WINDOWS

We also tried the mesh-based weight window generator included in MCNP4C. The mesh used was quite similar to the cell subdivision used with the cell-based weight window generator, with the mesh boundaries coinciding with material boundaries in many cases, otherwise with mesh intervals usually amounting to 7.5 cm in the x direction and with thin meshes just above and below the gap.

Successive iterations of the weight window calculation were carried out, much like we did with the progressive cell-based weight window generator, though in this case the target for the generator was always the composite tally cell.

Five fast neutron calculations with 200,000 histories each were carried out, replacing the weight windows after each calculation. The run times showed a curious variation. Expressed in minutes, they were: 0.44, 0.83, 16.58, 0.46, 0.47. It appears as if the third run, using the second set of generated weight windows, must have used much

heavier splitting. This did have the effect of reducing the fsd's, which were extremely high in the first two runs (**every** fsd exceeded 0.5!) to much more reasonable values (around 0.2). Apparently this enabled the program to produce much better weight windows, which then gave similar fsd's with much shorter run times.

As far as could be deduced from the results, the process had converged after the fourth run. The fifth was repeated with 20,000,000 histories. Table 6 compares this run, c4, with selected results from the calculations described above.

Table 6. Comparison of Fast Neutron Calculations with Cell-Based (a2, b7) and Mesh-Based (c4) Weight Windows; 20,000,000 Histories

	case	A2	b7	c4
	cell	fsd	fsd	fsd
flange	604	0.0159	0.0160	0.0228
cavity	501	0.0152	0.0156	0.0222
	601	0.0148	0.0155	0.0197
above port	408	0.0158	0.0442	0.0373
	508	0.0478	0.0906	0.0623
	608	0.0381	0.0612	0.0393
end of port	701	0.0149	0.0156	0.0198
	702	0.0181	0.0178	0.0276
	704	0.0217	0.0222	0.0357
	707	0.0183	0.0185	0.0248
	708	0.0502	0.0693	0.0420
	709	0.0215	0.0555	0.0364
		fom	fom	fom
flange		59.2	49.4	42.5
cavity		64.5	51.5	45.2
above port		59.7	6.5	15.9
end of port		67.3	52.1	56.7
time, min		66.75	79.31	45.07

Thus, for fast neutrons, the performance of the mesh-based weight window generator appears roughly comparable with that of the cell-based one.

Next we attempted to extend the calculation to photons. These were initially simply assigned the same importances as the neutrons had in the starting run, while for neutrons, regardless of energy, the weight windows generated in the preceding run were used. The weight window generator was then set to generate weight windows for neutrons in the same 3-group energy structure as before and for gammas.

200,000 histories were treated in run C5, giving reasonable-looking results in 12.65 minutes. The

ensuing weight windows were then used in the next run. This one, C6, took 865.55 minutes without any significant improvement in the fsd's, so the fom's dropped drastically. The run after that, C7, took 552.52 minutes, again failing to improve the precision. In fact, the gamma fluxes calculated in these runs seemed, if anything, to move farther from those obtained previously.

In Table 7 we compare results obtained previously for the gamma flux with those obtained in run C7. Note that run a4 involved 20,000,000 histories as compared with 200,000 for C7. For this reason we have multiplied the fsd's from run a4 by 10 to make them comparable with those for C7, and with this adjustment they are roughly similar. The run times given in the table, however, contain no such adjustment. Run a4 covered 100 times as many histories as C7 in almost the same time, which shows up in the figures of merit.

Table 7. Comparison of Coupled Calculations with Cell-Based (a4) and Mesh-Based (C7) Weight Windows; 20,000,000 and 200,000 Histories, Respectively

	case	a4	C7
	cell	fsd*10	fsd
flange	604	0.144	0.399
cavity	501	0.108	0.120
	601	0.111	0.155
above port	408	0.170	0.154
	508	0.296	0.120
	608	0.260	0.165
end of port	701	0.111	0.168
	702	0.134	0.285
	704	0.158	0.458
	707	0.145	0.584
	708	0.484	0.198
	709	0.202	0.142
		fom	fom
flange		8.7	0.011
cavity		15.5	0.126
above port		6.2	0.077
end of port		14.7	0.064
time, min		554.17	552.52

Thus, while the mesh-based weight window generator worked fairly well for fast neutrons, its results for gammas were disappointing. However, it is not clear how much significance, if any, should be attached to this finding. It is possible that a few further iterations would have given much improved results or that we made some mistake in using the mesh-based weight window generator. Perhaps we should have provided better starting weight

windows for intermediate and thermal neutrons and for gammas. Unfortunately schedule and funding limits precluded further work on this problem.

V. EXPONENTIAL TRANSFORM, FORCED COLLISIONS

We also studied the effect of using the exponential transform or forced collisions.

The exponential transform was applied to both neutrons and photons. The stretching was performed diagonally to the right and towards the gap with a stretching parameter of 0.7, except when some tally cell was nearer than the gap. In the latter case the stretching was usually directed towards the tally cell. When two or more directions were appropriate, an intermediate direction was chosen and the stretching parameter was reduced.

Table 8. Comparison of Coupled Calculations Without (a4) and With (a4x) Exponential Transform; 20,000,000 Histories

	case	a4	a4x
	cell	fsd	fsd
flange	604	0.0144	0.0117
cavity	501	0.0108	0.0088
	601	0.0111	0.0089
above port	408	0.0170	0.0169
	508	0.0296	0.0275
	608	0.0260	0.0229
end of port	701	0.0111	0.0089
	702	0.0134	0.0107
	704	0.0158	0.0128
	707	0.0145	0.0117
	708	0.0484	0.0496
	709	0.0202	0.0195
		fom	fom
flange		8.7	12.8
cavity		15.5	22.8
above port		6.2	6.2
end of port		14.7	22.2
time, min		554.17	566.43

We see that there is a modest improvement.

In the study of the effects of forced collisions, we limited ourselves to fast neutron calculations, since the main purpose of forced collisions in this problem would be to increase the sampling of fast neutron streaming along the gap. We used forced collisions in the cells just above and below the gap, with both positive and negative values for the forced collision parameter and with three absolute values for it: 0.5, 0.7 and 0.9. We preferred not to

use a value of 1, because particles crossing the gap back and forth might result in excessive multiplication of tracks.

The forced collision option would be much more useful if there were some way of biasing the flight direction of neutrons emerging from the forced collisions, in this case to make them move preferentially along the gap to the right. Unfortunately no such facility exists in MCNP4C (presumably because this would be impractical, involving excessively time-consuming calculations), and even combining forced collisions with the exponential transform is not allowed. The use of positive values for the forced collision parameter didn't work either. For all positive values

we sooner or later got an error stop with the message "the weight of the current particle is zero or less". We also got this error in a combined neutron-photon run with a forced collision parameter of -0.9 , though in this case more than 4,000,000 histories were followed before this happened, about twice as many as for the values $+0.7$ or $+0.9$. We didn't have time to investigate the reason for this trouble.

The fast neutron calculations with negative values for the forced collision parameter ran without trouble, and their fsd's and fom's are compared below with those for a run without forced collisions.

Table 9. Effects of Forced Collisions on Fast Neutron Calculations; 20,000,000 Histories

	case	a2	a2m5	a2m7	a2m9
		no fcl	fcl=-0.5	fcl=-0.7	fcl=-0.9
	cell	fsd	fsd	fsd	fsd
flange	604	0.0159	0.0138	0.0130	0.0127
cavity	501	0.0152	0.0133	0.0121	0.0121
	601	0.0148	0.0131	0.0123	0.0122
above port	408	0.0158	0.0161	0.0153	0.0150
	508	0.0478	0.0481	0.0448	0.0420
	608	0.0381	0.0398	0.0392	0.0395
end of port	701	0.0149	0.0131	0.0123	0.0123
	702	0.0181	0.0152	0.0148	0.0145
	704	0.0217	0.0179	0.0174	0.0171
	707	0.0183	0.0157	0.0148	0.0143
	708	0.0502	0.0514	0.0510	0.0485
	709	0.0215	0.0202	0.0200	0.0203
		fom	fom	fom	fom
flange		59.2	76.7	81.0	81.0
cavity		64.5	82.3	92.3	89.2
above port		59.7	56.0	58.2	58.3
end of port		67.3	85.0	89.7	86.0
time, min		66.75	68.95	73.55	76.5

Again we find a modest improvement, greater for the value -0.7 than for the other two parameter values, but suggesting that the optimum may be close to -0.8 .

Note that the use of forced collisions does not give any improvement in the tallies above the port. This is easy to understand, since the purpose of the use of forced collisions was to enhance streaming along the gap, but the particles scoring above the port are mainly such which left the gap early.

VI. CONCLUSIONS

We studied various methods of reducing the variance in MCNP4C calculations in a shielding problem containing a planar gap with a dogleg. The main emphasis was on the use of the weight window generator, but the exponential transform and forced collisions were also studied.

The main conclusion is that the weight window generator did turn out to be helpful, even in cases where the stochastic uncertainty of the resulting weight windows is large and manual adjustments

are impracticable. The two methods of generating cell-based weight windows for fast neutrons, the direct method of providing the best starting importances that our engineering judgment could provide, then setting the target for the weight window generator in the final tally cells themselves, and the progressive method of starting with simple (constant) importances and gradually putting the target farther and farther from the source, performed about equally well. We recommend the progressive method for inexperienced Monte Carlo users, while the direct method may be worthwhile for experienced practitioners.

Cell-based weight windows also performed reasonably well in the coupled neutron-photon calculations, whether they were derived starting with fast neutron calculations or going straight to the coupled calculations. We do, however, believe that the latter method may be impracticable in the more complicated problems encountered in real fusion neutronics calculations.

The mesh-based weight windows also worked satisfactorily for fast neutrons. They worked much less well for coupled calculations, but, as pointed out above, it is doubtful whether one can draw any conclusions about this without further study.

The exponential transform and forced collisions both brought a modest benefit, of the order of a 50 % improvement in the figures of merit.

¹ J.F. Briesmeister, Ed.: MCNP™—A General Monte Carlo N-Particle Transport Code, Version 4C. LA-13709-M (2000).

² H.Iida, D. Valenza, R. Plenteda, R. T. Santoro and J. Dietz "Radiation Shielding for ITER to allow for Hands-on Maintenance inside the Cryostat", J. of Nuclear Science and Technology, 19.Oct.1999

³ D. Valenza, H.Iida, R. Plenteda and R. T. Santoro "Proposal of shutdown dose estimate method by Monte Carlo code", Fusion Engineering and Design **55**, pp411-418 (2001)

⁴ Y. Chen and U. Fischer "Rigorous MCNP Based Shutdown Dose Rate Calculations: Computational Scheme, Verification Calculations and Application to ITER", *6th International Symposium on Fusion Nuclear Technology (ISFNT-6)*, San Diego, California, April 7-12, 2002. University of California, Center for Energy Research, San Diego, California.

PUBLICATION X

**Importances for MCNP Calculations
on a Shield with a Penetration**

14th Biennial Topical Meeting of the Radiation Protection
and Shielding Division of the American Nuclear
Society. Carlsbad, NM, USA 2006. Pp. 478–488.
Copyright 2006 by the American Nuclear Society, La
Grange Park, Illinois 60526, USA. Reprinted with
permission from the publisher.

Importances for MCNP Calculations on a Shield with a Penetration

Frej Wasastjerna

*VTT Technical Research Centre of Finland, P.O. Box 1000, FI-02044VTT, FINLAND
frej.wasastjerna@vtt.fi*

INTRODUCTION

This work was motivated by experience of shielding calculations on fusion-related facilities such as ITER and IFMIF using MCNP4C.^[1] These shielding calculations are very demanding, particularly due to the presence of penetrations along which neutrons can stream for a few meters. The work reported here can be considered a continuation of that reported by the author at the RPS2002 meeting.^[2]

The main tool for variance reduction in MCNP calculations of this kind is importances or weight windows, and the main conclusion of the previous work was that the weight window generator in MCNP4C is useful. The weight windows it provides gave a greater variance for a fixed number of histories than the manually chosen importances, but the time per history was so much shorter that the net result was a substantially better figure of merit.

However, this by no means obviates the need for manual variance reduction. There are two problems that need to be addressed:

(1) How should the shield be subdivided into cells for optimum performance? (If mesh-based rather than cell-based weight windows are used, the same question applies to the mesh.)

(2) Good starting importances are necessary for the weight window generator to give useful results. Even if the step-wise method is used, first generating weight windows for a tally somewhere inside the shield, then using these to take the neutrons farther into the shield and so on, good starting importances will help.

A possible solution to this problem is to use deterministic calculations to estimate importances, as has been described by many authors. However, this also involves difficulties. If two fully separate programs are used for the deterministic importance calculation and the actual (MC) flux calculation, the geometry must be modeled twice, which is prohibitive when even modeling it once may require many person-months or even years. If the two programs form a program system capable of using the same input file, this difficulty is avoided, but we do not have such a system in use at VTT. In any case, deterministic methods have difficulties in coping with streaming through long and narrow penetrations. Therefore, there remains an incentive to find a way of estimating importances that take streaming into account properly.

We consider the longitudinal variation of the importances (along the streaming direction) a nearly solved problem (see Appendix A). However, how to handle the transverse variation (the spatial dependence of the importances at right angles to the streaming direction) was not clear, and solving this problem was the goal of this work.

METHOD

The geometry we used for our test calculations was two-dimensional, with a steel + water shield (80 volume % stainless steel 316 L(N), ITER grade and 20 % water at a density of 0.9 g/cm³) 240 cm in thickness, penetrated by a plane slit 2 cm high. On the left side of the shield was a surface source of 14-MeV neutrons, and the neutron current on the right side was the main quantity to be tallied. In most cases we tallied only the current above 1 or 0.1 MeV, since, in the fusion applications we are interested in, most of the gamma radiation after shutdown is caused by activation reactions in this energy range.

In the direction of neutron streaming, the shield was divided into 7.5 cm thick layers, so that there were 32 such layers. In the lateral direction, the cell boundaries were set at 0.001, 0.002, 0.004, 0.008, 0.016, 0.032, 0.064, 0.125, 0.25, 0.5, 1, 2, 3, 4, 6, 8, 11.2, 16, 22.4 and 32 cm from the slit, with a void boundary condition beyond the last cell.

The calculations were performed with MCNP4C on a Linux cluster. The cross sections were taken from JEF2.2.03.

The program was set to generate weight window lower boundaries, which constituted the actual quantities of interest. These were then translated back into importances by dividing the weight window lower boundary for the reference cell (which was always set to 0.4) with the corresponding boundary for each cell. These importances, and in particular their lateral distributions, were then investigated. Two kinds of importance ratios were calculated: the ratio of the importance in a cell immediately adjacent to the slit (a "wall cell") to that in the slit itself, and the ratios of the importances in cells farther away from the slit to that in the wall cell.

In practical problems it will be unfeasible to use such a fine cell structure. We generally aim to use 3 lateral layers, with importances reduced by a factor of 4 and 16, respectively, from the cells adjacent to the penetration. Therefore we determined the locations at which the generated importances dropped below ¼ and 1/16 of the values in the wall cells.

To get good results, we typically ran hundreds of millions of histories. Longitudinal starting importances calculated as described in Appendix A were used, but mostly no lateral variations were present in the starting importances. Even so it sometimes happened that the cells farthest from the slit and about halfway along the shield thickness did not get any generated weight windows. However, these difficulties were limited to a few cells, so they do not detract from the usefulness of the results presented here.

SENSITIVITY STUDIES

Since real applications will differ in many ways from the cases studied here, we set out to study how the results were affected by changes in geometry, source spectrum, the energy range of interest and the shield material. Although we could not carry out an exhaustive investigation of this in view of the limits on time and funding, we could draw at least some tentative conclusions, which will be expressed here in terms of how steeply the generated importances decline with increasing distance from the penetration.

- Changing the geometry, to a slit 7 cm in height or to a duct of circular cross section with a diameter of 20 cm made the decline slightly steeper, but the change was minor. For a circular duct with a diameter of 2 cm the generated importances actually

increased with increasing distance from the duct, but this was probably an erroneous result caused by extremely poor statistics. We conclude that changes in the geometry of the shield penetration apparently do not make a big difference.

- We did not study the effect of changing the shield thickness, but we do not believe that it would change the results presented here, so long as the thickness is sufficient to make streaming dominate over bulk transport.
- The effect of changing from a 14 MeV source to a fission spectrum is small. Near the slit the decline of the importances becomes slightly steeper, farther away less steep, but these changes are not significant.
- Going from a cutoff energy of 1 MeV to 10^{-5} eV makes essentially no difference near the slit, but farther out the decline becomes less steep. The z boundary where the importance decreases by a factor of 16 from the wall cell moves out from 0.25 cm near the middle of the shield to about 1 cm.
- Changing the shield material made a big difference. For this reason we tested several different materials. The results are described below.

MATERIAL CHOICE

Four of the materials chosen were intended as extremely simplified versions of possible shield materials. These were water, quartz (as a simplified version of concrete), iron and tungsten. Light concrete, as specified for ITER, was also used, as was stainless steel 316 L(N) ITER grade, with and without 20 volume % water. A comparison of these seven materials led to the following conclusion: The importance drops off much more sharply with increasing distance from the slit for the most effective shielding materials than for the least effective ones.

This is physically reasonable. In a poor shielding material, even a neutron far from the slit may have a significant chance to reach the tally surface, but not in a good shielding material.

The extremely poor performance of pure iron in this respect was particularly noteworthy. We attribute it to cross section windows. Even though the cutoff at 0.1 MeV which we used eliminates the effects of the notorious window at about 25 keV, the windows above 0.1 MeV are apparently still enough to have a major influence.

RESULTS

The results are presented here for all materials, but only for the 2 cm slit with a 14 MeV source and for the energy range above 0.1 MeV, since only the material choice made a big difference.

Fig. 1 shows the importances in the slit itself, both estimated with the "handy method" of Appendix A ("est.imp.") and calculated from the generated weight windows for different materials. The agreement is as good as one can hope reasonably hope for, with most of the calculated importances agreeing with the estimates within about a factor of 2. As the stair-like "est.imp." curve shows, we didn't even try for greater accuracy.

The biggest differences are found for pure iron. Obviously the handy method underestimates the transport through the bulk shield in this case, where the cross section windows have a strong influence. For pure iron the flux halving length of 7.5 cm is too short.

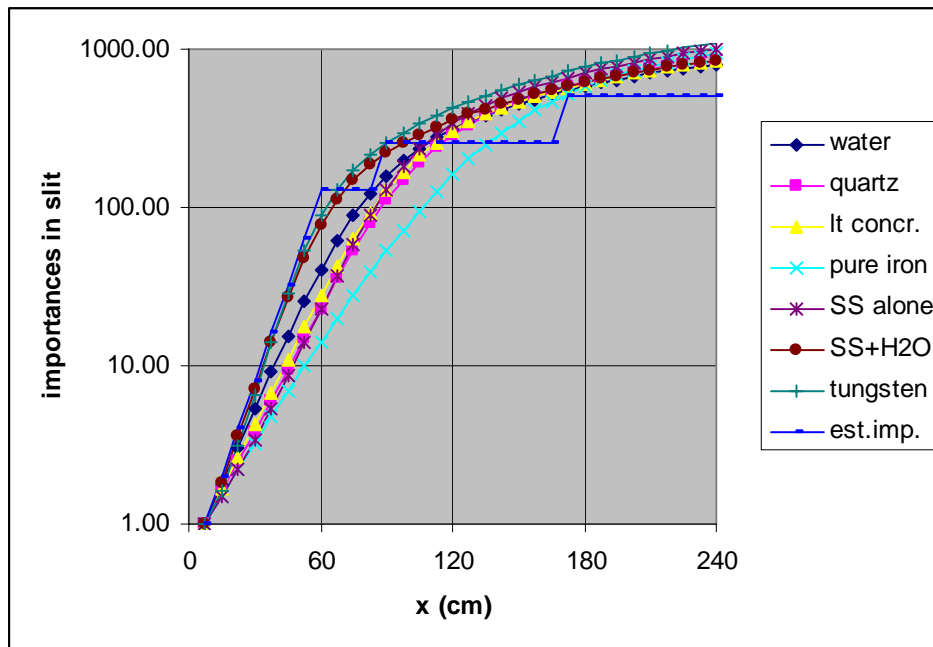


Fig. 1: Importances in the slit itself as functions of the longitudinal coordinate x

In any case, the importance in the void cells of the slit itself is of little relevance, since MCNP doesn't split particles in a void. The above results justify the use of the "handy method" for estimation of the longitudinal importance distribution in the slit, but we also need to investigate the lateral distribution.

First let us note that the lateral dependence of the importance is very flat in the rightmost layer of cells, $232.5 \text{ cm} < x < 240 \text{ cm}$. This is easy to understand, since any particle in this layer has a good chance of reaching the tallying surface at $x = 240 \text{ cm}$, regardless of its proximity to the slit. This dependence is also relatively flat in the leftmost cells, $0 < x < 7.5 \text{ cm}$. In between, the lateral variation of the importance is very pronounced.

Fig. 2 shows the ratio of the importance in the first 0.001 cm of the wall to the slit itself as a function of x (the position along the slit). This value is remarkably small in most of the shield. A reasonable approximation of this ratio would start at $1/16$, then drop gradually to $1/128$ at one quarter of the shield thickness, increase to $1/64$ at half the thickness, remain there to three quarters of the thickness and then rise gradually to 1. We don't know where the breakpoints should be located in a shield with a thickness different from 240 cm, however. And this recommendation is obviously not valid for pure iron.

The above gives us the importances in the cells immediately adjacent to the slit. There remains the question of determining the cell structure and importances farther from the slit. Fig. 3 shows how the importance declines with increasing distance from the slit surface in the middle of the shield.

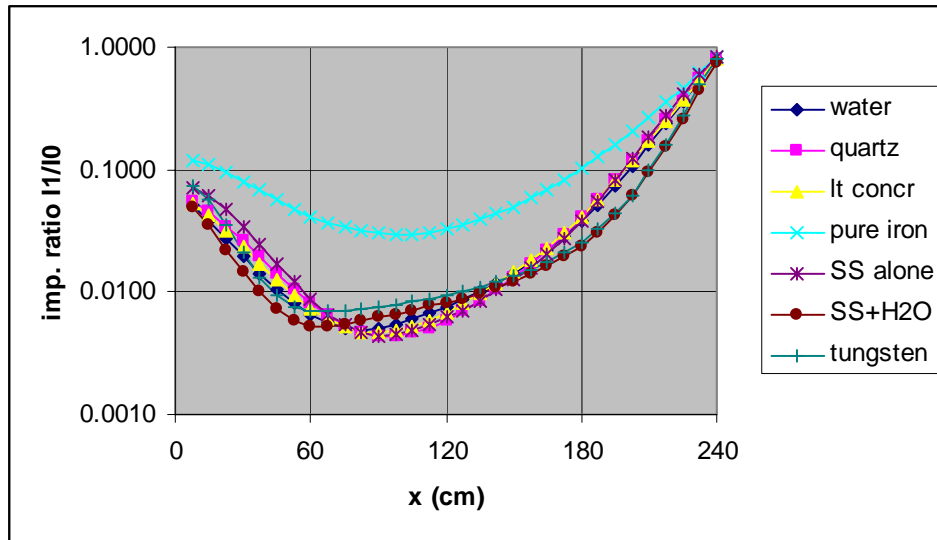


Fig. 2: Ratios of importance in the first 0.001 cm of the wall (I1) to that in the slit (I0) as functions of the longitudinal coordinate x

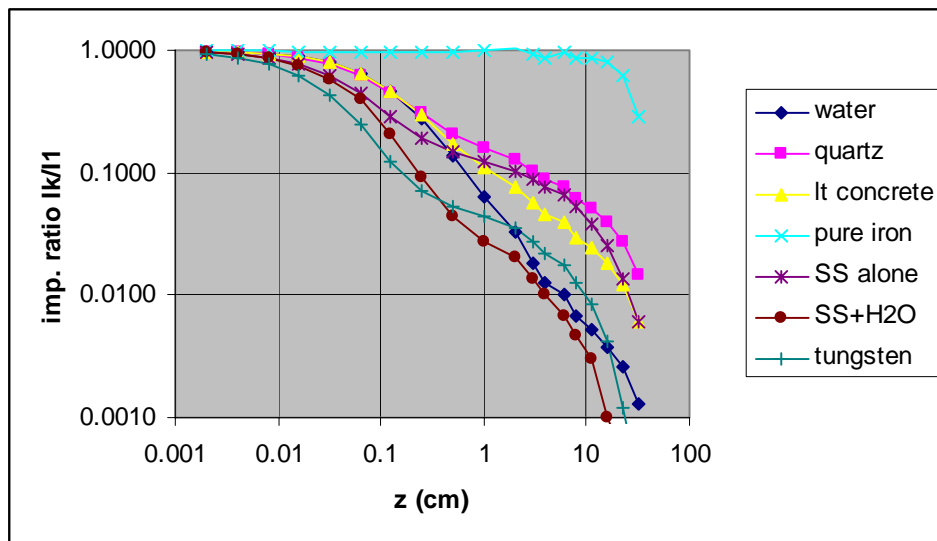


Fig. 3: Ratios of importance in the k 'th cell (I_k) to that in the first 0.001 cm of the wall (I1) as functions of the lateral coordinate z in the interval $112.5 \text{ cm} < x < 120 \text{ cm}$ (in the middle of the shield).

Since the geometries we typically deal with are complex enough already (some thousands of cells), we prefer not to use a large number of cells in the lateral direction.

We consider three layers of cells, each with an importance lower by a factor of 4, to be reasonable. From Fig. 3 one can conclude that for the best shielding materials, such as tungsten or a combination of 80 % stainless steel with 20 % water, the importance drops by a factor of 4 in the first 0.1 cm or less and by a factor of 16 at about 0.35 cm. For light concrete, the corresponding distances are about 0.3 and 2.5 cm, for stainless steel 0.16 and 6 cm. Pure iron behaves in its own idiosyncratic way.

Fig. 4 shows how the lateral importance distribution, expressed as the ratio of the importance at z to that at the slit surface $z = 0$, varies longitudinally through the shield for a single material, the 80 volume % stainless steel + 20 % water mixture. As was pointed out above, the distribution is quite flat at $i = 32$, the end of the shield, and also relatively flat at the beginning, steeper in between.

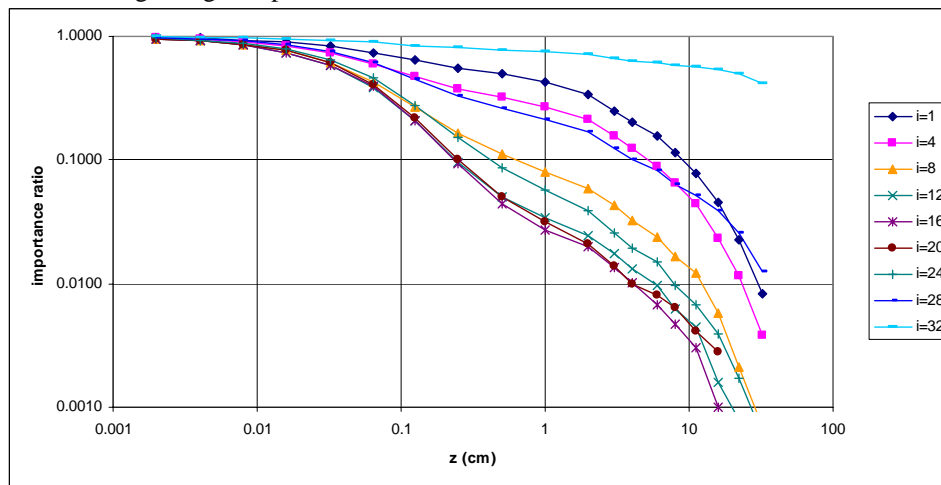


Fig. 4: Ratios of importance in the k 'th cell to that in the first 0.001 cm of the wall as functions of the lateral coordinate z at different longitudinal locations for 80 % SS + 20 % water. $i = 1$ is the first layer of the shield, $i = 32$ is the last.

AN APPLICATION

To demonstrate and test how these importances work, we carried out some calculations with them. For comparison we also did some calculations with old importances, the way we would have done before this investigation.

When using the old importances, we set the z boundaries at 2 and 8 cm from the slit surface; with the new importances, we set them at at 0.064 and 0.5 cm. (In practice all 4 boundaries were present, but the importances were changed only at the appropriate boundaries.)

The tables show the importances for different cells in both the x and z directions. The first case used no lateral importance variations whatever, only longitudinal importances. The second and third cases used lateral variations also, in the old way. In the second case the importances were separable in the x and z directions, which is sometimes necessary when using universes. In the third case, the importances were

modified to give a laterally flat distribution at the end of the shield, which is more realistic though unfortunately not always feasible.

With the new importances we also had both a separable and a non-separable case. For the separable case, we first divided the importances in the slit by 64 to get the importances in the cells immediately adjacent to the slit, on the basis that this seems like a reasonably representative average of what Fig. 2 shows. Then there were two further reductions by a factor of 4, going farther from the slit. In the non-separable case, we took into account the x dependencies shown by Figs. 2 and 4.

There was a further change, compared with the old method. If we had used an importance of 1 in the first cell in the slit, as we would traditionally have done, the importances of the cells at the left end of the shield and far from the slit would have been very small (1/1024 in the separable case), which would have involved an inordinate amount of Russian roulette for newly started neutrons. Instead we renormalized the importances so that we got more reasonable values in the material-filled cells at the start of the shield. This way the importances in the slit were quite large, but this has no practical significance, since MCNP doesn't split particles in a void.

The importances used in each calculation, the figure of merit and fractional standard deviation for the total current exiting the shield and the number of histories per minute are shown in Tables I through V. The fractional standard deviations (fsd's) are comparable, because each calculation ran for 525 minutes on a single processor in a Linux PC.

i (x location index)	I (importance)
1	1
2	2
3	4
4	8
5	16
6	32
7	64
8-11	128
12-22	256
23-32	512
FOM	16.34
histories/min	96,973
fsd	0.0107

Table I: Calculation with old, exclusively longitudinal importances

The first calculation, using importances depending only on the x coordinate (Table I), worked fairly well. Introducing our old guesses concerning the lateral variation of the importances (Tables II and III) actually made things worse, decreasing the figure of merit by more than a factor of 2. Whether separable or non-separable importances were used made no significant difference.

Table II: Calculation with old separable importances

z intervals (cm)	-1...0	0...2	2...8	8...32
Material	void	80 % SS + 20 % water		
i (x location index)	I (importances)			
1	1	1	0.25	0.0625
2	2	2	0.5	0.125
3	4	4	1	0.25
4	8	8	2	0.5
5	16	16	4	1
6	32	32	8	2
7	64	64	16	4
8-11	128	128	32	8
12-22	256	256	64	16
23-32	512	512	128	32
FOM	7.808			
histories/min	45,820			
fsd	0.0155			

Table III: Calculation with old non-separable importances

z intervals (cm)	-1...0	0...2	2...8	8...32
Material	void	80 % SS + 20 % water		
i (x location index)	I (importances)			
1	1	1	0.25	0.0625
2	2	2	0.5	0.125
3	4	4	1	0.25
4	8	8	2	0.5
5	16	16	4	1
6	32	32	8	2
7	64	64	16	4
8-11	128	128	32	8
12-22	256	256	64	16
23-28	512	512	128	32
29	512	512	128	64
30	512	512	256	128
31	512	512	256	256
32	512	512	512	512
FOM	7.921			
histories/min	46,416			
fsd	0.0155			

Changing to the new separable importances (Table IV) resulted in a slight improvement over Tables II and III but the figure of merit did not reach the same level as when using only longitudinal importances.

Table IV: Calculation with new separable importances

z intervals (cm)	-1...0	0...0.064	0.064...0.5	0.5...32
Material	void	80 % SS + 20 % water		
i (x location index)	I (importances)			
1	256	4	1	0.25
2	512	8	2	0.5
3	1024	16	4	1
4	2048	32	8	2
5	4096	64	16	4
6	8192	128	32	8
7	16384	256	64	16
8-11	32768	512	128	32
12-22	65536	1024	256	64
23-32	131072	2048	512	128
FOM	9.475			
histories/min	73,697			
fsd	0.0142			

However, the new non-separable importances (Table V) worked significantly better, giving the best figure of merit, improved over Table I by a factor of 2.

That non-separable importances work better than separable ones is easy to understand, since separable importances cannot match the way the optimal importance distribution scrunches up near the penetration in the middle of the shield but spreads out near the end. The surprising thing is the absence of any significant difference between the old separable and non-separable importances. This may be due to the different cell subdivisions. Near the end of the shield, there are likely to be few fast neutrons farther from the slit than 2 cm, so the importance used in this region doesn't matter much, while that between 0.064 cm and 0.5 cm and even that beyond 0.5 cm does matter.

The observation that using longitudinal importances alone worked so well is interesting and, at the moment, unexplained.

CONCLUSIONS

We have shown that, in shields constructed of a good shielding material, the cell boundaries needed to define the lateral distribution of importances or weight windows around a penetration should be quite close to that penetration, of the order of a few millimeters or less. We have also found a way of manually constructing importances that are probably close to optimal for the geometry considered here, and this method is expected to be applicable to many other geometries with a shield penetrated by slits or ducts. These importances are, however, only intended for use as a starting point, allowing

efficient generation of cell-based weight windows. These weight windows will presumably further improve the calculation efficiency. Unfortunately we did not have time to test that before the deadline for completion of this paper.

Table V: Calculation with new non-separable importances

Case	nnos2 (new, non-separable importances)			
z intervals (cm)	-1...0	0...0.064	0.064...0.5	0.5...32
Material	void			
i (x location index)	I (importances)			
1	32	2	1	0.5
2	64	4	2	1
3	128	4	2	1
4	256	8	2	1
5	512	8	2	1
6	1024	16	4	1
7	2048	16	4	1
8-11	4096	32	8	2
12-16	8192	64	16	4
17-22	8192	128	32	8
23-26	16384	256	64	16
27	16384	512	128	64
28	16384	1024	256	128
29	16384	2048	1024	512
30	16384	4096	2048	2048
31	16384	8192	4096	4096
32	16384	16384	16384	16384
FOM	32.82			
histories/min	222,910			
fsd	0.0076			

For maximum efficiency, a non-separable importance distribution is required. In some cases the geometry model does not allow this. Our results suggest that, in such instances, one might as well make the lateral importance distribution flat and use only the longitudinal distribution. It seems likely that the optimal longitudinal distribution in that situation would not be the one calculated for the penetration itself as described in Appendix A but the product of that and the ratio shown in Fig. 2, i.e., the importance distribution for the walls of the penetration. The reason for this is that the importance in a void has no significance in MCNP.

Appendix A: Estimation of Longitudinal Importances

To estimate the importance as a function of position in the direction of streaming (longitudinal position), we follow the principle that the number of tracks should be roughly constant as one goes from the source to the tally. For this we estimate neutron transport through the bulk material and the streaming separately.

For the transport through bulk material, we assume that the neutron current attenuates exponentially. Based on ITER experience, we assume a halving of the flux for each 7.5 cm. Thus the importance doubles for each 7.5 cm. (This is the reason why we generally use cells with a thickness of about 7.5 cm in the direction of the neutron current, especially at the beginning of a shield.)

For streaming through voids, we assume that the neutron current is proportional to the solid angle subtended by the beginning of the duct as seen from the location under consideration. Thus the importance increases in inverse proportion to this solid angle.

We then choose the lower of these two importances, so that the importance is inversely proportional to the dominant part of the current. This usually means that, near the beginning of the shield, the importance will increase in the exponential fashion dictated by bulk attenuation. Farther on the streaming is well collimated, so it will dominate and the importance grows much more slowly.

As a final step, we calculate the nearest power of 2 that does not exceed the estimated importance, and then use this as the final importance.

This method is closely related to the "Handy Method" of Iida et al.^[3] for estimation of flux or current in a shield. It is not quite identical, but close enough that we borrow that name for this method. One difference is that Iida used the sum of the bulk transport and streaming, while we use the greater of the two. The conversion to a power of 2 is also, of course, missing from Iida's method, since it makes sense only for importances. It means that the ratio of importances is always an integer, which ensures conservation of weights in each individual splitting event (when using MCNP), not just averaged over all splits at a given surface.

REFERENCES

1. J.F. Briesmeister, Ed.: MCNPTM—A General Monte Carlo N-Particle Transport Code, Version 4C. LA-13709-M (2000).
2. F. Wasastjerna: A Study of Variance Reduction Methods in MCNP4C in a Slot with a Dogleg. RPSD2002, Santa Fe, New Mexico, USA, 2002-04-14...18.
3. H. Iida, R. T. Santoro, D. Valenza, and V. Khripunov, "A Handy Method For Estimating Radiation Streaming Through Holes In Shield Assemblies", Fusion Engineering and Design 43 (1998) 1-13.

Author(s) Wasastjerna, Frej		
Title Using MCNP for fusion neutronics		
<p>Abstract</p> <p>Any fusion reactor using tritium-deuterium fusion will be a prolific source of 14 MeV neutrons. In fact, 80% of the fusion energy will be carried away by these neutrons. Thus it is essential to calculate what will happen to them, so that such quantities as the tritium breeding ratio, the neutron wall loading, heat deposition, various kinds of material damage and biological dose rates can be determined. Monte Carlo programs, in particular the widely-used MCNP, are the preferred tools for this. The International Fusion Materials Irradiation Facility (IFMIF), intended to test materials in intense neutron fields with a spectrum similar to that prevailing in fusion reactors, also requires neutronics calculations, with similar methods.</p> <p>In some cases these calculations can be very difficult. In particular shielding calculations – such as those needed to determine the heating of the superconducting field coils of ITER or the dose rate, during operation or after shutdown, outside ITER or in the space above the test cell of IFMIF – are very challenging. The thick shielding reduces the neutron flux by many orders of magnitude, so that analog calculations are impracticable and heavy variance reduction is needed, mainly importances or weight windows. On the other hand, the shields contain penetrations through which neutrons may stream. If the importances are much higher or the weight windows much lower at the outer end of such a penetration than at the inner end, this may lead to an excessive proliferation of tracks, which may even make the calculation break down.</p> <p>This dissertation describes the author's work in fusion neutronics, with the main emphasis on attempts to develop improved methods of performing such calculations. Two main approaches are described: trying to determine near-optimal importances or weight windows, and testing the "tally source" method suggested by John Hendricks as a way of biasing the neutron flux in angle.</p>		
ISBN 978-951-38-7129-1 (soft back ed.) 978-951-38-7130-7 (URL: http://www.vtt.fi/publications/index.jsp)		
Series title and ISSN VTT Publications 1235-0621 (soft back ed.) 1455-0849 (URL: http://www.vtt.fi/publications/index.jsp)		Project number 28596
Date November 2008	Language English, Swedish abstr.	Pages 68 p. + app. 136 p.
Name of project		Commissioned by
Keywords fusion neutronics, MCNP, variance reduction, importances, weight windows, tally source method		Publisher VTT Technical Research Centre of Finland P.O. Box 1000, FI-02044 VTT, Finland Phone internat. +358 20 722 4520 Fax +358 20 722 4374



Seriens namn, nummer och
rapportkod

VTT Publications 699
VTT-PUBS-699

Författarna Wasastjerna, Frej		
Namn Fusionsneutronik med MCNP		
Referat En fusionsreaktor som använder sig av tritium-deuteriumfusion kommer att vara en mycket stark källa till neutroner med en energi av 14 MeV. Dessa kommer i själva verket att bära med sig 80 % av fusionsenergin. Det är alltså väsentligt att beräkna vad som kommer att hända med dem, så att man kan bestämma sådana storheter som tritiumbränslevärdet, den av neutronerna förorsakade väggbelastningen, värmedepositionen, olika slags materialskador och biologiska dosrater. Monte Carlo-program, speciellt MCNP, är det mest allmänt använda redskapet för sådana beräkningar. IFMIF (International Fusion Materials Irradiation Facility), avsedd att testa material i ett intensivt neutronflöde med ett spektrum som liknar det i fusionsreaktorer, kräver också neutronberäkningar, med liknande metoder. I vissa fall kan dessa beräkningar vara mycket svåra. I synnerhet strålskyddsberäkningar, sådana som behövs för att bestämma värmeutvecklingen i ITERs supraledande fältspolar eller dosraten, i verksamhet eller efter avstängning, utanför ITER eller i utrymmet ovanför IFMIFs testcell, är särdeles krävande. Det tjocka strålskyddet minskar neutronflödet med många storleksordningar, så att analoga beräkningar är ogenomförbara och stark variansreduktion är nödvändig, främst med viktighet eller viktönsken. Å andra sidan innehåller skyddet genomföringar längs vilka neutroner kan strömma. Om viktigheterna är mycket högre eller viktönsken mycket lägre i yttre ändan av en sådan genomföring än i den inre ändan, kan en partikkelhistoria yngla av sig i ett orimligt antal spår, vilket kan få beräkningen att bryta samman. Denna avhandling beskriver disputandens arbete i fusionsneutronikbranschen med huvudvikten lagd vid hans försök att utveckla förbättrade beräkningsmetoder. Två huvudsakliga sätt att göra detta beskrivs: försök att bestämma närapå optimala viktigheter eller viktönsken, och testning av "tally source"-metoden, föreslagen av John Hendricks som ett sätt att biasera neutronflödet med avseende på vinkel.		
ISBN 978-951-38-7129-1 (häftad) 978-951-38-7130-7 (URL: http://www.vtt.fi/publications/index.jsp)		
Series namn och ISSN VTT Publications 1235-0621 (häftad) 1455-0849 (URL: http://www.vtt.fi/publications/index.jsp)		Projekt nummer
Datum November 2008	Språk engelska, svensk ref.	Sidor 68 s. + bil. 136 s.
Projektets namn		Uppdragsgivare
Nyckelord fusion neutronics, MCNP, variance reduction, importances, weight windows, tally source method		Utgivare VTT PB 1000, 02044 VTT Tel. 020 722 4520 Fax 020 722 4374

Any fusion reactor using tritium-deuterium fusion will be a prolific source of 14 MeV neutrons. It is essential to calculate what will happen to them, so that such quantities as the tritium breeding ratio, the neutron wall loading, heat deposition, material damage and biological dose rates can be determined. Monte Carlo programs, in particular MCNP, are the preferred tools for these calculations.

In some cases these calculations can be very difficult. In particular shielding calculations - such as those needed to determine the heating of the superconducting field coils of ITER or the dose rate, during operation or after shutdown, outside ITER - are very challenging. In an analog Monte Carlo calculation very few neutrons will make it through a thick shield, so heavy reliance on variance reduction is necessary. The most important such technique is geometry splitting. Neutrons that have made some progress through the shield are split so that each history branches into several tracks. This may be repeated many times. This technique ensures that a greater number of tracks will penetrate the shield, but it is problematic when there are slits or ducts through which neutrons may stream.

This thesis describes the author's work in fusion neutronics, with the main emphasis on attempts to develop improved methods for such calculations. Two main approaches are described: trying to determine near-optimal importances or weight windows to control splitting, and testing the "tally source" method suggested by John Hendricks as a way of preferentially following those neutrons whose flight direction gives them the best chances of penetrating a shield with ducts.

Julkaisu on saatavana

VTT
PL 1000
02044 VTT
Puh. 020 722 4520
<http://www.vtt.fi>

Publikationen distribueras av

VTT
PB 1000
02044 VTT
Tel. 020 722 4520
<http://www.vtt.fi>

This publication is available from

VTT
P.O. Box 1000
FI-02044 VTT, Finland
Phone internat. +358 20 722 4520
<http://www.vtt.fi>
